New Approaches to Sensitivity Enhancement in Solid-State Nuclear Magnetic Resonance Spectroscopy

WENG KUNG PENG

July 2008

New Approaches to Sensitivity Enhancement in Solid-State Nuclear Magnetic Resonance Spectroscopy

A dissertation submitted to
THE GRADUATE SCHOOL OF ENGINEERING SCIENCE
OSAKA UNIVERSITY
in partial fulfillment of the requirements for the degree of
DOCTOR OF PHILOSOPHY IN SCIENCE
BY

WENG KUNG PENG

July 2008

Life has never been more rewarding knowing that you are actually contributing to humankind, and to share the dream of those who strive hard to make this world a better place to live. This book is dedicated to those who share the same dream.

Abstract

A work on sensitivity enhancement by means of cross polarization mediated by dipole-dipole coupling of heteronuclear spins-$\frac{1}{2}$, in Nuclear Magnetic Resonance (NMR) spectroscopy of solid-state diamagnetic and paramagnetic systems is presented. Two novel schemes, Nuclear Integrated Cross Polarization (NICP) and Simultaneous ADIabatic Spin-locking Cross Polarization (SADIS CP) are proposed. The transfer mechanisms were analyzed and its performances were verified experimentally.

Conventional Cross Polarization technique (and other single frequency/amplitude modulated schemes) utilize initial $\frac{\pi}{2}$-pulse for excitation on the source spins. This is followed by continuous-wave (cw) irradiation spin-locking (frequency or amplitude modulation maybe applied on one of the channels to counter the effect of fast sample spinning) applied on both the source and target spins, for mixing both spins. In NICP, instead of using initial $\frac{\pi}{2}$-pulse, a single phase irradiation of adiabatic frequency sweep from far off-resonance to on-resonance is applied on the source spins while keeping the cw irradiation on the target spins. This method provides efficient spin-lock on each individual spin-packets of the source spins even in the presence of considerable spectral distribution and/or line broadening. Much broadened Hartmann-Hahn matching profiles for a wide-range of chemical isotropic shifts were obtained for our experiment under fast sample spinning and high static field. In addition, higher signal intensity gains (with an additional gain of up to 3.20 folds as compared to Kolbert's scheme, which utilizes an initial $\frac{\pi}{2}$-pulse followed by adiabatic spin-locking from on-resonance to off-resonance on the source spins) were recorded.

A further improvement of performance for NICP is viable with SADIS CP scheme. In this scheme, adiabatic frequency sweep from far off-resonance to on-resonance is applied to both the source and target spins, simultaneously. We analyzed its Rabi-oscillation and reported the first evidence of reducing the time-dependent Hartmann-Hahn mismatching factor, which allows polarization transfer over a large bandwidth to be sped up, despite having a smaller time-dependent

effective dipolar coupling. This effect was studied by gradually turning on the additional adiabatic frequency sweep spin-locking on the target spins, while keeping the frequency sweep width on the source spins constant. Furthermore, the Hartmann-Hahn matching profile is further broadened. We observed the ^{1}H-^{13}C transfer in L-Alanine (diamagnetic system) that by turning on an additional frequency sweep on target channel, while keeping all other experimental parameters were kept the same as NICP, an additional signal gain of up to 31% was achieved. This scheme offers new solution to issues such as (i) wideband polarization transfer even in the presence of large bandwidth offset effect on both the source and target spins, and (ii) spins with fast relaxation on both the source and target spins.

SADIS CP was further tested on solid-state paramagnetic sample under very-fast sample spinning and high static field. Solid-state paramagnetic sample, which is notoriously known for large spectral distribution and fast relaxation spins due to the effect of large electronic magnetic moment on its nuclear spins, has been an issue with currently existing cross polarization schemes. We proved that essential and robust spin-locking on both channels did induce substantial gain in polarization transfer. An additional signal gain of up to 2.33 folds as compared to amplitude-ramp cross polarization scheme (RAMP CP) was observed.

Foreword

'Difficulty is Opportunity, Pain is Lesson, Sharing is Joy'.

It was a Monday afternoon and we decided that it would be wonderful to demonstrate our pulse technique, SADIS CP in highly paramagnetic sample. The next thing I did was going into our workshop, switching on the milling machine and preparing to build a printed circuit board (PCB) to develop my own personal NMR spectrometer. Yes, you are right. I was about to develop my own NMR spectrometer based on the architecture of OPENCORE NMR, a brain child of my mentor, Dr. Takeda. Milling machine has high precession 'printing' capability of few hundreds micron to mount 'micro-sized' electronic devices. For example, the dimension of a chip-capacitor 1608 is 800x1600 μm. It was so small that we have to use microscope to solder each device manually. Huh, sound like a very long procedure before I can actually start NMR measurement ! No, actually this is part of the journey in research. Considering that in RESEARCH, there is no final DESTINATION but it is the JOURNEY itself, so one might as well enjoy along the way !

We decided to build our own spectrometer simply because there is a need for higher specification (especially frequency jump of a few MHz) than what the commercial spectrometer does offer us. This has taught me a lot to grasp the idea

'to be able to do good science, one must be able to start from the very bottom of the problem'.

I am certainly grateful to happen to be in this Graduate School of Engineering Science, which exposed me to engineering stuff while doing science at the same time. Building a spectrometer especially had exposed me a lot to Electrical Engineering such as Digital Logic, Very-High-Description-Languange (VHDL) programming, rf-transmission engineering, pcb design, passive filter fabrication and Direct Digital Synthesis (DDS). It reminds me of the hardship, pain and persistency of those who involved in building simple NMR transreceiver in the early onset of NMR

(back to the early 50's), when commercial spectrometer was not available. Without it, there would certainly be no magnetic resonance today. When science began, technology starts to roll and the cycle continues.

I was initially brought into Japan with the strong recommendation of Prof. Masahiro Kitagawa, after a-year-long of tight selection process in my home country, Malaysia. Ministry of Education, Culture, Sports, Science and Technology offer a handful full-scholarships world wide, known as Monbusho-scholarship, through their respectively embassy. This award which has prestige similar to Fulbright Scholar as in United State and British Chevening Scholar as to United Kingdom, has upheld its prestigious ever since its commencement.

Being an expert in electronic devices and Quantum Information Science, our laboratory mainly works on achieving high polarization for initialization stage for quantum operation in solid-state NMR. I was humbled by the complexity and difficulty of Quantum Information Science, especially when one has to build new and sophisticate hardware as a testbed for future technology, while risking that the idea may not work at all ! This turn out to be a blessing in disguise, as I began to be more realistic and honest with myself. It was then, Dr. Takeda who introduced me to solid-state NMR and I began with doing NICP, a pulse sequence which was later published in CPL.

It was early in the morning about 4 am when I stumbled on a phenomenon which seemed to give me an extra signal enhancement in much shorter time than NICP itself. What drove me there was just my simple curiostiy and basic intuition of wanting to understand a physical phenomena. Obviously, without any theoretical backup yet then, I failed to convince my supervisor on the very next day. Finally, it was when I managed to track down that it was actually due to faster/efficient polarization transfer which can be described numerically in terms of its Rabi oscillation. It took me almost 1.5 yrs to convince him ! Throughout the journey, theoretical derivation, simulation, re-verifying and re-verifying (I forgot how many times) the phenomena experimentally were done to fine tuning our understanding towards this new idea. This work was then published as a pulse

sequence with acroynm, SADIS CP, appeared in JMR. This dissertation mainly concerning NICP, SADIS CP (initially carried out on diamagnetic sample), how we have successfully demonstrated its application for sensitivity enhancement in solid-state paramagnetic spectroscopy (manusricpt is currently under reviewed at press time) as well, and building our own NMR spectrometer for future extension work.

The Author

Contents

List of Figures

List of Tables

Thesis Overview

An introductory idea of solid-state NMR and Cross Polarization (CP) is presented in Chapter 1. A general theoretical framework and results on numerical simulation of both our new schemes NICP [1] and SADIS CP [2], are presented in Chapter 3. Experimental verifications are given in Chapter 4, Chapter 5 and Chapter 6.

The first idea of double resonance was first demonstrated by Hartmann-Hahn in 1962, it was then preceded by work of proton-enhanced rare spins by Alex Pines in 1972, which is known as cross polarization. Over the years, CP evolved as development in NMR technology took place. Chapter 2 is dedicated to show a historical development of CP and our works. NICP (Chapter 4), which borrowed the idea from ICP, (work on electron-to-nuclear polarization), was successfully demonstrated in nuclear-to-nuclear polarization transfer. This technique, is suitable to effectively spin-lock large spectral distribution of the source spins, such as proton and fluorine. We show theoretically that adiabatic inversion of 2 spin-system in zero-quantum subspaces is similar to single spin adiabatic inversion in conventional rotating frame. Besides being useful for source spins with large spectral distribution, NICP is also compatible for experiment under fast magic-angle sample spinning (MAS).

Following NICP, another novel scheme was introduced by our group to speed up the polarization over a large bandwidth. This can be achieved with simultanoeus application of frequency sweep on both the source and target spins, which we call Simultaneous ADIabatic Spin-locking Cross Polarization, with acroynm SADIS CP. Theoretical description and results on numerical simulation are presented in Chapter 3 and experimental verification in Chapter 5 and Chapter 6. SADIS CP is robust against the effect of fast sample spinning, capable of wideband excitation and faster transfer (which is suitable for systems with fast relaxation time), turnout to be a general technique for all other currently existing cross-polarization schemes.

To my knowledge, we are the first group to show that polarization transfer over a large bandwidth can be sped up by reducing the time-dependent Hartmann-Hahn

mismatching throughout the whole contact time. Simplified description of the dynamics of two interacting spins as revealed by its Rabi oscillation (in Chapter 3), allows us to draw to conclusions that: (a) the maximum amount of instanstaneous polarization transfer is described by the amount of Hartmann-Hahn mismatching, and (b) effective exchange coupling (or its scaling factor) only describes how fast the oscillations between two spins and not the ultimate amount of polarization transfer. The amount of polarization transfer can only be described by the effective exchange coupling provided that the time-dependent Hartmann-Hahn mismatching is fixed. We have successfully observed the effect of time-dependent Hartmann-Hahn mismatching and clearly shown the effect of turning on additional frequency sweeping on the target spins, which is translated into higher sensitivity gain in diamagnetic organic system (refer to Chapter 5).

We have also shown that SADIS CP performs remarkably well for sensitivity enhancement on solid-state paramagnetic sample (Chapter 6) [3]. Conventional Cross Polarization and its variations (single channel frequency/amplitude modulated CP) had not been a popular choice for sensitivity enhancement in paramagnetic solids, mainly, due to the large broadening and the effect of fast relaxation. With this demonstration, we show that significant enhancement in paramagnetic system can be obtained provided that the spin-locking efficiency can be improved. In order to perform SADIS CP on other highly paramagnetic species, initial frequency-jump of several MHz is required. A new NMR spectrometer (Chapter 6) based on Dr. Takeda's work has been developed for this purpose.

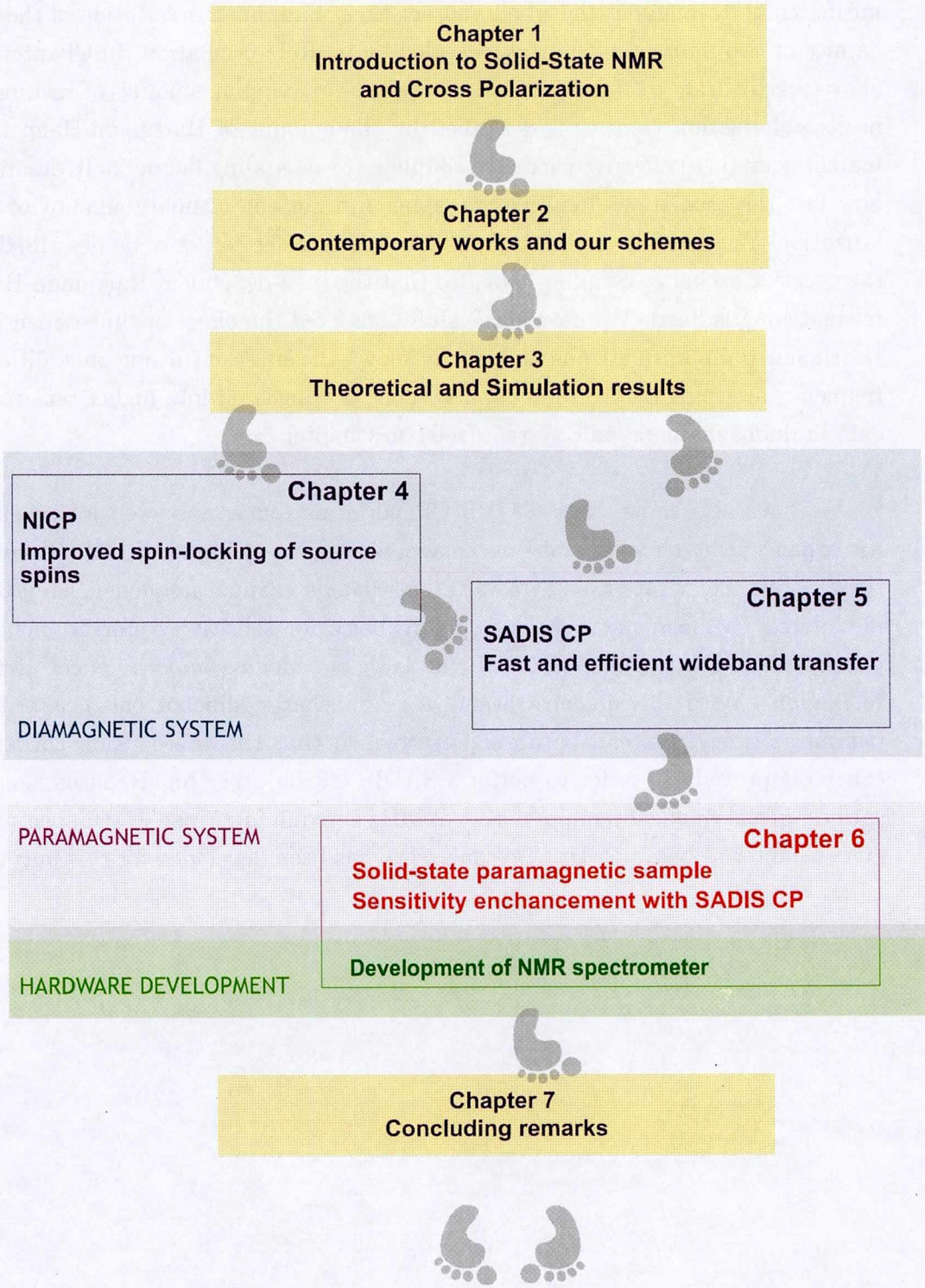
Chapter 1
Introduction to Solid-State NMR
and Cross Polarization
Chapter 2
Contemporary works and our schemes
Chapter 3
Theoretical and Simulation results
Chapter 4
NICP
Improved spin-locking of source spins
Chapter 5
SADIS CP
Fast and efficient wideband transfer
DIAMAGNETIC SYSTEM
PARAMAGNETIC SYSTEM
Chapter 6
Solid-state paramagnetic sample
Sensitivity enchancement with SADIS CP
Development of NMR spectrometer
HARDWARE DEVELOPMENT
Chapter 7
Concluding remarks

Part I

Introduction to Solid-State NMR and Historical Development of Cross Polarization

1 Solid-State NMR and its development

1.1 NMR, Spectroscopy and Spin-Dynamics

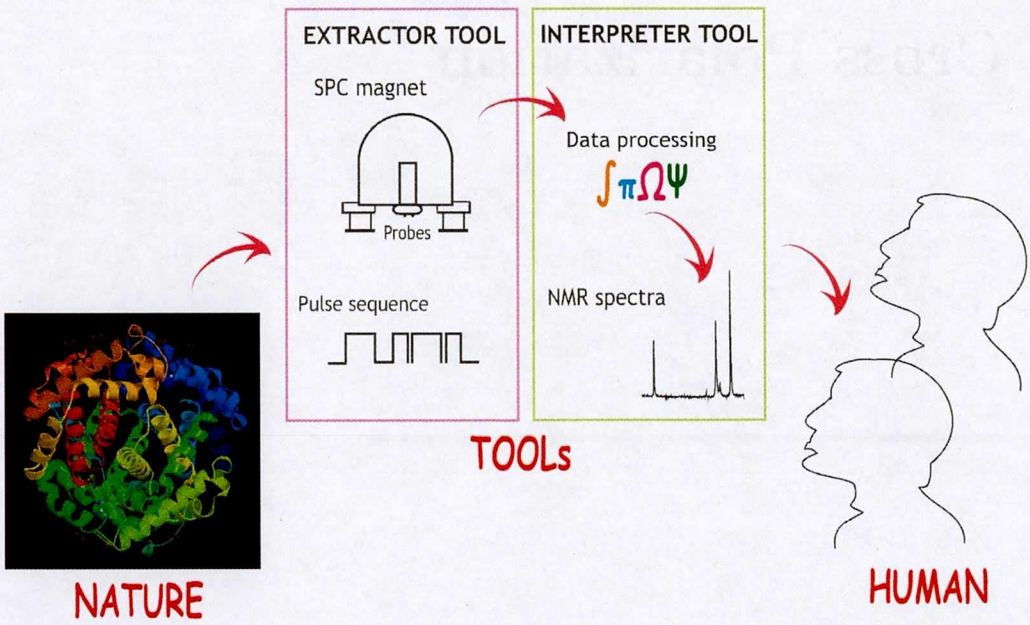

Figure 1.1: Graphical idea of how NMR is used as a tool for spectroscopy.

What is spectroscopy? You are actually performing a spectroscopy right now when you are reading this script. In layman term, spectroscopy means 'seeing' or 'looking' at something. Have you ever wonder how this simple spectroscopy works? When light is shown to an object and reflected to our eyes (through cornea), an image will be formed and finally detected by our retina. This image will be interpreted as some kind of 'information' by our brain. The concept here is extracting information and interpretating them. This wonder works, because we have been naturally blessed with eye and brain.

What about things which are too small, too far, or too dark to be seen with

our bare eye? With the parallel progress of science and technology, human being had then been able to probe into states which can not be observed directly with our bare eye. From the same principle as what our Mother Nature gave us, more complex form of spectroscopy requires an intermediate state or TOOLs, which can generally be divided into two classes; an extractor tool and an interpretor tool. These extractor tools are usually hardware built by engineers, to interact with the system and detect its responses. The obtained responses will then by interpreted by some form of mathematical algorithms into a language which can be recognized by scientist/human being.

Nuclear Magnetic Resonance spectroscopy is as shown in Fig.1.1. A sample is placed under a strong longitudinal static field, B_o, to differentiate each unique nuclear spin due to its surrounding. A much smaller magnitude of oscillating field B_{rf}, is then applied perpendicularly to B_o, to excite these nuclear spins, which happen to fall under the region of radio-frequency (rf). A rotation of the nuclear magnetic moment produces rotating magnetic field and since the changing of the magnetic fields produces electric currents in coil, we can detect the oscillation of the electric current with the same coil (also known as Faraday coil). This NMR signal is known as free-induction decay (FID). Since, the FID is also in rf range, we could actually 'listen' to the molecule, very much like asking the molecule 'who are you ?' and being replied with 'I am Handai Taro'. More often than not, this FID is actually a combination of a few FIDs, meaning that there are too many people shouting their own names at the same time and therefore we can't recognize clearly who they are. We need an interpreter tool to translate these FIDs into information recognized by human being. One popular method is through Fourier Transform (FT) which works on transforming the time-domain oscillation signal into resolved peaks in frequency-domain data.

Unlike other spectroscopy techniques, NMR has more than "looking into the states", her beauty probably lies on the spin-dynamics. With appropriate pulse sequences, we can actually interact with the internal system, through external pertubation. Smartly choreographing the spins, quantum mechanical behaviour is revealed in which can be exploited to do simple quantum gate-operations and even

spin-memory system.

1.2 The Birth of NMR

Nuclear magnetic resonance was first described and measured in molecular beams by Isidor Rabi in 1938. Eight years later, the first successful NMR experiments in condensed matter were carried out by Edward Mills Purcell, Torrey, and Pound [4] at Harvard University. At the same time, Felix Bloch [5] worked on nuclear induction independantly at Stanford University. Both Bloch and Purcell shared the Nobel Prize in physics in 1952 in recognization of their indigenous effort.

Harald Cramer, member of the Royal Academy of Sciences, addressed the laureate in his speech by saying

'Dr. Bloch and Dr. Purcell !! You have opened the road to new insight into the microworld of nuclear physics. Each atom is like a subtle and refiend instrument, playing its own faint, magnetic melody, inaudible to human ears. By your methods, this music has been made perceptible, and the characteristic melody of an atom can be used as an identification signal. This is not only an achievement of high intellectual beauty - it also places an analytic method of the highest value in the hands of scientists.'

Born in Illinois and educated in Purdue University, Purcell graduated as an electrical engineer. His interest had then turned into physics, in which he took his Ph.D degree from Harvard University. Purcell had worked on the development and application of RADAR during World War II at Massachusetts Institute of Technology's Radiation Laboratory. His work during that project on the production and detection of radiofrequency energy, and on the absorption of such energy by matter, had probably served as an inspiration to his discovery of NMR. He then pursued his interest in relaxation phenomena, nuclear magnetic behaviour at low temperature and measurement of atomic constants.

Bloch was born in Zurich, Switzerland. He had an early education in the Eidgenossische Technische Hochschule, Zurich. Similarly to Purcell, he initially studied engineering and his interest soon changed to physics. Graduating in 1927 he continued his physics studies at the University of Leipzig, where he took his doctorate in 1928. He remained in German Academia, studying with a few other big names like, Werner Heisenberg, Wolfgang Pauli, Niels Bohr and Enrico Fermi. In 1933, he emigrated to US to work at Stanford University in 1934. During World War II, he worked on atomic energy at Los Alamos National Laboratory, before resigning to join the radar project at Harvard University.

They noticed that magnetic nuclei, like ^{1}H and ^{31}P, could absorb rf energy when placed in a magnetic field of a strength specific to the identity of the nuclei. It was this simple phenomena, that had paved way to today's technology such as Magnetic Resonance Imaging (MRI) and NMR Quantum Computation.

1.3 The Bizarre Properties of Magnetism

Generally speaking magnetism come from three sources [6], (a) circulation of the electric current, (b) the magnetic moments of the electrons, and (c) the magnetic moments of the atomic nuclei. Unlike (a) which is due to circulation, (b) and (c) are intrinsic properties of a particle, just like mass, electric charge and spin.

All magnetic substances have the capabilities to interact with magnetic fields and this interaction is expressed by magnetic moment, μ. Some substances have permanent magnetic moment such as ferromagnetic and anti-ferromagnetic systems while for other it is induced e.g. paramagnetic and diamagnectic systems. This induced magnetism can only posses magnetic moment in the presence of external magnetic field and its magnetic moment is given by

$$\mu_{induced} = \mu_o^{-1} V \chi \mathbf{B}, \tag{1.1}$$

where the permeability of free space, $\mu_o = 4\pi$ x 10^{-7} Hm^{-1} is a constant, $\mathbf{B}$ is the magnetic flux density, V is the object volume and χ is the magnetic suscepibility and is dimensionless. The magnetization per volume,

$$M = \frac{\mu_{induced}}{V} = \mu_o^{-1}\chi\mathbf{B}. \tag{1.2}$$

For paramagnetic sample, χ is positive while diamagnetic sample, χ is negative (Fig. 1.2). Paramagnetic susceptibilities tend to be larger in magnitude as compare to its counterpart (Fig. 1.3). Diamagnetic susceptibility in metalloprotein (paramagnetic ion center surrounded by thousands of atoms), can however, be in the same order with paramagnetic susceptibility [7]. Diamagnetism always present due to the interaction of the magnetic field with the motion of the electrons in their orbits.

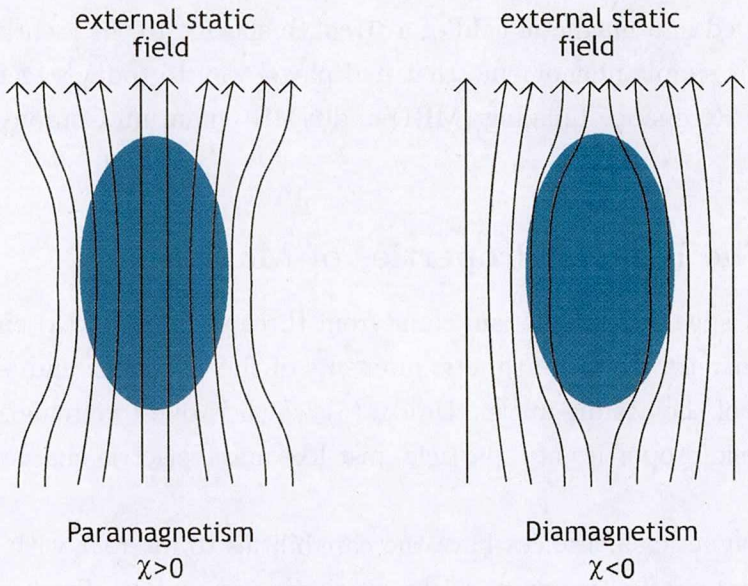

Figure 1.2: The effect on the shape of the distortion on applied magnetic field is described by positive and negative magnetic susceptibility.

Permanent magnetism inside electron and nuclei is closely linked to its spin, which is given by the spin magnetic moment as,

$$\boldsymbol{\mu} = -\gamma\mathbf{S} \tag{1.3}$$

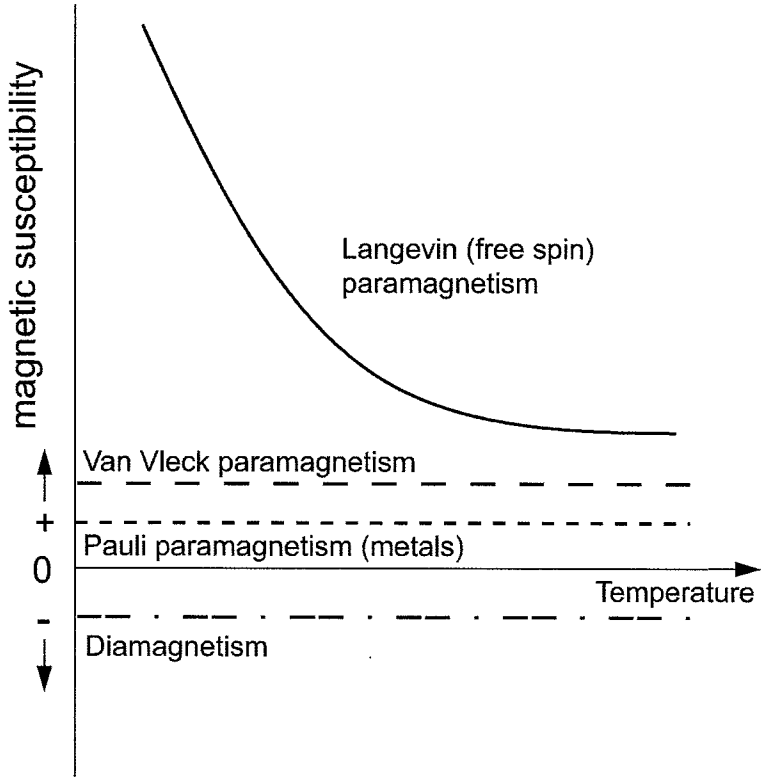

Figure 1.3: Characteristic of magnetic susceptibility of paramagnetic and diamagnetic substances as a fucntion of temperature.

where **S** is the spin angular momentum vector and γ is called gyromagnetic ratio. Magnetic moments of nuclei are usually of order of 10^{-3} times smaller than the magnetic moment of the electron. We will see in later chapter how this interaction between them give raise to nuclear paramagnetism effect.

If an external magnetic field is applied to this object, the magnetic moment of the nuclei start precessing around the external field so as to minimize the magnetic energy. This precession frequency is known as Larmor frequency and is expressed as

$$\omega = -\gamma B_o \tag{1.4}$$

where B_o is the magnitude of the external field. Each isotope is unique and its properties are as shown as Table 1.1.

Isotope	Notation	Spin	Natural Abundance	Gyromagnetic Ratio, γ [10^6 rads^{-1}T^{-1}]	Larmor Frequency at 9.4 T, $\omega/2\pi$ [MHz]
^{1}H	I	$\frac{1}{2}$	~100	267.522	~-400.0
^{12}C		0	98.9	-	-
^{13}C	S	$\frac{1}{2}$	1.1	67.283	~-100.6
^{14}N		1	99.63	19.338	~-28.9
^{15}N		$\frac{1}{2}$	0.37	-27.126	~+40.6

Table 1.1: A few selected nuclear isotopes and its properties.

1.4 Solid-State NMR and fundamental

1.4.1 Interaction in NMR and Hamiltonian

Chemical Shift Local magnetic fields experienced by each nuclear spin are different due to its unique electronic environment. For example a methyl, CH_3 and a methine, CH experience slightly different electron cloud, therefore we could tell which carbon they belongs to. This is known as chemical shift. For this homonuclear system, this small chemical shift differences can be shown when a large external magnetic field is applied to the system. Their respective Larmor frequency is then shifted according to the external field by a factor of

$$\omega = -\gamma B_o(1 - \sigma). \tag{1.5}$$

Since it is arbitrary due to its dependancy on the external field, per per million (ppm) measurement is used to identify the system. For standard reference, it is referred to well-known system such as tetramethylsilane (TMS). For heteronuclear system such as ^{13}C and ^{1}H , the chemical shift is much larger and can therefore be well-identified.

Direct Dipole-Dipole Coupling In solid-state, dipole-dipole interaction is the main source of coupling and it is frequently used for structural determination. Each nuclear spin posses its own magnetic moment which, generates local magnetic field according to the direction of the spin magnetic moment. This nuclear spin interacts with other nuclear spins that are present around its surrounding. This mutual interaction is called dipole-dipole interaction. The hamiltonian for dipole-dipole interaction is given by

$$H_d = -d_o[A + B + C + D + E + F], \tag{1.6}$$

where

$$\begin{aligned}
A &= I_z S_z(3\cos^2\theta - 1) \\
B &= -\frac{1}{4}[I_+S_- + I_-S_+](3\cos^2\theta - 1) \\
C &= \frac{3}{2}[I_zS_+ + I_+S_z]\sin\theta\cos\theta e^{-i\phi} \\
D &= \frac{3}{2}[I_zS_- + I_-S_z]\sin\theta\cos\theta e^{+i\phi} \\
E &= \frac{3}{4}[I_+S_+]\sin^2\theta e^{-2i\phi} \\
F &= \frac{3}{4}[I_-S_-]\sin^2\theta e^{+2i\phi}
\end{aligned}$$

and d_o is the coupling constant defined by $\frac{\mu_o}{4\pi}\frac{\gamma_I\gamma_S\hbar}{r^3}$ (in unit rads^{-1}), where r is the internuclear distance. θ and ϕ are the polar angles of the internuclear axis to the static field and to the xy-plane, respectively. The hamiltonian for homonuclear spins in rotating frame (a frame which rotates at Larmor frequency, ω_o around the z-axis of the laboratory frame, $\mathbf{B_o}$) due to its dipole-dipole interaction is given by

$$H_d^\star = -d_o R_z^{-1}(\omega_o t)[A + B + C + D + E + F]R_z(\omega_o t). \tag{1.7}$$

A and B terms are unaffected by the transformation, C-F terms become time-dependent and can be dealt with by using average hamiltonian theory [8]. Upon averaging, to the first order these terms did not survive. The first order (which is the lowest order, often confusingly denoted as $\overline{H}^{(0)}$) average hamiltonian in the

rotating frame thus become,

$$\begin{aligned}
\overline{H}_d^{(0)} &= -d_o(3\cos^2\theta - 1)[A + B] \\
&= -d_o(3\cos^2\theta - 1)[I_z S_z - \frac{1}{4}(I_+ S_- + I_+ S_-)] \\
&= -d_o(3\cos^2\theta - 1)[I_z S_z - \frac{1}{2}(I_x S_x + I_y S_y)] \\
&= -d_o(3\cos^2\theta - 1)\frac{1}{2}(3I_z S_z - \mathbf{I.S}), \qquad (1.8)
\end{aligned}$$

where **I.S** represents $I_z S_z + I_y S_y + I_x S_x$. Notice that, $I_x = \frac{1}{2}(I_+ + I_-)$ and $I_y = \frac{1}{2i}(I_+ - I_-)$, therefore $I_x S_x + I_y S_y = \frac{1}{2}(I_+ S_- + I_+ S_-)$. If the spins are of different isotropic species, only A term survived after the transformation and the secular part of the heteronuclear dipole-dipole hamiltonian is given by

$$\overline{H}_d^{(0)} = -d_o[A] = -d_o(3\cos^2\theta - 1)[I_z S_z]. \qquad (1.9)$$

For short-hand purposes, $\overline{H}_d^{(0)}$ is usually simplified to H_d. B term is important to homonuclear dipolar coupling but not to heteronuclear dipolar coupling to the first order approximation. We can imagine the B term as corresponding to the transverse component of the local field. This component is due to a spin precess at the Larmor frequency of that spin only if both the nuclear spins are of the same nuclide. However, two heteronuclear spins can also be made to communicate with each and other by putting them into resonance as shown by Hartmann-Hahn. Cross polarization is also mediated by such couplings and the details will be explained in the following chapter.

Quadrapolar Interaction For nuclear spin which is greater than $\frac{1}{2}$, the electric quadrupole moment of the nucleur interacts strongly with the electric field gradients generated by the electron clouds. The secular quadrapolar interaction is given here as

$$H_Q = \omega^Q(3I_z^2 - \mathbf{I.S}), \qquad (1.10)$$

ω^Q is called quadrupolar frequency. This interaction is not of interest in this work.

1.4.2 Density Matrix and Coherences

The density matrix for a spin-pair of a ensemble of noninteracting spin-$\frac{1}{2}$ is given by the averaged outer product (ket-bra multiplication) of the wavefunctions

$$\begin{aligned}\widehat{\rho} &= \overline{|\psi\rangle\langle\psi|} \\ &= \begin{pmatrix} c_{\alpha\alpha} \\ c_{\alpha\beta} \\ c_{\beta\alpha} \\ c_{\beta\beta} \end{pmatrix} \begin{pmatrix} c^{\star}_{\alpha\alpha} & c^{\star}_{\alpha\beta} & c^{\star}_{\beta\alpha} & c^{\star}_{\beta\beta} \end{pmatrix},\end{aligned} \tag{1.11}$$

and after multiplication of the column vector and the row vector,

$$\widehat{\rho} = \begin{pmatrix} \overline{c_{\alpha\alpha}c^{\star}_{\alpha\alpha}} & \overline{c_{\alpha\alpha}c^{\star}_{\alpha\beta}} & \overline{c_{\alpha\alpha}c^{\star}_{\beta\alpha}} & \overline{c_{\alpha\alpha}c^{\star}_{\beta\beta}} \\ \overline{c_{\alpha\beta}c^{\star}_{\alpha\alpha}} & \overline{c_{\alpha\beta}c^{\star}_{\alpha\beta}} & \overline{c_{\alpha\beta}c^{\star}_{\beta\alpha}} & \overline{c_{\alpha\beta}c^{\star}_{\beta\beta}} \\ \overline{c_{\beta\alpha}c^{\star}_{\alpha\alpha}} & \overline{c_{\beta\alpha}c^{\star}_{\alpha\beta}} & \overline{c_{\beta\alpha}c^{\star}_{\beta\alpha}} & \overline{c_{\beta\alpha}c^{\star}_{\beta\beta}} \\ \overline{c_{\beta\beta}c^{\star}_{\alpha\alpha}} & \overline{c_{\beta\beta}c^{\star}_{\alpha\beta}} & \overline{c_{\beta\beta}c^{\star}_{\beta\alpha}} & \overline{c_{\beta\beta}c^{\star}_{\beta\beta}} \end{pmatrix}, \tag{1.12}$$

and finally rewritten as (following the notation by Levitt [6])

$$\widehat{\rho} = \begin{pmatrix} \rho_{\alpha\alpha} & \rho_{\alpha+} & \rho_{+\alpha} & \rho_{++} \\ \rho_{\alpha-} & \rho_{\alpha\beta} & \rho_{+-} & \rho_{+\beta} \\ \rho_{-\alpha} & \rho_{-+} & \rho_{\beta\alpha} & \rho_{\beta+} \\ \rho_{--} & \rho_{-\beta} & \rho_{\beta-} & \rho_{\beta\beta} \end{pmatrix}. \tag{1.13}$$

Among the elemnents, four diagonal elements representing the population,

$$\begin{pmatrix} \textit{population} & & & \\ & \textit{population} & & \\ & & \textit{population} & \\ & & & \textit{population} \end{pmatrix}, \tag{1.14}$$

and twelve off-diagonal elements representing the coherences between the states. These coherences are categorized into two groups: the Single Quantum (SQ) coherence and the Multiple Quantum (MQ) coherence. MQ consists of Zero-Quantum (ZQ) transition and Double-Quantum (DQ) transition. The SQ transitions occupy

$$\begin{pmatrix} & SQ & SQ & \\ SQ & & & SQ \\ SQ & & & SQ \\ & SQ & SQ & \end{pmatrix} \tag{1.15}$$

while the MQ coherences occupy

$$\begin{pmatrix} & & & DQ \\ & & ZQ & \\ & ZQ & & \\ DQ & & & \end{pmatrix}. \tag{1.16}$$

These coherences can be illustrated by arrow diagram as shown in Fig. 1.4.

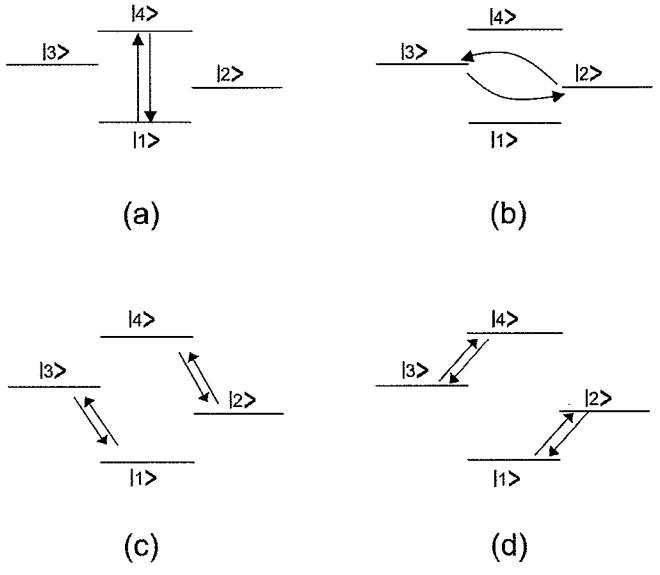

Figure 1.4: Arrow diagram of (a) DQ transition and (b) ZQ transition. Both (c) and (d) are SQ transitions.

In general, the spin-density operator can be expressed as a sum of product operator terms given by

$$\rho = a\mathbf{I} + bI_z + c2I_xS_y + ... \tag{1.17}$$

The product operators are as given in the Table 1.2,

Populations	I_z, S_z, I_zS_z
Single Quantum Coherences	$I_x, I_y, S_x, S_y, I_xS_z, I_yS_z, I_zS_x, I_zS_y$
Multiple Quantum Coherences	$I_xS_x, I_yS_y, I_xS_y, I_yS_x$
Scalar element	$\mathbf{I}/2$

Table 1.2: A summary of the product operators for 2 spins system, I and S are grouped according to their coherence orders. Note that $I_{1\alpha} = I_\alpha \otimes E$ and $I_{2\alpha} = E \otimes I_\alpha$, where I_α and $\alpha = x, y, z$ are the Pauli operators. For brevity, $I_{1\alpha} = I_\alpha$ and $I_{2\alpha} = S_\alpha$ are oftenly used.

1.5 High Resolution Solid-State NMR

Unlike liquid-state NMR, which give high sensistivity and sharp resolution, solid-state NMR is lack of it. Solid-state material is dominated mostly with huge anisotropic interactions such as hetero/homo-nuclear dipolar coupling which give essentialy broad and featureless spectrum and therefore provide no direct information. An excellent example is provided by water whose proton NMR linewidth is about 0.1 Hz, while that for ice is about 10^5, which is six orders of magnitude broader. In mobile fluids, the rapid isotropic motions of the nuclei average out the anisotropic interactions. Since not all samples can be found in liquid-state nor keeping its chemical properties with dilution, there is a huge demand on high-resolution solid-state NMR. Removing the unwanted interactions, increasing the wanted signal and improving the resolution between peaks are all the on-going research challenges. Among the routinely used techniques for high resolution solid-state NMR are (i) cross polarization to enhance the sensitivity, (ii) fast mechanical sample spinning, known as magic-angle spinning used to remove undesirable anisotropic interactions (iii) application of rf-irradiation to decouple unwanted interactions and finally, (iv) recoupling used to 'make alive' desire interaction and also for those afforable (v) employment of higher static field.

1.5.1 Double Resonance and Cross Polarization

Cross polarization (CP) [9, 10] is routinely used in diamagnetic solid-state NMR spectroscopy to enhance sensitivity of nuclear spin species having relatively small gyromagnetic ratios such as ^{13}C and ^{15}N, by transfering a large polarization from spins such as ^{1}H or ^{19}F. The I spin here on may be refered to as source spin while the S spin is refered to as target spin. The original idea nuclear double resonance was shown by Hartmann and Hahn [9], and then successfully demonstrated in proton-enhanced sensitivity enhancement of rare spins by Pines, Gibby and Waugh [10].

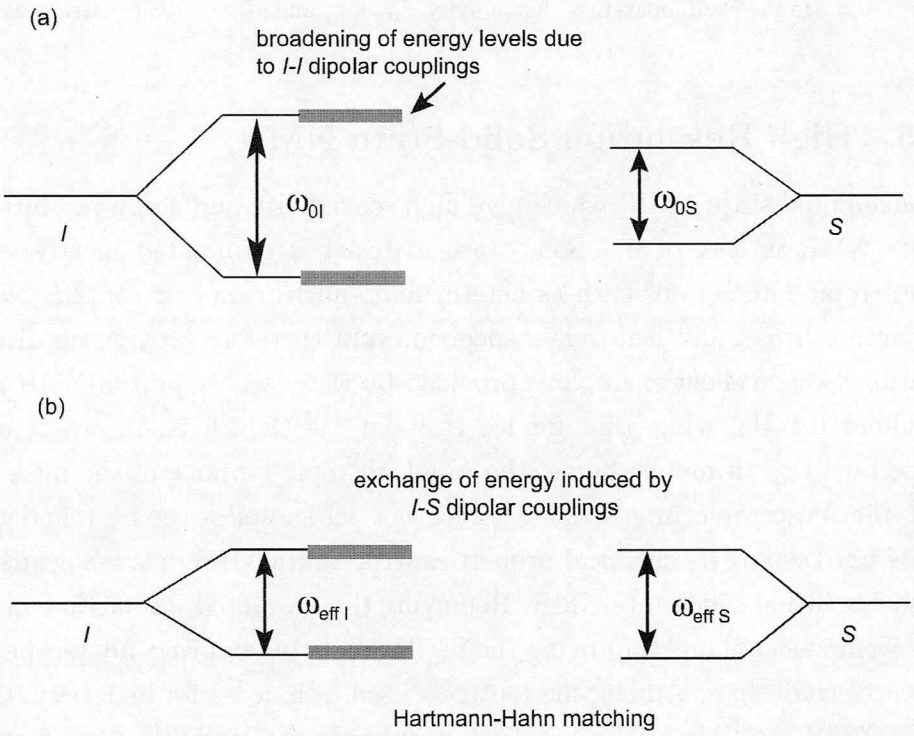

Figure 1.5: (a) Energy levels of I and S spin in laboratory frame. (b) Matching of energy levels of I and S spins in the rf rotating frame.

If a solid containing I and S spins with gyromagnetic ratio of γ_I and γ_S respec-

tively, subjected to strong external magnetic field, then their energy level splits according to its Larmor frequency as shown in Fig. 1.5. Practically, there is a distribution of $I-I$ homonuclear couplings, therefore the energy levels are broadened. When rf-irradiations were applied to both nuclear spins, the two spins system becomes an oscillatory time-dependant term in laboratory frame. It is convenient to choose a new reference frame, which rotate with applied rf-fields and a new z-axis, known as doubly tilted rotating frame. When nutation frequencies of I and S spins, are matched, energy exchange mediated by the flip-flop terms between both spin take place. This is known as Hartmann-Hahn condition,

$$\gamma_I B_{1I} = \gamma_I B_{1S}, \tag{1.18}$$

or simply their respective nutation frequency,

$$\omega_{1I} = \omega_{1S}. \tag{1.19}$$

In the present of isotropic chemical shift or application of frequency/amplitude modulation, Hartmann-Hahn should be expressed in a more general equation as their respective effective field,

$$\omega_{\mathrm{effI}} = \omega_{\mathrm{effS}}. \tag{1.20}$$

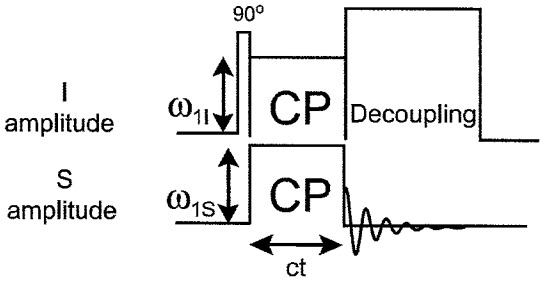

Figure 1.6: Pulse sequence of the original idea of Hartmann-Hahn CP. CW irradiations were applied on both channels. S is observed under high-power decoupling.

Figure 1.6 shows a typical pulse sequence for cross polarization. Strong continuous-wave (CW) rf-irradiations are applied to lock each nuclear spins on the x-y plane,

so that polarization transfer can take place. This strong forced precession is known as spin-locking and the amount of time spent is known as contact time, *ct*. For full transfer to occur, spin-locking must be able to lock both the source and target spins effectively and long enough before the magnetizations decay take place. This magnetization decay in this rotating frame is known as spin-lattice relaxation in rotating frame or $T_{1\rho}$.

Sensitivity enhancement of a factor $\frac{\gamma_I}{\gamma_S}$ is then possible, provided that (i) the number of abundant spins are very much larger than the rare spins, and (ii) relaxation of both the source and target spins are long enough. Furthermore, often faster relaxation rate of abundant spins allow shorter recycle delay, which will increase the SNR as compared to direct excitation of the rare spins. In this case, however, the signal intensity per unit time, remains the same.

1.5.2 Visualizing CP with matrix representation

In this section, I will show a simplified version of cross polarization of two isolated spins system in the form of matrix representation. As such, one will be able to visualize how polarization transfer works in the form of matrix. Consider, if rf-irradiation of ω_{1I} and ω_{1S} are applied to I and S spins respectively, the rotating Hamiltonian of IS spin-pair is given by,

$$H = -\omega_{1I}I_x - \omega_{1S}S_x - \triangle\omega_I I_z - \triangle\omega_S S_z + 2bI_zS_z, \tag{1.21}$$

where b is the heteronuclear dipolar coupling and $\triangle\omega$ is the offset resonance. Since only the magnetization along the effective fields is of interest, it is convenient to transform the hamiltonian to doubly tilted rotating frame. Defining the effective fields to an angle $\tan\theta_I = \omega_{1I}/\triangle\omega_I$ and $\tan\theta_S = \omega_{1S}/\triangle\omega_S$, and diagonalizing with propagator $U = \exp(-i\theta_I I_y)\exp(-i\theta_S S_y)$, the following hamiltonian is obtained,

$$
\begin{aligned}
H^T = -\omega_{eI} I_z - \omega_{eS} S_z + 2b \sin\theta_I \sin\theta_S (I_x S_x) \\
+2b \cos\theta_I \cos\theta_S (I_z S_z) \\
-2b \cos\theta_I \sin\theta_S (I_z S_x) \\
-2b \sin\theta_I \cos\theta_S (I_x S_z),
\end{aligned} \tag{1.22}
$$

where the their effective field is given by $\omega_{e\epsilon} = (\omega_{1\epsilon}^2 + \triangle\omega_{\epsilon}^2)^{\frac{1}{2}}$. The (third, fourth, fifth, sixth) terms are (DQ, population, SQ, SQ) respectively. For simplicity, when both the rf-irradiations were applied on-resonance (θ= 90°), making all the $\sin\theta$ terms equal to 1 while the $\cos\theta$ terms equal to zero, reducing the total hamiltonian to only the third terms. Therefore,

$$
H^T = -\omega_{1I} I_z - \omega_{1S} S_z + 2b I_x S_x. \tag{1.23}
$$

Further, rewritting them into single transition operators,

$$
H^T = -\Delta I_z^{\mathrm{ZQ}} - \Sigma I_z^{\mathrm{DQ}} + b(I_x^{\mathrm{ZQ}} + I_x^{\mathrm{DQ}}), \tag{1.24}
$$

where the time-independant coefficients are given by,

$$
\Delta = \omega_{1I} - \omega_{1S}, \tag{1.25}
$$

$$
\Sigma = \omega_{1I} + \omega_{1S}, \tag{1.26}
$$

and the single transition operator for the new x-axis along the ZQ and DQ subspaces are given by,

$$
I_x^{\mathrm{ZQ}} = \frac{1}{2}[I_+ S_- + I_- S_+], \tag{1.27}
$$

$$
I_x^{\mathrm{DQ}} = \frac{1}{2}[I_+ S_+ + I_- S_-]. \tag{1.28}
$$

These two subspaces are also known as flip-flop term and flop-flop term, respectively. Along the new z-axis,

$$
I_z^{\mathrm{ZQ}} = \frac{1}{2}[I_z - S_z], \tag{1.29}
$$

$$
I_z^{\mathrm{DQ}} = \frac{1}{2}[I_z + S_z]. \tag{1.30}
$$

One can visualize them in the form of matrix representation,

$$\begin{pmatrix} \frac{\Sigma}{2} & & & \frac{b}{2} \\ & -\frac{\Delta}{2} & \frac{b}{2} & \\ & \frac{b}{2} & -\frac{\Delta}{2} & \\ \frac{b}{2} & & & \frac{\Sigma}{2} \end{pmatrix}. \tag{1.31}$$

Notice that the diagonal terms are actually experimental controlable parameters, which mean that we can drive the 'population' of polarization transfer with suitable rf-irradiations !

1.5.3 Fast, Very-Fast, Ultra-fast Sample Spinning

Human being finds ways to emulate Nature by taking 'hint' on how its Mother Nature works. Since naturally isotropic motion is not present in solids as in liquid-state, applying mechanical rotation on the sample fixed at an angle θ_m inclined to the static field, the spatial space coordinate can be 'averaged-out'. This θ_m angle is known as magic-angle. The pioneers of this works were Andrew [11] and then independantly demonstrated by Lowe [12].

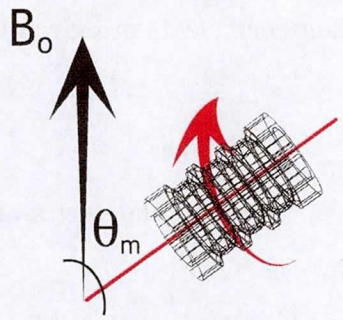

Figure 1.7: Rotor aligned to an angle, θ_m tilted to the static field. This is known as magic-angle.

Removal of line broadening originating from chemical shift anisotropy (CSA) can be achieved with such techniques, and give rise to narrowed line or/and spectral. If the sample is spunned fast enough (faster than its coupling), direct dipole-dipole couplings (both heteronuclear and homonuclear) can also be removed. We

will only focus on the effect of heteronuclear dipolar interaction under fast magic-angle sample spinning (MAS), which is related to this work. Consider when the sample is static, the time-independent heteronuclear dipolar interaction is given by

$$H_d = -d_o I_z S_z (3\cos^2\theta - 1), \tag{1.32}$$

as shown in Eq. 1.9. It is clear that if this term $(3\cos^2\theta - 1)$ were somehow to be made to zero, the coupling will be removed and therefore the magic-angle here is given by $\theta_m = \cos^{-1}\frac{1}{\sqrt{3}}$. Actually, one can recreate this 'magic angle' by folding an A4 paper across the diagonal. When the sample is spun at this magic angle, the dipolar coupling becomes time-dependant, which can be described by a fourier series,

$$D(t) = \sum_k d_k e^{ik\omega_r t} \tag{1.33}$$

where $k = \pm 1, \pm 2$, and

$$d_{\pm 1} = -\frac{\gamma_I \gamma_S \hbar}{4r^3}\sqrt{2}\sin(2\beta)e^{\pm i\gamma} \tag{1.34}$$

$$d_{\pm 2} = -\frac{\gamma_I \gamma_S \hbar}{4r^3}\sqrt{2}\sin^2\beta e^{\pm 2i\gamma}. \tag{1.35}$$

From Eq.1.33, it is clear that the dipolar coupling appears at certain integer of its fourier components and is said to be modulated by MAS.

At the early onset of MAS discovery, spinning frequency of 1-2 kHz was already very remarkable. With the advancement of MAS engineering, smaller and smaller diameter rotor which improves the spinning speed were made available. It was during the 90's, when 15-20 kHz of spinning modules were commercially available, there was a surge of application in solid-state NMR to observe rare-spins such as ^{13}C. At this spinning speed, CSA and heteronuclear couplings between ^{13}C-^{1}H is basically well-removed, and therefore, high resolution spectroscopy of ^{13}C can be achieved. This fast MAS actually came in conflict with the idea of cross polarization and will be explained further in the following chapter (refer to Fig.

2.1). Today, spinning of up to 90 kHz is made possible by Ago Samoson in Estonia. Wide range of application such as using very-fast MAS (VFMAS) to observe polycrystallines highly paramagnetics organic sample. Among the early work was by Ishii [48, 54, 55, 56], who defined VFMAS as somewhere between 20-40 kHz. At this spinning speed ^{13}C-^{1}H and ^{1}H-^{1}H dipole-dipole couplings are removed, and thereby producing high resolution spectra. Our idea of cross-polarization techniques was used in combination with VFMAS as presented in chapter 6.

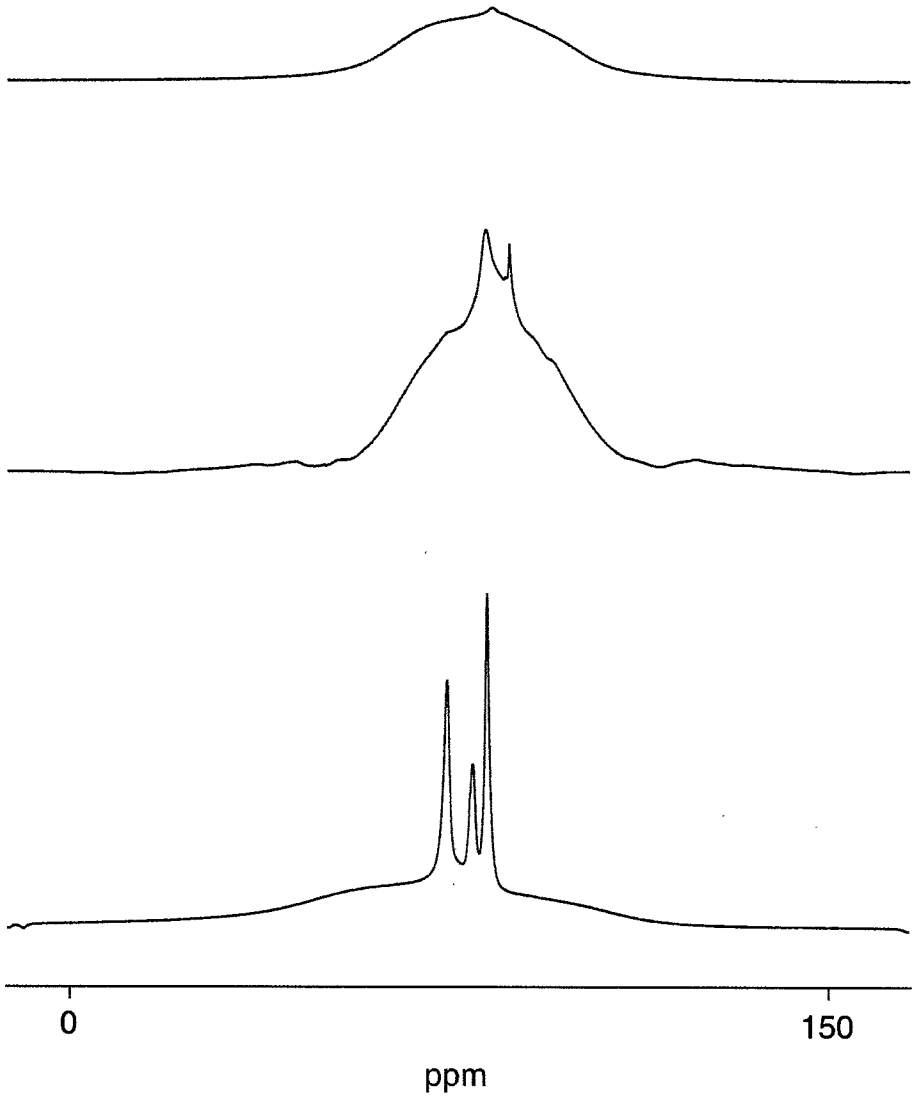

Figure 1.8: ^{1}H polycrystalline L-alanine spectrum showing the effect of MAS on the spectral resolution and its sensitivity. When the sample is observed at static (top) condition, the spectra is broad and featureless, strongly dominated by anisotropic interaction and direct dipole-dipole coupling. When the spinning speed is increased to 18 kHz (middle), overlapping peaks appear but poorly resolved, revealing that anisotropic interactions has not been completely removed. When VFMAS of 35 kHz (bottom) spinning speed was applied, anisotropic interactions as well as homonuclear proton couplings were well-removed, thereby producing distinguishable isotropic peaks.

1.5.4 Decoupling

In order to eliminate broadening of resonance lines of rare S spins due to heteronuclear dipolar interactions with abundant I spins, high power continuous wave irradiation near the Larmor frequency of I spins can be applied. The efficiency of such heteronuclear decoupling can be improved with suitable phase modulation such as the one shown by Two Pulse Phase Modulation (TPPM) [13] and many other advance techniques [14, 15, 16, 17]. Removal of homonuclear dipolar coupling can be achieved by averaging the spin space with application of pulse such as Lee-Goldburg (LG) irradiation [18], Combined Rotation And Multiple-Pulse Spectroscopy (CRAMPS) [19] and multiple pulse [20, 21] techniques.

1.5.5 High static development and its implication

One straight-forward but expensive way to improve the resolution is to increase the static field. Over the years, the trend to employ high static field had been obvious.

1962	fisrt superconducting magnet Varian 220 MHz
1973	360 MHz superconducting NMR spectrometer by Bruker
1987	600 MHz magnet by Varian, Bruker, Oxford Instruments
2006	950 MHz actively shielded Bruker magnet

As NMR spectrometer is designed to operate at higher magnetic fields, the issues of uniform excitation or uniform spin inversion became relevant. Broadband polarization transfer, broadband decoupling, and isotropic mixing faced severe challenges as the hard-pulse technique is appproaching the limit. When the chemical shift dispersion is increased, the matching the Hartmann-Hahn condition of each isotropic chemical shift is split over a large offset. Therefore, simultenously satisfying all Hartmann-Hahn conditions over a large chemical shift dispersion by means of hard-pulse becoming an uphill task if not impossible. We will see later how high field came into conflict with cross polarization and how we had improved CP schemes (Chpater 4 and Chapter 5) to cater for this problem.

2 Cross Polarization and Contemporary works

2.1 Evolution of Cross Polarization

The first idea of double resonance was first demonstrated by Hartmann-Hahn [9] in 1962, it was then followed by work of proton-enhanced rare spins observation by Alex Pines [10] in 1972. This original CP technique [10] (Fig. 1.6), employs a $\frac{\pi}{2}$ pulse at I spins followed by simultaneous continuous-wave (CW) irradiations at I spins and S spins so that the Hartmann-Hahn condition is satisifed. The matching profile is broad (refer to Fig. 2.1(a)) and the half-width at half height is roughly defined by the magnitude of the homonuclear $I - I$ couplings or heteronuclear $I - S$ couplings, whichever is larger. Therefore, so as long as the mismatching is much smaller than those couplings, polarization transfer is still possible, albeit at the expense of decreased transfered magnetization. Three years later, CP combined with slow magic angle spinning (MAS) [11, 12], known as CPMAS, was first demonstrated by Schaefer [22]. Since the spinning speed of a few kHz, which is less than the typical dipolar linewidth, polarization transfer with CP is still viable. It has then became one of the most successful methodologies in solid-state NMR, and is utilized to investigate static structure and dynamics of solid materials.

Since 1990s, eversince fast MAS (10-20 kHz) is commercially available, a lot of modifications to the pulse sequence have been proposed to improve the efficiency of polarization transfer. For example, under high speed MAS [11, 12, 23, 24, 25], the Hartmann-Hahn matching profile splits into sidebands (refer to Fig. 2.1(b)). As a result, efficiency of the polarization transfer becomes sensitive to the mismatch of the rf amplitudes. In order to make transfer robust against the mismatch, a number of techniques [26, 27, 28, 29, 30, 31, 32, 33] have been proposed which employ modulation of rf amplitude or frequency during the contact time. They include Amplitude-Modulated Cross Polarization (AMCP) [26], Adiabatic Passage through the Hartmann-Hahn condition (APHH) [27, 28, 29], Amplitude-Modulated Adiabatic Passage Cross Polarization (AMAP-CP) [30], Ramped-Amplitude Cross Polarization (RAMP-CP) [31], Hartmann-Hahn matching via adiabatic frequency sweep (FSCP) [32], sinusoidally frequency-modulated Cross Polarization [33] (Fig. 2.3), and so forth. Since the magnitude of the effec-

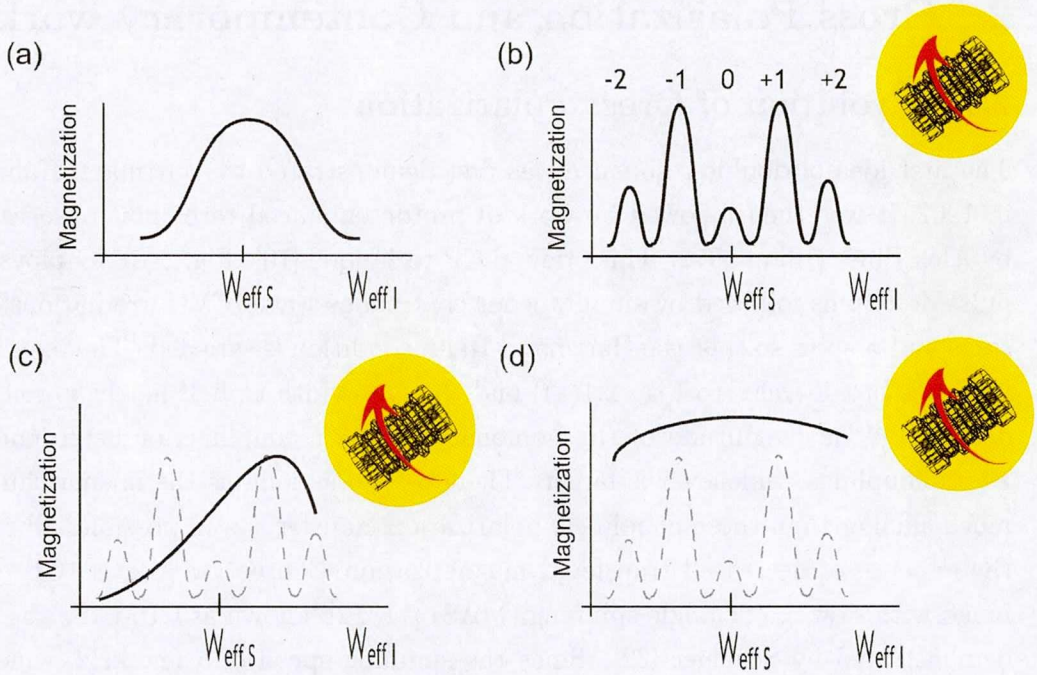

Figure 2.1: Broad Hartmann-Hahn matching profile for (a) static sample. Matching profile splitted into narrow sidebands under fast MAS application measured with (b) simultaneous CW irradiation, (c) single frequency/amplitude channel schemes and (d) SADIS CP.

tive field in the rotating frame changes in time, the Hartmann-Hahn condition can be made to be fulfilled on the way during the contact time.

Another viewpoint for improving the CP performance has recently been put forth, in which the efficiency of spin-locking is enhanced while the favorable properties of the modulation schemes are still retained. In the proposed technique, referred to as Nuclear Integrated Cross Polarization (NICP) [1] (Fig. 2.4), the initial $\frac{\pi}{2}$ pulse on the I spin is removed, and the frequency of the I channel is adiabatically swept from far-off resonance toward on-resonance. The far-off to on-resonance frequency sweep serves the following two purposes. (i) Even in the presence of considerable spectral distribution due to chemical shift or dipolar line broadening, the I spin packets follow, i.e., locked along the effective field, which is initially pointing in the z direction and gradually tilted toward the xy plane.

Since it is the locked components of the I spin packets that participate in polarization transfer, this approach leads to increase in the enhancement factor when available/tolerable rf power is not large enough to flip the entire spin packets with the $\frac{\pi}{2}$ pulse in the previous CP techniques. (ii) The magnitude of the effective field takes the maximum value at the beginning of the sweep and decreases gradually. Thus, transfer is expected to be insensitive to rf-mismatch as shown in Fig. 2.1(c).

These techniques (except NICP) were initially proposed during the 90's to compensate for the effect of rf-mismatching due to application of fast MAS. Here on, I would like to refer all these schemes [1, 26, 27, 28, 29, 30, 31, 32, 33] as Single Amplitude/Frequency modulated schemes (SAF). As amplitude/frequency modulation on single channel, which were then thought to be sufficient to compensate for the rf-mismatching due to fast MAS, not much attention were paid to the effect of fast relaxation effect and huge spectral broadening which may occur in both the source and target spins such as in paramagnetic sample.

In 2007, we presented another novel scheme by employing adiabatic frequency sweeping simultaneously on both the source and target spins, which we call Simultaneous ADIabatic Spin-locking Cross Polarization (SADIS CP) [2] (Fig. 2.4). Unlike any other SAF schemes that had been proposed till then, there had been much controversies and doubts over the role of employing an additional frequency sweep, due to introduction of another sine factor in the magnitude effective dipolar coupling. Its coefficient is known as the scaling factor. This issue was then clarified (Chapter 5), when we clearly shown the effect of speeding up the polarization transfer by switching on the additional frequency sweep (which is SADIS CP) and switching off (which correspond to NICP), whereby the 'time-dependant Hartmann-Hahn mismatching effect' outweigth the 'dipolar coupling scaling factor effect'. To my knowledge, we are the first group to show that polarization transfer over a large bandwidth can be speeded up by reducing the time-dependant Hartmann-Hahn mismatching throughout the whole contact time.

Here, we summarize the advantageous of SADIS CP as compared to NICP, which represents the SAF family. (i) Simultanoeus sweep reduces the amount

of Hartmann-Hahn offset throughout the whole sequence as compared to that in NICP, therefore allowing faster polarization transfer. (ii) Offset irradiation leads to higher effective field. The higher effective field, in general, results in a longer spin-lattice relaxation time in the rotating frame. The property that the effective field is initially the largest is particularly attractive, because both the I and S magnetization can be well kept during the sequence. Offset assisted power reduction is also attractive for application to power lossy biological samples [34]. (iii) The favorable properties of NICP mentioned above are retained in this new approach. Besides being succesfully demonstrated in diamagnetic (L-Alanine) sample, SADIS CP was also shown to work remarkably well in paramagnetic sample (Cu(II)(D,L-Alanine)$_2$.H_2.O) [3].

Figure 2.2: Historical development CP schemes and its compatibility.

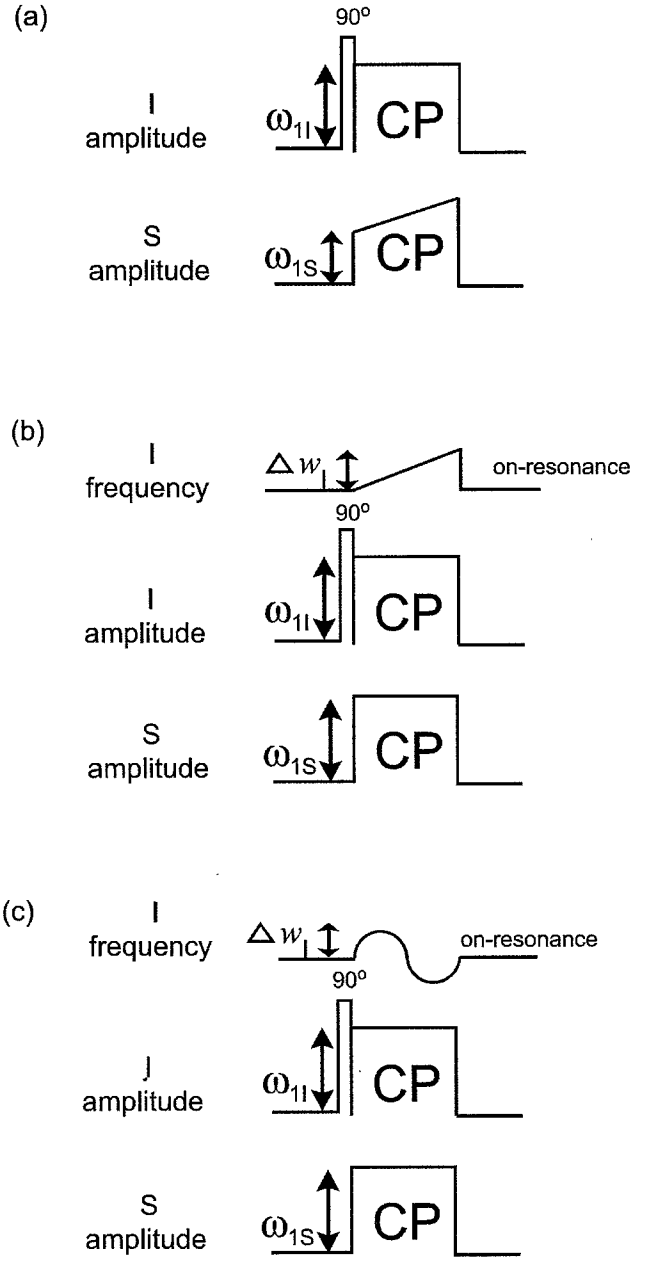

Figure 2.3: (a) Pulse sequence for RAMP CP, (b) FSCP and (c) sine-modulated CP.

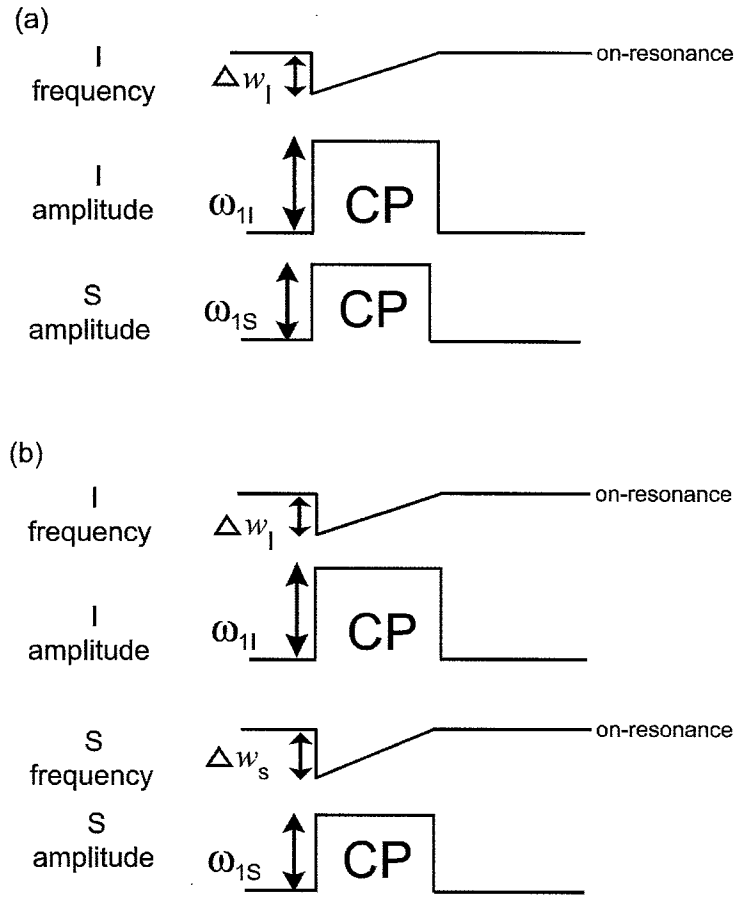

Figure 2.4: Our proposed pulse sequences (a) NICP, and (b) SADIS CP

Part II

Theoretical and Simulation Results

3 Spin-dynamics of Interacting Spins and Polarization Transfer under the influence of Adiabatic Amplitude/Frequency Sweep

Abstract

In this section, a general formalism of the spin dynamics of two interacting spins, or known as the Rabi oscillation, which serves as the fundamental of understanding simple polarization transfer, is described. This general theoretical framework is suitable under circumstances such as (a) static or sample spinning, (b) single crystal or polycrystalline, and (c) time dependent (or independent) amplitude and/or frequency modulation.

3.1 Isolated IS-spin model

Let us consider an isolated heteronuclear spin pair $I = \frac{1}{2}$ and $S = \frac{1}{2}$ and suppose that linear frequency sweeps are applied simultaneously to the I and S spins under rf irradiations with intensities ω_{1I} and ω_{1S}, respectively. For simplicity, homonuclear dipolar interactions among the abundant protons are neglected. This assumption will be justified in the following chapter 4 and chapter 5. We write the rotating-frame Hamiltonian as

$$H = -(\Delta\Omega_I(t) + \Omega_I)I_z - \omega_{1I}I_x - (\Delta\Omega_S(t) + \Omega_S)S_z - \omega_{1S}S_x + D(t)I_zS_z. \quad (3.1)$$

Here, Ω_I and Ω_S are the isotropic chemical shifts for I and S. $D(t)$ is the magnitude of the dipolar interaction between them, which is modulated by MAS and is given by

$$D(t) = d_{IS}[G_1 \cos(w_r t) + G_2 \cos(2w_r t)] \tag{3.2}$$

where w_r is the spinning frequency and G_k (k = 1,2) depends on the orientation of the internuclear vector in a reference frame fixed to the rotor. d_{IS} is the dipolar coupling constant. In the pulse sequence of SADIS CP as depicted in Fig. 3.1(c), the frequency-offset terms $\Delta\Omega_I$ and $\Delta\Omega_S$ change in time according to

$$\Delta\Omega_\epsilon(t) = -\Delta\omega_\epsilon(1 - \frac{t}{T}) \tag{3.3}$$

where $\epsilon = I$ or S, T is the period of frequency sweep, and $\Delta\omega_\epsilon$ is the frequency sweep width. Note that the special case of SADIS CP in which $\Delta\omega_S = 0$ (no frequency sweep on the S channel) corresponds to the NICP sequence described in Fig. 3.1(b). The implication of such doing such modulation, which is the key point to this work, will be discussed in details in the later section.

We assume that the rate of frequency sweep is slow enough for both I and S and consider the doubly tilted rotating frame in which the effective fields for both spins point in the z axis. When the adiabatic conditions are met, transformation from the rotating frame into the doubly tilted rotating frame does not have significant effects on the density matrix, whereas the Hamiltonian H^{TR} in this new frame is given by

$$H^{\mathrm{TR}} = H_Z + H_D, \tag{3.4}$$

where

$$H_Z = \omega_{eI}(t) I_z + \omega_{eS}(t) S_z \tag{3.5}$$

$$H_D = D(t)[I_z \cos(\alpha_I(t)) + I_x \sin(\alpha_I(t))][S_z \cos(\alpha_S(t)) + S_x \sin(\alpha_S(t))], \tag{3.6}$$

with

$$\omega_{e\epsilon}^2(t) = \omega_{1\epsilon}^2 + (\Delta\Omega_\epsilon(t) + \Omega_\epsilon)^2, \tag{3.7}$$

and

$$\alpha_\epsilon(t) = \tan^{-1} \frac{\omega_{1\epsilon}(t)}{\Delta\Omega_\epsilon(t) + \Omega_\epsilon}. \tag{3.8}$$

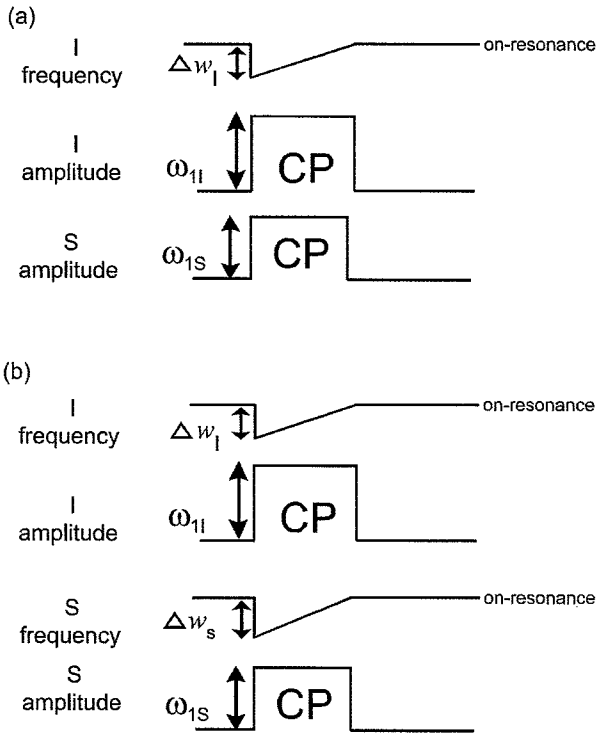

Figure 3.1: Pulse sequence for (a) NICP, and (b) SADIS CP.

The evolution of the system is governed by the propagator $U(t)$ given by

$$U(t) = T\exp\left[\int_0^t dt' H^{\mathrm{TR}}\right] = U_0(t)U_1(t), \tag{3.9}$$

where

$$U_0(t) = T\exp\left[\int_0^t dt' H_Z\right], \tag{3.10}$$

$$U_1(t) = T\exp\left[\int_0^t dt' \widetilde{H}_D\right], \tag{3.11}$$

with

$$\widetilde{H}_D = U_0^{-1}(t)H_D U_0(t) \tag{3.12}$$

$$= D(t)[S_z\cos(\alpha_S(t)) + (S_x\cos(\omega_{eS}t) - S_y\sin(\omega_{eS}t))\sin(\alpha_S(t))]$$
$$\times[I_z\cos(\alpha_I(t)) + (I_x\cos(w_{eI}t) - I_y\sin(w_{eI}t))\sin(\alpha_I(t))]. \tag{3.13}$$

When the time-dependent Hartmann-Hahn condition

$$\Delta_{\mathrm{HH}}(t) \equiv \omega_{eI}(t) - \omega_{eS}(t) - nw_r = 0, (n = -2, -1, 1, 2) \tag{3.14}$$

is satisfied, interference between the spatial and spin parts in $\widetilde{H}_D$ leads to the non-vanishing average Hamiltonian

$$\overline{\widetilde{H}}_D = \frac{1}{8} d_{IS} G_n \sin\alpha_I(t) \sin\alpha_S(t) (I_+ S_- + I_- S_+). \tag{3.15}$$

In order to discuss the exchange of the spin states between I and S, we focus only on the zero-quantum (ZQ) subspace spanned by states $|+-\rangle$ and $|-+\rangle$, in which the secular Hamiltonian H^{ZQ} is represented by

$$H^{\mathrm{ZQ}} = 2\Delta_{\mathrm{HH}}(t) I_z^{\mathrm{ZQ}} + \frac{1}{4} D_{\mathrm{eff}}(t) I_x^{\mathrm{ZQ}}, \tag{3.16}$$

where $D_{\mathrm{eff}}(t)$, which we call the effective dipolar frequency, is given by

$$D_{\mathrm{eff}}(t) = d_{IS} G_n \sin\alpha_I(t) \sin\alpha_S(t), \tag{3.17}$$

and I_z^{ZQ} and I_x^{ZQ} are the ZQ fictitious spin-$\frac{1}{2}$ operators given by

$$I_z^{\mathrm{ZQ}} = \frac{1}{2} [|+-\rangle\langle+-| - |-+\rangle\langle-+|], \tag{3.18}$$

$$I_x^{\mathrm{ZQ}} = \frac{1}{2} [|+-\rangle\langle-+| + |-+\rangle\langle+-|]. \tag{3.19}$$

We assume that initially the state $|+-\rangle$ is idempotently populated, so that the ZQ density matrix $\rho^{\mathrm{ZQ}}(t=0)$ is

$$\rho^{\mathrm{ZQ}}(t=0) = \begin{pmatrix} 1 & 0 \\ 0 & 0 \end{pmatrix} = \frac{1}{2}\mathbf{1} + I_Z^{\mathrm{ZQ}}. \tag{3.20}$$

When the I and S spins have exchanged their spin states, the density matrix would be

$$\rho^{\mathrm{ZQ}}(t=ct) = \begin{pmatrix} 0 & 0 \\ 0 & 1 \end{pmatrix} = \frac{1}{2}1 - I_Z^{\mathrm{ZQ}}. \tag{3.21}$$

Hence, the transverse magnetization $< S_x >$ of the S spin is correlated with $< I_Z^{ZQ} >$ through

$$< S_x > (t) = \frac{1}{2} - < I_Z^{\mathrm{ZQ}} > \tag{3.22}$$

$$= \frac{1}{2} - \mathrm{Tr}[I_Z^{\mathrm{ZQ}} \rho^{\mathrm{ZQ}}(t)]. \tag{3.23}$$

Since the problem has now been reduced to the two-level system, geometric state representation is possible, i.e., a general state ρ^{ZQ} in the ZQ-subspace is given by employing a vector $\mathbf{M}$ as

$$\rho^{\mathrm{ZQ}}(t) = \mathrm{M}_x(t) I_x^{\mathrm{ZQ}} + \mathrm{M}_y(t) I_y^{\mathrm{ZQ}} + \mathrm{M}_z(t) I_z^{\mathrm{ZQ}}, \tag{3.24}$$

and the dynamics of $\mathbf{M}$ is governed by the Bloch equation [35]

$$\frac{d}{dt}\mathbf{M} = \mathbf{M} \times \omega_{\mathrm{eff}}^{\mathrm{ZQ}}, \tag{3.25}$$

where $\boldsymbol{\omega}_{\mathrm{eff}}^{\mathrm{ZQ}}$ is the vector of effective field in the ZQ-subspace which is represented by

$$\boldsymbol{\omega}_{\mathrm{eff}}^{\mathrm{ZQ}} = \begin{pmatrix} (\omega_{\mathrm{eff}}^{\mathrm{ZQ}})_x \\ (\omega_{\mathrm{eff}}^{\mathrm{ZQ}})_y \\ (\omega_{\mathrm{eff}}^{\mathrm{ZQ}})_z \end{pmatrix} = \begin{pmatrix} \frac{1}{4} D_{\mathrm{eff}}(t) \\ 0 \\ 2\Delta_{\mathrm{HH}}(t) \end{pmatrix}. \tag{3.26}$$

Substituting Eq.(3.26) into Eq.(3.25), we arrive at

$$\frac{d}{dt} \begin{pmatrix} M_x \\ M_y \\ M_z \end{pmatrix} = \begin{pmatrix} 2\Delta_{\mathrm{HH}}(t) M_y \\ \frac{1}{4} D_{\mathrm{eff}}(t) M_z - 2\Delta_{\mathrm{HH}}(t) M_x \\ -\frac{1}{4} D_{\mathrm{eff}}(t) M_y \end{pmatrix}. \tag{3.27}$$

3.2 Adiabatic inversion in ZQ subspace in NICP

In this section, we show that adiabatic inversion of 2-spin system in ZQ-subspace is similar to single spin adiabatic inversion in conventional rotating frame. Here we pick NICP as an example. We have $\sin\alpha_S(t)= 1$, since CW irradiation is applied to carbon channel. Dropping the nonsecular terms, we express the zero-quantum Hamiltonian H^{ZQ} as

$$H^{\mathrm{ZQ}} = \begin{pmatrix} \Delta(t) - n\omega_r & \frac{1}{8}d_{IS}G_n \sin\alpha_I \\ \frac{1}{8}d_{IS}G_n \sin\alpha_I & -\Delta(t) + n\omega_r \end{pmatrix} \tag{3.28}$$

$$= 2(\Delta(t) - n\omega_r)I_z^{\mathrm{ZQ}} + \frac{1}{4}d_{IS}G_n \sin\alpha_I I_x^{\mathrm{ZQ}}. \tag{3.29}$$

According to the vector representation scheme for a general two-level system [36], H^{ZQ} gives the "effective field", $\boldsymbol{\omega}_{\mathrm{eff}}^{\mathrm{ZQ}} = (\frac{1}{4}d_{IS}G_n \sin\alpha_I, 0, 2(\Delta(t) - n\omega_r))$ in the ZQ subspace. Fig. 3.2 (a) and (b) describe how $(\omega_{\mathrm{eff}}^{\mathrm{ZQ}})_z$ and $(\omega_{\mathrm{eff}}^{\mathrm{ZQ}})_x$ change in time during NICP for $\omega_{1I}/2\pi = 35$ kHz, $\omega_{1S}/2\pi = 45$ kHz, $\Delta\omega_I/2\pi = 100$ kHz, and $\tau = 7.2$ ms. For simplicity, we assumed here that $\omega_r = 0$ and chose a IS dipolar interaction (40 kHz) arbitrarily.

As is found in Fig. 3.2 (c) or (d), the trajectory of the effective field in the ZQ subspace during NICP is reminiscent to that in the conventional rotating frame under a passage from far above-resonance to below-resonance. By an analogy with the conventional adiabatic inversion, one can also expect that the "inversion" takes place in the ZQ subspace, if the change of the ZQ effective field in time is sufficiently slow. The condition for the slow passage, which may be referred to as the adiabatic condition in the ZQ subspace, can be derived in the same manner as in the case of the conventional adiabatic condition [38], as follows. Using a general formula for vector kinetics, change of $\boldsymbol{\omega}_{\mathrm{eff}}^{\mathrm{ZQ}}$ in time is described by

$$\frac{d}{dt}\boldsymbol{\omega}_{\mathrm{eff}}^{\mathrm{ZQ}} = \boldsymbol{\Omega} \times \boldsymbol{\omega}_{\mathrm{eff}}^{\mathrm{ZQ}} + \Omega_1 \boldsymbol{\omega}_{\mathrm{eff}}^{\mathrm{ZQ}}, \tag{3.30}$$

where the vector $\boldsymbol{\Omega}$ and the scalar Ω_1 have dimension of frequency. Since $(\omega_{\mathrm{eff}}^{\mathrm{ZQ}})_y = 0$ in the present case, the only non-vanishing component of $\boldsymbol{\Omega}$ is Ω_y, whose expres-

sion is obtained from Eq. (3.30) as

$$\Omega_y = \frac{d_{IS}G_n}{2(\omega_{\text{eff}}^{\text{ZQ}})^2}\left[\Delta(t)\dot{\alpha}\cos\alpha - \dot{\Delta}(t)\sin\alpha\right]. \tag{3.31}$$

The adiabatic condition is satisfied when Ω_y has a negligible Fourier component at the frequency $\omega_{\text{eff}}^{\text{ZQ}}$, or $\Omega_y \ll \omega_{\text{eff}}^{\text{ZQ}}$. That is, if

$$\frac{d_{IS}G_n}{2}\left[\Delta(t)\dot{\alpha}(t)\cos\alpha - \dot{\Delta}(t)\sin\alpha\right] \ll \left(\omega_{\text{eff}}^{\text{ZQ}}\right)^3 \tag{3.32}$$

is satisfied, NICP causes inversion in the ZQ subspace. Since inversion in the ZQ subspace is equivalent to swap of populations between the states $|+-\rangle\langle+-|$ and $|-+\rangle\langle-+|$, polarization transfer is shown to take place by NICP.

If the two-spin system is well isolated, the adiabatic inversion in the ZQ subspace causes complete exchange of spin polarizations between I and S, when only a single sideband of the Hartmann-Hahn matching profile is swept through. However, if a sweep is performed through multiple sidebands, polarization would be transferred back [28]. The way to avoid such multiple contacts in NICP is to choose ω_{1I} such that $\omega_{1S} + \omega_r < \omega_{1I} < \omega_{1S} + 2\omega_r$.

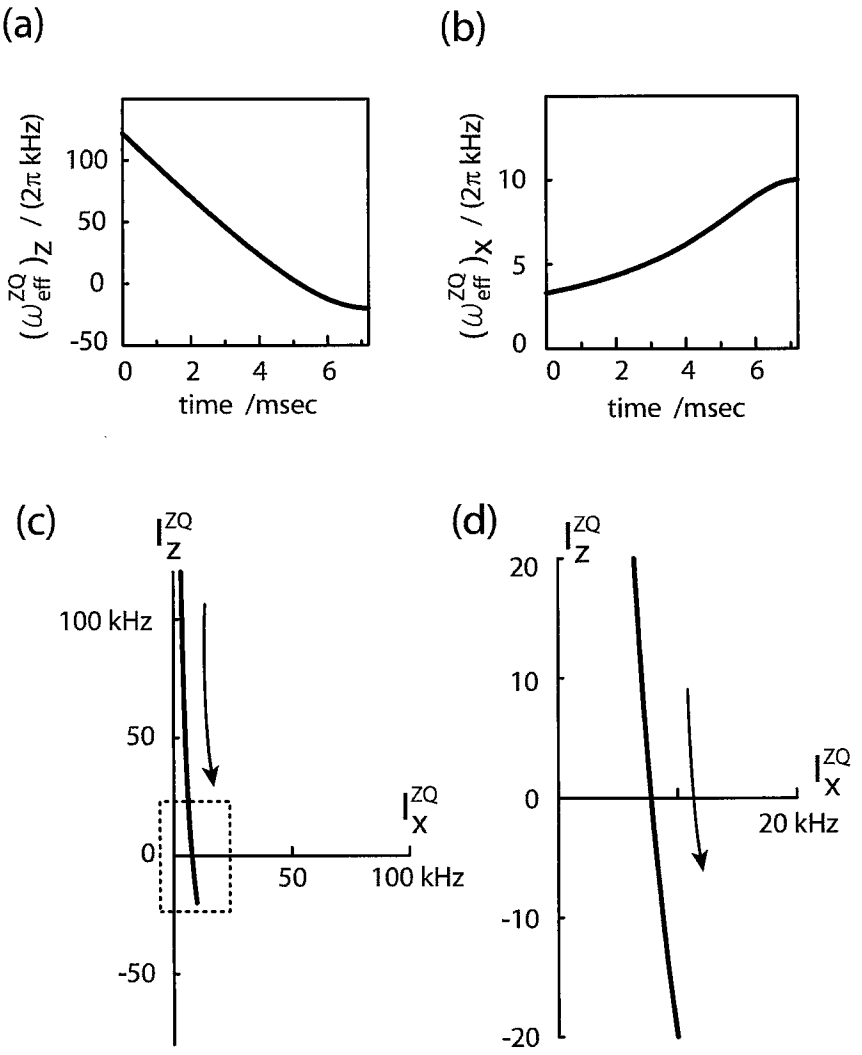

Figure 3.2: (a)(b) Calculated z and x components of the ZQ effective field $\omega_{\text{eff}}^{\text{ZQ}}$ for $\omega_{1I}/2\pi = 35$ kHz, $\omega_{1S}/2\pi = 45$kHz, $\Delta_I/2\pi = 100$ kHz, and $\tau = 7.2$ ms. For simplicity, $\omega_r = 0$ was assumed and an arbitrary IS dipolar interaction (40 kHz) was chosen. The trajectory of the effective field in the ZQ subspace, shown in (c), gives a crude but visual account for exchange of the spin states and thereby transfer of polarization, in analogy with the inversion of magnetization in the rotating frame by a passage from above to below resonance. (d) is an expanded view of the region indicated by a dotted square in (c).

3.3 Polarization buildup and Rabi oscillation

3.3.1 CW irradiation on source and target spins

When cw-irradiation (without any frequency sweep) is applied on both the channels, which is the pulse sequence for Conventional Cross Polarization [10] (Fig. 1.6), the two-spin system interaction for a single crystallite shows a 'normal' Rabi oscillation, where the frequency of the oscillation corresponds to the dipolar coupling frequency of the two spins. In such transfer, the magnitude of dipolar frequency remains constant throughout the whole contact time. Note that, the dipolar coupling constant, $\frac{d_{IS}}{2\pi} = \frac{1}{2\pi}\frac{\mu_o\gamma_I\gamma_S\hbar}{4\pi r^3}$ (in unit Hz), while the secular dipolar frequency $d = \frac{1}{2\pi}\frac{\mu_o\gamma_I\gamma_S\hbar}{4\pi r^3}(3\cos^2\theta - 1)$, is a function of angle orientation. For example, if the $\frac{d_{IS}}{2\pi} = 4.5$ kHz, then the dipolar frequency is $d(\theta = 0) = \frac{d_{IS}}{2\pi}(3\cos^2 0 - 1) =$ 4.5 kHz $\times 2 =$ 9 kHz and the period for one oscillation is $t = \frac{1}{d(\theta=0)} = 0.11$ ms (Fig. 3.3).

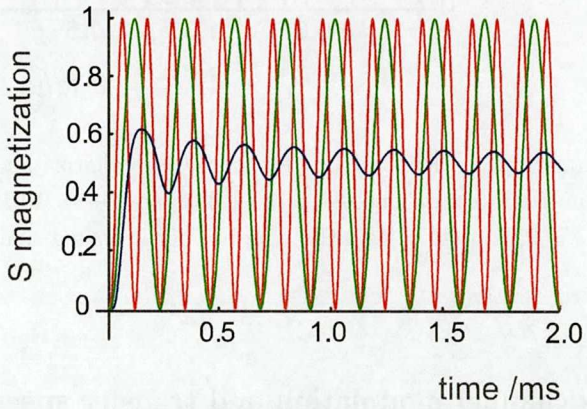

Figure 3.3: Numerical calculated (refer to Appendix A) buildup curves for CW irradiation on both channels with frequency sweeps switched off on both channels. The dipolar coupling constant, $\frac{d_{IS}}{2\pi} = 4.5$ kHz for two different crystallite orientations, (i) $\theta = 0$ (red line), and (ii) $\theta = \pi/2$ (green line) were shown. Hartmann-Hahn matching parameters were $\frac{\omega_{1S}}{2\pi} = 35$ kHz, $\frac{\omega_{1I}}{2\pi} = 35$ kHz, for a contact time, $T = 2$ ms. The powder-averaged signal is shown in (blue line).

As for the case of powder sample, the signal intensity, is the weighted-sum signal contributed by each crystallite distributed over theta angle of 0 to π (Fig. 3.3). The

maximun polarization transfer is approximately 0.6, achieved at a time approximately $\frac{1}{2d(\theta=\frac{\pi}{2})}$, and then the polarization transfer settle down to an equilibrium-exchange between the two spins. If the polarization transfer (Fig. 3.4) were set to occur at a mismatched Hartmann-Hahn condition for e.g. $\frac{\omega_{1S}}{2\pi}$ = 35 kHz and $\frac{\omega_{1I}}{2\pi}$ = 10 kHz, the maximun magnetization transfer will be less than 1. The intensity will drops approximately according to a gaussian function, as shown in Fig. 2.1(a), as the Hartmann-Hahn matching condition is departed.

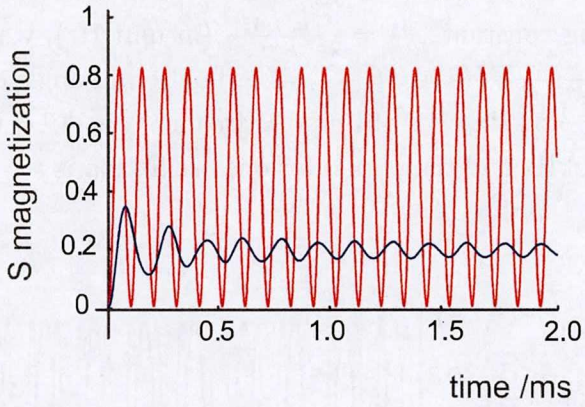

Figure 3.4: Numerically calculated buildup curve for polarization transfer occur at a mismatched Hartmann-Hahn condition, $\frac{\omega_{1S}}{2\pi}$ = 35 kHz, and $\frac{\omega_{1I}}{2\pi}$ = 10 kHz (red line). The other parameters were $\theta = 0$, and $\frac{d_{IS}}{2\pi}$ = 4.5 kHz. The powder-averaged signal is shown in (blue line).

3.3.2 Single channel modulation and transfer speed

In this section, we compare the transfer speed for the case when the amplitude-modulation on one of the channel is carried-out, a pulse sequence known as RAMP CP. RAMP CP is usually used to relax the Hartmann-Hahn mismatching in the case of sample spinning or when there is a large distribution of chemical shifts. Two variations of RAMP CP, partial-RAMP CP and full-RAMP CP as shown in Fig. 3.5 were analyzed. As revealed in Fig. 3.5(c) and Fig. 3.5(d), the Δ_{HH} for full-RAMP CP is much larger than partial-RAMP CP.

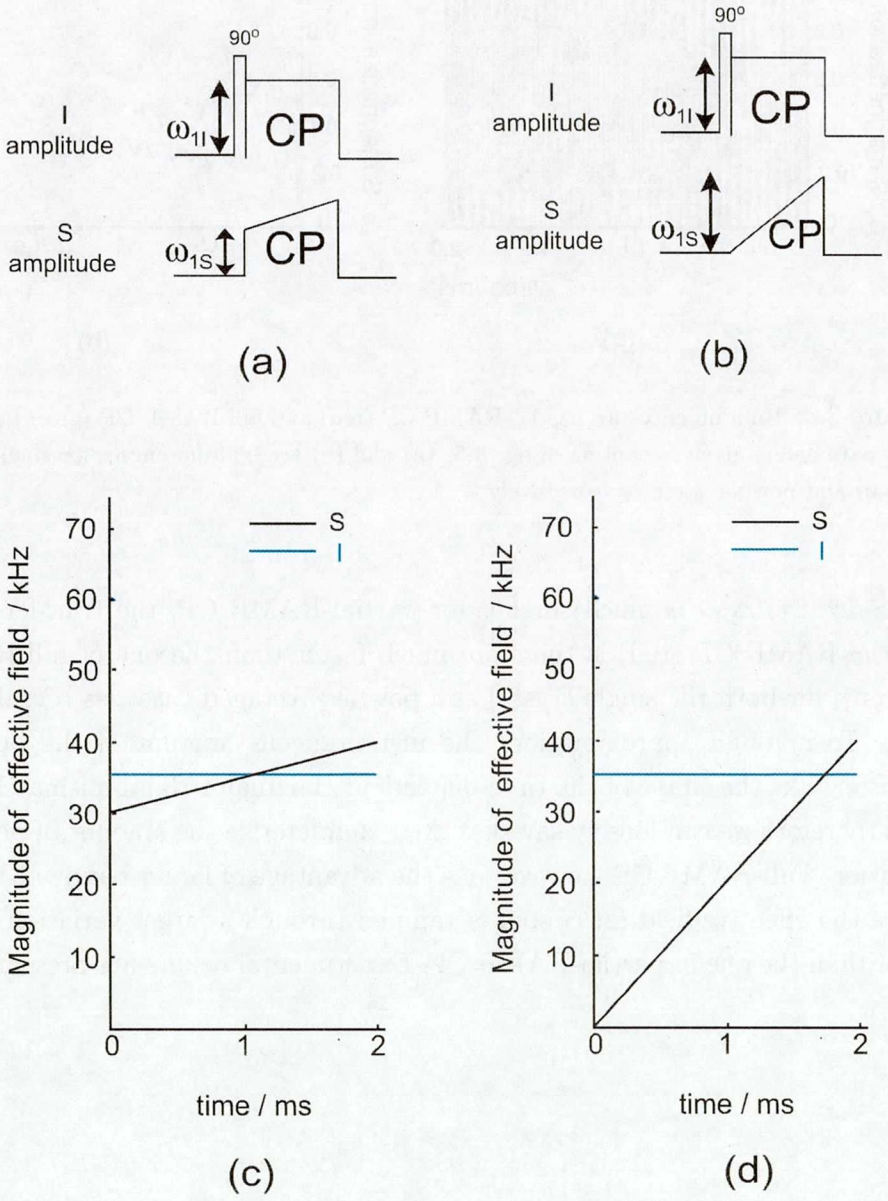

Figure 3.5: Pulse sequence for (a) partial-RAMP CP, and (b) full-RAMP CP. (c) and (d) are the time-dependent of the effective field for I and S spins for (a) and (b), respectively. For partial-RAMP CP ($\frac{\omega_{1S}}{2\pi} = 30 - 40$ kHz), and full-RAMP CP ($\frac{\omega_{1S}}{2\pi} = 0 - 40$ kHz). The other parameters were $\frac{\omega_{1I}}{2\pi} = 35$ kHz, T= 2 ms, and $\frac{d_{1S}}{2\pi} = 10$ kHz.

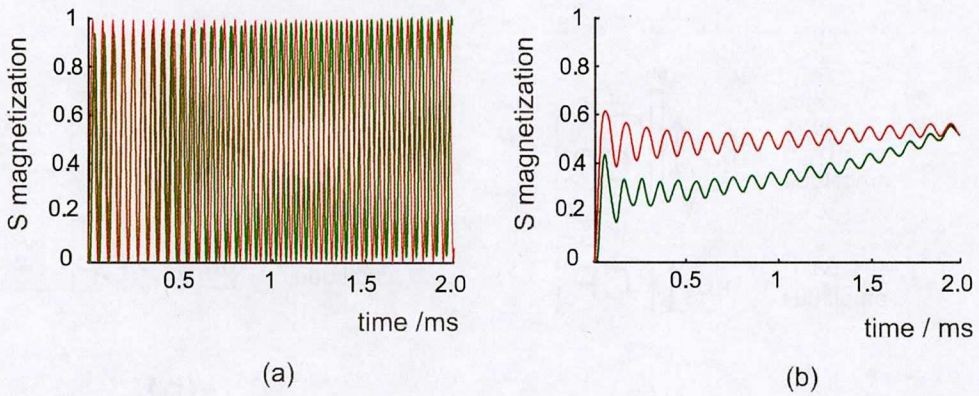

Figure 3.6: Buildup curve for partial-RAMP CP (red) and full-RAMP CP (green) as evaluated with parameters given in caption of fig. 3.5. (a) and (b) are buildup curves for single crystallite ($\theta = 0$) and powder sample, respectively.

Since the Δ_{HH} is much smaller for partial-RAMP CP, the transfer speed for partial-RAMP CP (red) is therefore much faster than the one of full-RAMP CP (green), for both the single crystal and powder-averaged cases, as revealed in Fig. 3.6. To a rough approximation, the instantaneous amount of the polarization transfer take the shape of the time-dependent Hartmann-Hahn mismatching, Δ_{HH} and therefore we can loosely say that Δ_{HH} characterize the amount of polarization transfer. Full-RAMP CP, however has the advantage of larger bandwidth coverage since the effective field for S spin is ramped through a larger variation of magnitude than the one in partial-RAMP CP. Experimental results are presented in Sec. 5.4.

3.3.3 Simultaneous amplitude/frequency modulations: 'Reduced time-dependent Hartmann-Hahn mismatching'

In order to make a simple comparison on transfer efficiencies between SADIS CP and NICP, (refer to Chapter 5 for experimental results) we consider one specific crystallite orientation in a static sample. We also neglect the effect of relaxation here, which will be discussed later. Assuming the initial magnetization $(0, 0, 1)$, we evaluated numerically (Fig. 3.7) the dynamics of the S magnetization for an arbitrarily given set of parameters ($\frac{\omega_{1S}}{2\pi}$= 35 kHz, $\frac{\omega_{1I}}{2\pi}$= 40 kHz, $\frac{\Delta\omega_I}{2\pi}$= 80 kHz, T= 2 ms, and d_{IS}= 45 kHz). The difference between SADIS CP (blue line) and NICP (green line) is the application of the frequency sweep on the S channel, in which $\frac{\Delta\omega_S}{2\pi}$= 90 kHz for SADIS CP while $\frac{\Delta\omega_S}{2\pi}$= 0 kHz for NICP.

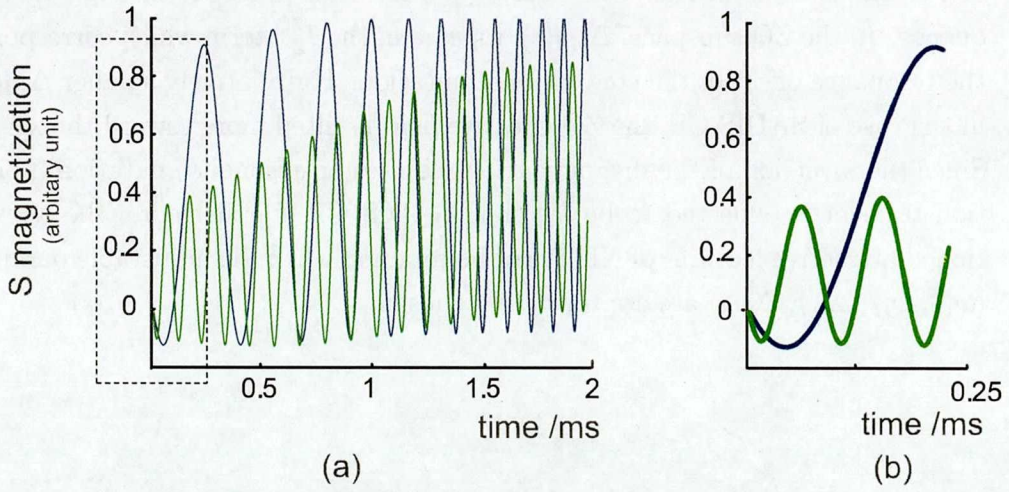

Figure 3.7: (a) Numerically calculated buildup curves for SADIS CP (blue line) and NICP (green line). $\frac{\Delta\omega_S}{2\pi}$ = 90 kHz and $\frac{\Delta\omega_S}{2\pi}$ = 0 were used for SADIS CP and NICP, respectively. Other parameters were $\frac{\omega_{1S}}{2\pi}$ = 35 kHz, $\frac{\omega_{1I}}{2\pi}$ = 35 kHz $\frac{\Delta\omega_I}{2\pi}$ = 80 kHz, and T = 2 ms. (b) a zoom portion for (a) from 0 ms to 0.25 ms.

As shown in Fig. 3.7, the calculated buildup of the S magnetization is faster in SADIS CP than in NICP. Thus, the same amount of S polarization can be achieved with SADIS CP in a relatively shorter period of time as compared to NICP. This feature is particularly attractive for spins with short relaxation times,

where polarization transfer should be as fast as possible before overwhelmed by the effect of relaxation. The oscillation at the $I-S$ dipolar frequency is also visible in the buildup curve. It is worth noting here that the effective dipolar frequency $D_{\rm eff}(t)$ given in Eq.(3.17) is lower in SADIS CP than in NICP by the scaling factor $\sin\alpha_S(t)$. For this reason, NICP shows faster oscillation than SADIS CP, as revealed in Fig. 3.7. In NICP, however, the buildup of the amplitude profile of the oscillation is rather slower because of the larger Hartmann-Hahn offset. In actual situations, this oscillation is expected to be suppressed due to distribution of the $I-S$ dipolar frequency in powder samples, and due to the effect of homonuclear dipolar interactions among the I spins.

The efficient polarization transfer in SADIS CP is ascribed to the smaller time-dependent Hartmann-Hahn offset $\Delta_{\rm HH}$(t) than that in NICP throughout the sequence. In the ZQ subspace, $\Delta_{\rm HH}$(t) appears in the $I_Z^{\rm ZQ}$ term which corresponds to the resonance offset in the conventional nutation. For relatively smaller $\Delta_{\rm HH}$(t) as in the case of SADIS CP, the ZQ effective field is tilted more toward the xy-plane. Since the inversion of the magnetization requires on-resonance nutation, polarization transfer is expected to be faster in SADIS CP. Furthermore, the aforementioned attractive features of NICP can be retained when the adjustable parameters (ω_{1S}, ω_{1I}, $\Delta\omega_I$, $\Delta\omega_S$) are appropriately chosen.

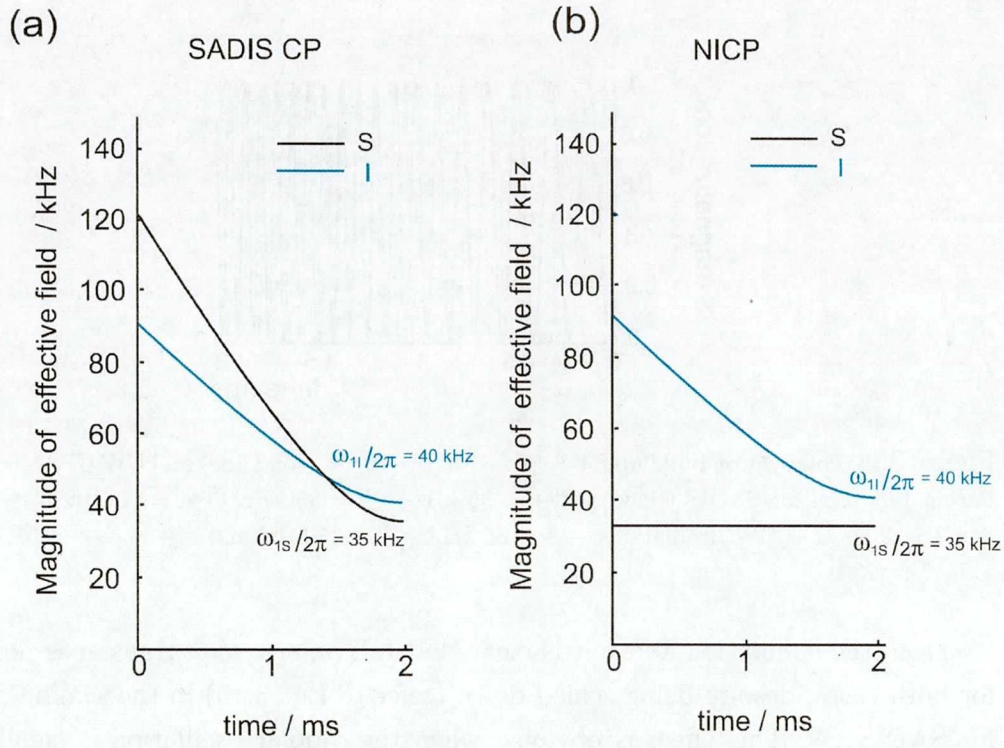

Figure 3.8: Time dependence of the magnitude of the effective field in (a) SADIS CP for the S spin (black lines) and I spin (blue lines) with $T = 2.0$ ms, with $\Omega_S = 0$, $\frac{\omega_{1S}}{2\pi} = 35$ kHz, and $\frac{\Delta\omega_S}{2\pi} = 90$ kHz, $\Omega_I = 0$, $\frac{\Delta\omega_I}{2\pi} = 80$ kHz, and $\frac{\omega_{1I}}{2\pi} = 40$ kHz. (b) Time dependence of the magnitude of the effective field in NICP for the S spin (blue lines) and I spin (black lines). Parameters are the same in (a) except for $\frac{\Delta\omega_S}{2\pi} = 0$.

3.3.4 Buildup for exact matching in SADIS CP

We compare the case where both the frequency modulation functions on I and S spin are set exactly the same in SADIS CP, which resulted in zero for time-dependent Hartmann-Hahn mismatching, and CW irradiation on both channels with exact rf-amplitude matching, as shown in Fig. 3.9.

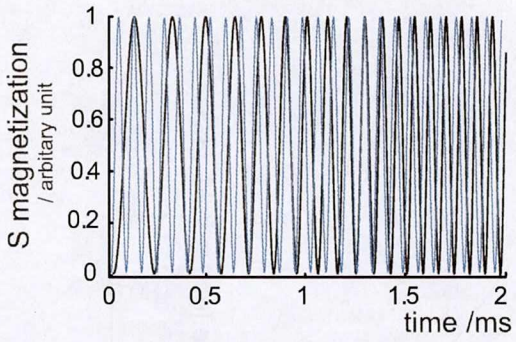

Figure 3.9: Polarization build up for S spin with SADIS CP (solid line) and CW CP (blue line). Parameters used for SADIS CP were $\frac{\omega_{1S}}{2\pi} = 35$ kHz, $\frac{\omega_{1I}}{2\pi} = 35$ kHz, $\frac{\Delta\omega_I}{2\pi} = 80$ kHz, $\frac{\Delta\omega_S}{2\pi} = 80$ and $T = 2$ ms. For CW irradiations, $\frac{\omega_{1S}}{2\pi} = 35$ kHz, $\frac{\omega_{1I}}{2\pi} = 35$ kHz, and $\frac{\Delta\omega_I}{2\pi} = \frac{\Delta\omega_S}{2\pi} = 0$.

From the simulation above it is clear that full polarization transfer is possible for both cases, despite being scaled down (refer to Eq. 3.15) in the scaling factor for SADIS CP. This effect is obvious, when the dipolar oscillation is smaller at the beginning of the transfer (where the initial off-resonance is large) and becames larger as it goes on-resonance. Since the scaling factor for CW-CP is much larger than that of SADIS CP, the transfer has completed within a shorter time-frame. As such, for the case where only a single S spin is present, using CW-CP is sufficient. However, for SADIS CP, since the effective fields were swept across large different values, the probability of Hartmann-Hahn matching over a large bandwidth can be increased. This is not true for the case of CW-CP because both the effective fields remain constant over time.

3.3.5 SADIS CP: Insensitive to large chemical shift offset

For cases like paramagnetic system, where large distribution of chemical shift offsets are present, it is desirable that the transfer do not degrade over chemical shift offset. As shown in Fig. 3.10, for the same magnitude of $\frac{\omega_{1S}}{2\pi}$, application of additional rf-frequencies sweeping (as in the case of SADIS CP), Hartmann-Hahn crossing is still viable for various S spins of chemical shift offset ranging from $\Omega_S = 0$ kHz to $\Omega_S = 300$ kHz. While for RAMP CP, as Hartmann-Hahn crossing did not take place for spins where the chemical shift offset for S spins beyond $\Omega_S = 125$ kHz and as a result, the transfered S intensity dropped over the chemical shift offset distribution as shown in Fig. 3.11.

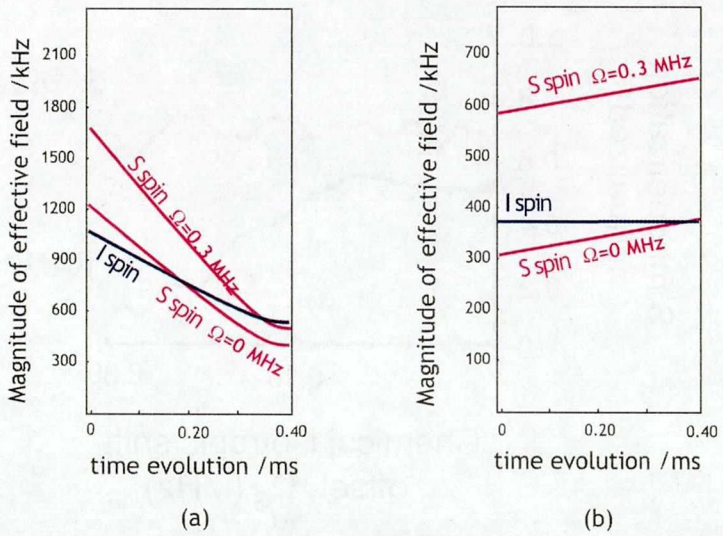

Figure 3.10: Time dependent of the magnitude of the effective field in SADIS CP (left) for the S spin (red lines) and I spin (blue lines) with $T = 0.40$ ms, for $\Omega_S = 0$ and 300 kHz, $\Omega_I = 0$, $\frac{\omega_{1S}}{2\pi} = 350$ kHz, and $\frac{\Delta\omega_S}{2\pi} = 1200$ kHz, $\frac{\omega_{1I}}{2\pi} = 580$ kHz and $\frac{\Delta\omega_I}{2\pi} = 1000$ kHz. (b) Time dependent of the magnitude of the effective field in RAMP CP (right) for the S spin (red lines) and I spin (blue lines). Other parameters were $\frac{\omega_{1S}}{2\pi} = 300 - 350$ kHz, and $\frac{\Delta\omega_S}{2\pi} = 0$ kHz, $\frac{\omega_{1I}}{2\pi} = 340$ kHz and $\frac{\Delta\omega_I}{2\pi} = 0$ kHz.

One interesting feature about SADIS CP is that given an optimal contact time, the maximum magnitude powder-averaged signal goes beyond the transfer bound

achieveable with Conventional CP and RAMP CP. As shown in Fig. 3.3, for CW-CP, at short contact time the maximun amount of possible polarization has surged up to about 0.6, while at longer contact time, the amount of polarization stabilizes and oscillates around 0.5. For RAMP CP, the maximum amount of polarization transfer is 0.5 as shown in Fig. 3.11. With SADIS CP, our simulation result shows that at 400 μs, a transfer of 0.7 can be achieved. As the contact time is further increased a maximum of 1 is possible (results not shown). Intuitively, this shows that the adiabatic component [39, 40] of some of the unfortunate crystallittes are high enough and we can drive its signal orientation to the same direction. Research is currently still under progress.

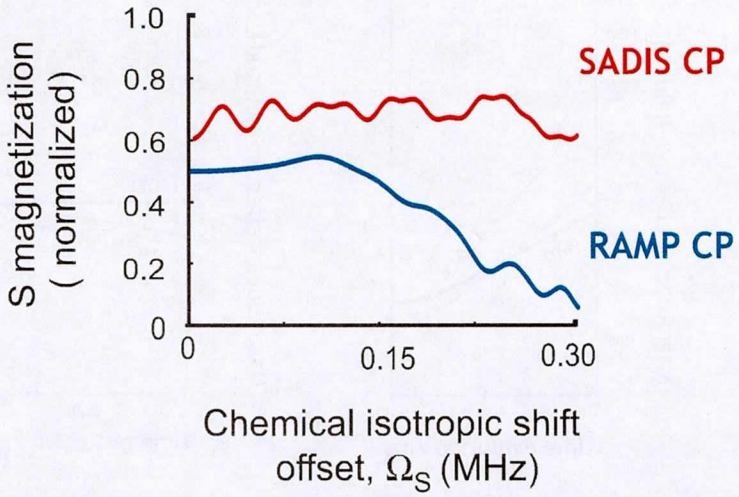

Figure 3.11: Numerically calculated powder-averaged signal intensity of S spins at various chemical isotropic shift offsets, Ω_S with respect to a fixed carrier-frequency, ranging from 0-300 kHz. Carrier-frequency for I channel is assumed to be applied at on-resonance for all cases. Polarization transfer for SADIS CP (red) is almost insensitive over large chemical isotropic shift distribution. For RAMP CP (blue), the signal intensity drops as the chemical isotropic shift offset increases. Heteronuclear dipolar coupling constant for all the spins with different chemical isotropic shift are assumed to be $d_{IS} = 40$ kHz. The other rf-amplitude and frequency sweep width parameters used were given in caption of Fig. 3.10.

Part III

Experimental Verifications and Discussions

4 NICP: Cross Polarization under high-field and fast-MAS

Abstract

The idea of integrated cross polarization which has been utilized for electron-to-nucleus polarization transfer is applied to nucleus-to-nucleus polarization transfer. Instead of using a $\frac{\pi}{2}$ pulse followed by a $\frac{\pi}{2}$ phase-shifted locking pulse like in the conventional cross polarization, irradiation with a single phase is applied together with adiabatic frequency sweep from far off-resonance toward on-resonance. This is capable of locking individual spin packets even in the presence of considerable spectral distribution and/or line broadening. Thus, this technique can provide efficient polarization transfer for spin species having large chemical shifts and experiments in high static fields.

Recent technological development has brought very fast MAS into practice, which can considerably improve spectral resolution [23, 24, 25]. On the other hand, the Hartmann-Hahn matching profile splits into narrow sidebands under fast MAS, making polarization-transfer experiments sensitive to rf-intensity mismatch. In order to improve such mismatch-tolerance, a number of techniques have been proposed which employ modulation of rf amplitude or frequency [26, 27, 31, 28, 32, 29, 33, 30]. In parallel, the available static magnetic fields have been increased remarkably, which is preferred to further enhance sensitivity and

spectral resolution. However, like fast MAS led to the problem of the sensitive Hartmann-Hahn condition, rise in static field has also brought a challenge into CP due to the increased spectral distribution or resonance-line broadening by isotropic and anisotropic chemical shifts. Large spectral distribution inevitably leads to off-resonance irradiation, which results in incomplete spin lock. Since only those components of the spin magnetization which is locked along the effective field contribute to polarization transfer, high fields comes into conflict with CP.

What will be required henceforth is a new CP technique which is compatible with both fast MAS and high fields, that is, a CP technique that is robust against rf-mismatch and is capable of wideband spin lock. The purpose of this work is to present one such technique. Instead of applying a $\frac{\pi}{2}$ pulse followed by the locking pulse whose phase is shifted by $\frac{\pi}{2}$ with respect to the first pulse, this technique uses irradiation with a single phase together with an adiabatic frequency sweep from far off-resonance toward on-resonance. In this technique, the effective field has the maximum amplitude at the beginning and is decreased gradually as the frequency gets close to on-resonance. Thus, the Hartmann-Hahn condition is fulfilled during the sweep for a wide range of rf amplitudes. In previous works on frequency sweep CP (FSCP) [32], a $\frac{\pi}{2}$ pulse is initially applied and then frequency is swept from on-resonance to far off-resonance.

Although the Hartmann-Hahn condition is relaxed, the problem of incomplete spin lock remain unsolved. On the other hand, the present technique is free from the initial $\frac{\pi}{2}$ pulse and employs the converse frequency sweep, making it possible to lock the individual spin packets with relatively low rf powers. Improvement in spin locking efficiency is also expected in homogeneously-broadened spin systems such as protons in rigid solids. The present approach would also be advantageous when strong rf irradiation should be avoided for investigations of heat-sensitive biological materials.

The technique in which adiabatic passage serves for both efficient spin lock and error-tolerant Hartmann-Hahn matching has originally been demonstrated in electron-to-proton polarization transfer [41, 42, 43, 44, 45, 46, 47], and originally

called integrated solid effect, and then integrated cross polarization (ICP). Accordingly, we call the present nuclear-spin-version technique Nuclear Integrated Cross Polarization (NICP). We demonstrate NICP in powder mixture of L-alanine and glycine, and show that the Hartmann-Hahn matching profile is as insensitive as FSCP, and the ^{1}H-^{13}C polarization transfer is more efficient than that by the FSCP scheme, as a consequence of effective locking of the homogeneously broadened ^{1}H spins even with relatively low rf amplitudes.

4.1 Improvement of spin-locking efficiency on the source spins

4.1.1 Experimental verification

Powder mixture of non-labeled L-alanine and glycine was packed in a Doty 5 mm rotor, and experiments were carried out in a magnetic field of 11.7 T at room temperature with a spinning speed of 10 kHz. The carrier frequencies for the ^{1}H and ^{13}C resonances were 499.789 MHz and 125.686 MHz, respectively. After performing the NICP sequence, the ^{13}C magnetizations of the methyl (CH_3), the methylene (CH_2), the methine (CH), and the carboxyl (COOH) groups were measured under Two Pulse Phase Modulation (TPPM) ^{1}H decoupling [13]. NICP experiments were performed for various ^{1}H irradiation amplitudes (ω_{1I}), while that (ω_{1S}) at the ^{13}C spins was fixed to 45 kHz. For better spin lock performance, the ^{1}H irradiation amplitude was tangentially turned on at the beginning of the frequency sweep.

For comparison, we have also performed the conventional CP and the FSCP experiments, whose pulse sequences are shown in Fig. 4.1(a) and (c). In conventional CP and FSCP, a $\frac{\pi}{2}$ pulse was firstly applied, and then was the locking pulse whose phase was shifted by $\frac{\pi}{2}$ with respect to the first pulse. No rf modulation was used in conventional CP, while frequency sweep from on-resonance to far off-resonance was employed in FSCP.

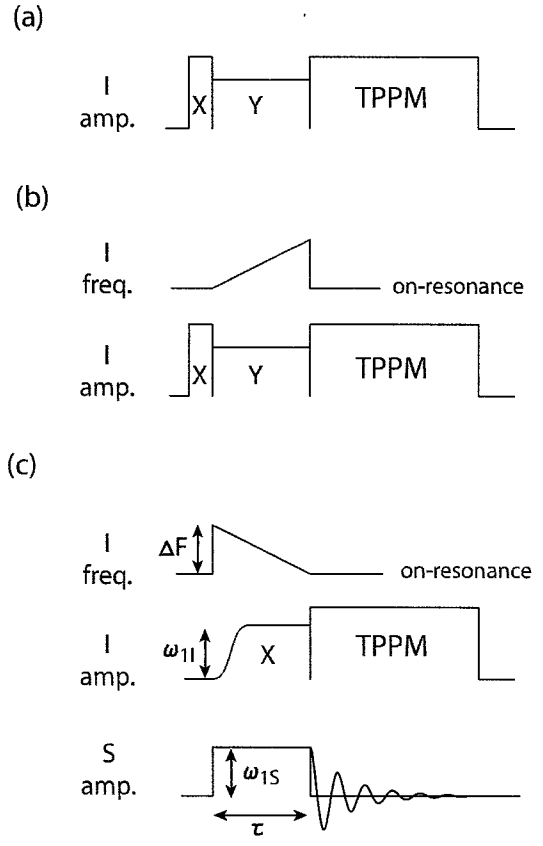

Figure 4.1: Pulse sequence for (a) Conventional Cross Polarization Spin locking of source spins with (b) NICP: far-off to on-resonance rf sweep, (c) FSCP: on to off-resonance rf-sweep. CW irradiation is applied to carbon channel in both techniques.

4.1.2 Results and Discussions

Among a number of experiments for various contact times and frequency sweep widths, the optimal results are shown in Fig. 4.2 for conventional CP (squares), FSCP (triangles), and NICP (circles). In the conventional CP experiment, the Hartmann-Hahn matching profiles show sidebands splitted by the spinning frequency (10 kHz) for the methyl and the carboxyl group, which is ascribed to relatively weak dipolar couplings between the ^{13}C and the ^{1}H spins. Such a sideband splitting was considerably suppressed in FSCP, because the amplitude of the ^{1}H effective field is ramped by the frequency sweep, so that the Hartmann-Hahn

condition can be fulfilled for wide range of irradiation amplitudes. As demonstrated in Fig. 4.2, the flat matching profiles were also realized in NICP. This is because the trajectory of the effective field during NICP is nearly the same as that during FSCP except for its direction. Moreover, the ^{13}C magnetizations obtained in NICP were considerably larger than those in conventional CP and FSCP. This is ascribed to that the rf amplitude $\omega_{1I}/2\pi = 56$ kHz used for the initial $\frac{\pi}{2}$ pulse in conventional CP and FSCP was not sufficiently large as compared to the ^{1}H resonance-line broadening of the order of several tens of kilohertz, so that some amount of the spin packets could not be locked and were lost. On the other hand, the amplitude of the initial effective field ($\sim$ 100 kHz) in NICP was large enough to effectively lock the ^{1}H spin and let all the spin packets to participate in the polarization transfer process, even when the rf intensity was relatively small as compare to the spectral width. It is worth noting that although the availability of high rf amplitude is not the prerequisite for NICP, it is certainly beneficial to have high rf amplitude to align back the effective field of I spins to the xy-plane.

We have also found that the optimal sets of contact time and frequency-sweep width are nearly the same for the four carbon groups in NICP. The theoretical account for this favorable feature will require evaluation of the ZQ adiabatic condition in (3.32) by taking account of powder averaging and sample spinning.

The characteristic of NICP that the effective field has the maximum amplitude at the beginning of the sequence would also be advantageous for polarization transfer from spin species having relatively large chemical shifts such as ^{19}F and ^{31}P as well as protons in paramagnetic compounds where anisotropic paramagnetic shifts can be as large as 1000 ppm [48]. Although broadband spin locking may be achieved by employing higher rf power, it would be even more formidable for experiments in high static fields, which are preferred to gain both sensitivity and resolution. On the other hand, NICP realizes efficient spin lock with relatively low rf power, and is conveniently implemented with moderate power amplifiers. This feature is also advantageous for biological materials containing water and salts, where rf-induced sample heating can be a serious problem.

In summary, we proposed a new technique for CP, namely, the NICP technique, in which adiabatic frequency sweep is applied to the I spin from far off-resonance toward on-resonance, while cw irradiation is applied to the S spin. Since the magnitude of the effective field is decreased gradually as the frequency is swept toward on-resonance, NICP can, like the existing amplitude-ramped or frequency-modulated schemes can, realize a flat Hartmann-Hahn matching profile even for high spinning speeds. Adiabatic passage from far off- to on-resonance is capable of lock the individual spin packets even in the presence of considerable spectral distribution and/or line-broadening. Thus, NICP is useful when available rf power is limited, or for polarization transfer from spin species having large chemical shifts, or for experiments in high static fields.

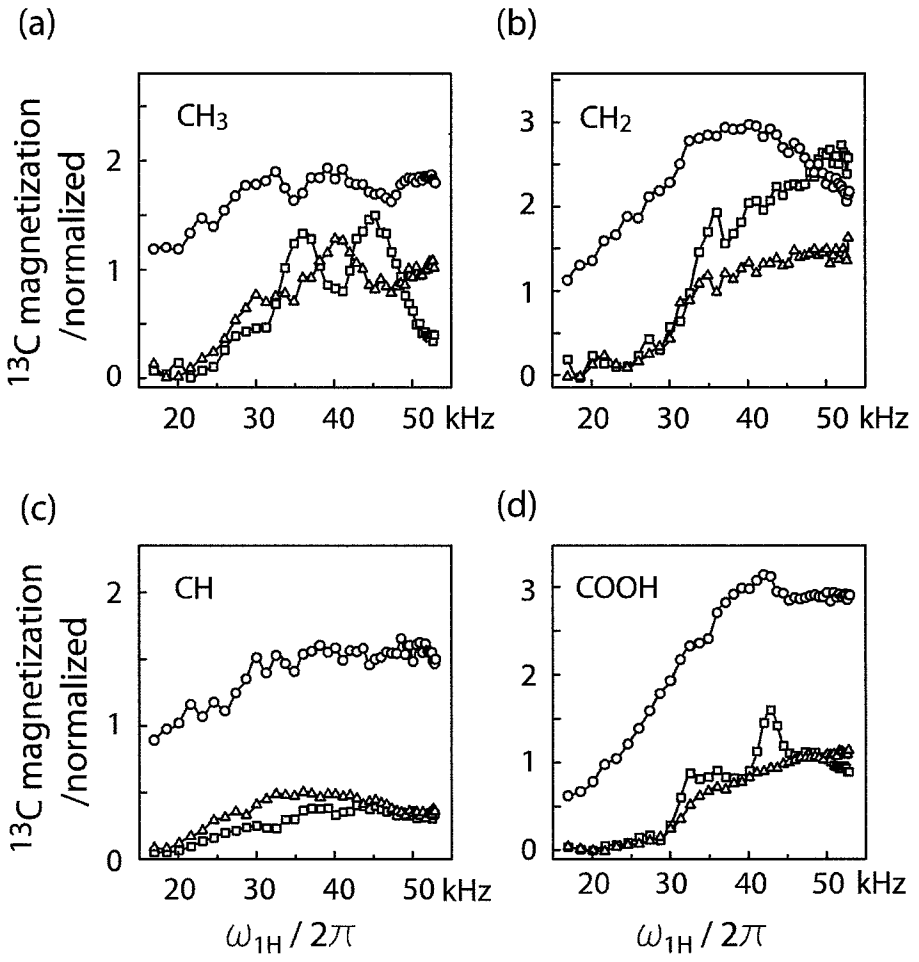

Figure 4.2: ^{13}C magnetizations of (a) the methyl (CH_3), (b) the methylene (CH_2), (c) the methine (CH), and (d) the carboxyl (COOH) groups in powder mixture of L-alanine and glycine obtained with conventional CP (squares), FSCP (triangles), and NICP (circles) for various ^1H irradiation amplitudes. The spinning frequency was 10 kHz, and the carrier frequencies for the ^1H and ^{13}C channels were 499.789 MHz and 125.686 MHz, respectively. Among a number of experimental results for various contact times and frequency-sweep widths, the optimal results were shown here for each carbon group. In conventional CP, the optimal contact times were 0.2 ms, 5.5 ms, 0.2 ms, and 5.5 ms for the methyl, the methylene, the methine, and the carboxyl groups, respectively. In FSCP, the optimal sets of contact time and sweep width were (0.2 ms, 50 kHz), (5.5 ms, 80 kHz), (0.2 ms, 34 kHz), and (5.5 ms, 50 kHz), and in NICP were (7.2 ms, 100 kHz), (7.2 ms, 200 kHz), (7.2 ms, 100 kHz), and (7.2 ms, 100 kHz). The ^{13}C magnetizations were normalized with respect to those in thermal equilibrium.

5 SADIS CP: Fast, Efficient and Wideband Cross Polarization

Abstract

In this work, we propose a new and efficient heteronuclear cross polarization scheme, in which adiabatic frequency sweeps from far off-resonance towards on-resonance are applied simultaneously on both the source and target spins. This technique, which we call as Simultaneous ADIabatic Spin-locking Cross Polarization (SADIS CP), is capable of efficiently locking both the source and target spins with moderate power even in the presence of large spectral distribution and fast relaxation. It is shown that by keeping the time dependent Hartmann-Hahn mismatch minimal throughout the mixing period, polarization transfer can be accelerated. Experiments are demonstrated in a powder sample of L-alanine.

In order to further increase the attainable magnetization, we present in this work an improved scheme for NICP, in which adiabatic frequency sweeps from far-off resonance toward on-resonance are applied simultaneously on both the source and target spins. This technique, which we call as Simultaneous ADIabatic Spin-locking Cross Polarization (SADIS CP), has the following advantages. (i) Simultanoeus sweep reduces the amount of Hartmann-Hahn offset throughout the whole sequence as compared to that in NICP, therefore allowing faster polarization transfer. (ii) Offset irradiation leads to higher effective field. The higher effective field, in general, results in a longer spin-lattice relaxation time in the rotating frame.

The property that the effective field is initially the largest is particularly attractive, because both the I and S magnetization can be well kept during the sequence. Offset assisted power reduction is also attractive for application to power lossy biological samples [34]. (iii) The favorable properties of NICP mentioned above are retained in this new approach. We present here the principle behind SADIS CP and demonstrate its performance in ^{1}H-^{13}C double resonance experiments using a powder sample of L-alanine. As shown later, the above merits are more than enough to compensate the cost of the decreased I-S dipolar interaction with offset irradiation.

5.1 Hartmann-Hahn matching condition under fast MAS

The time-dependent Hartmann-Hahn offset should be kept small as long as the Hartmann-Hahn condition is satisfied for the individual target spins. Generally speaking, experiments should be arranged in such a way that the magnitude of the effective fields are initially different, and so they are the other way around at the end of the sequence. For example, for the case of simple isolated two-spin system under sample spinning,
(1) at $t = 0$

$$\omega_{eI} + w_r \leq \omega_{eS} \leq \omega_{eI} + 2w_r, \tag{5.1}$$

and
(2) at $t = T$

$$\omega_{eS} + w_r \leq \omega_{eI} \leq \omega_{eS} + 2w_r, \tag{5.2}$$

or vice versa so that the crossing will be limited to $|n|= 1$ matching condition, where the magnitude of the dipolar coefficient is the largest. The reversal of the magnitude relation between the effective fields guarantees that the Hartmann-Hahn condition is satisfied during the simultaneous sweep.

5.2 Experimental aspects

Experiments were performed at room temperature in a magnetic field of 11.7 T using a home-built triple resonance probe equipped with a Varian 4 mm spinning module. Carrier frequencies for the ^{13}C and ^{1}H channels were 125.675 MHz and 499.789 MHz, respectively. We compare SADIS CP with both NICP and Conventional Cross Polarization, and the pulse sequences are as shown in Fig. 5.1. The ^{13}C NMR signals in a polycrystallines sample of ^{13}C-labelled L-alanine were measured at a spinning frequency of 13.5 kHz under ^{1}H TPPM decoupling [13]. Recycle delays were 60 s for ^{13}C direct observation and 2 s for all other CP experiments.

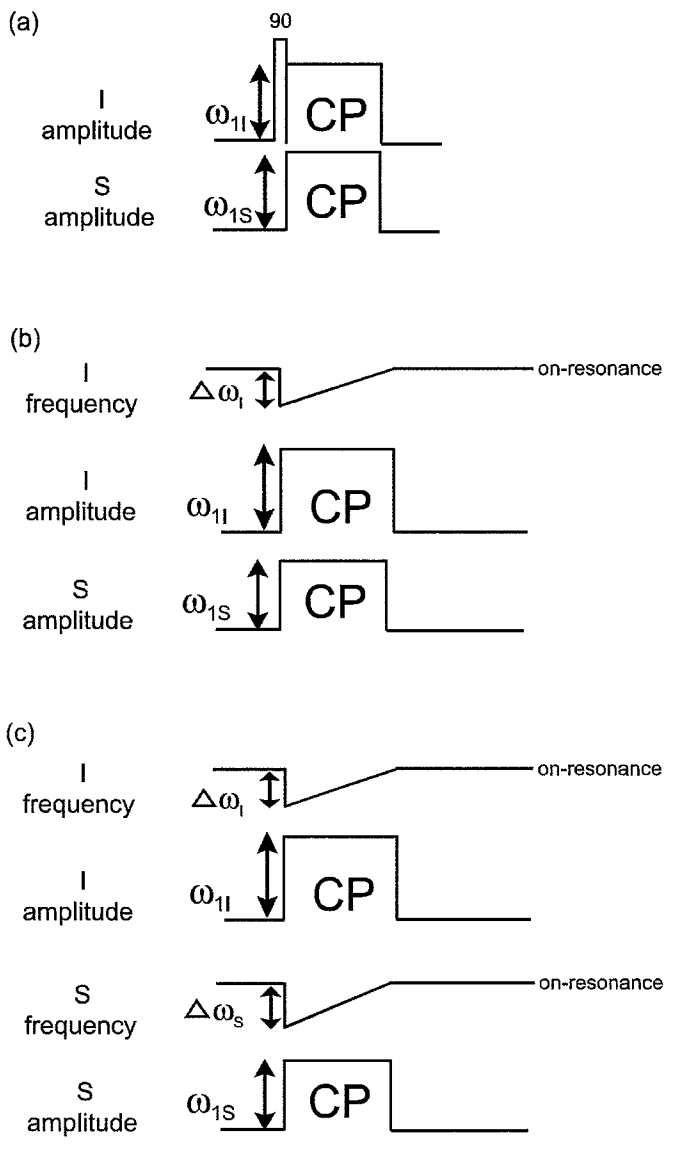

Figure 5.1: Pulse sequence for (a) Conventional Cross Polarization, (b) NICP, and (c) SADIS CP.

5.3 Results and discussions

5.3.1 'Contact-time' dependent behaviour

Figure 5.2 shows the signal intensities of the methyl, methine, and carboxyl ^{13}C spins for various contact times in the conventional CP, NICP, and SADIS CP techniques. By 'contact time' we refer to the time interval T of the frequency-sweep for NICP and SADIS CP. The signal intensities are normalized with respect to the signal obtained in thermal equilibrium with direct excitation with sufficiently long recovery delay time of 60 s. In the conventional CP experiment, separate measurements were carried out for the individual carbon groups by setting the carrier frequency at on-resonance and adjusting the $n= +1$ Hartmann-Hahn condition, and the maximum enhancement factors recorded were 2.26, 2.32, 1.52 for the methyl, methine, and carboxyl ^{13}C spins with contact times of 0.16, 0.10, and 0.68 ms, respectively. This result indicates that it is impossible to choose a common set of optimal contact time and rf power. This problem would be more serious for samples with large chemical shift distribution or experiments under high static field where the Hartmann-Hahn matching profile is shifted according to the individual chemical shifts. The relatively smaller signal enhancement for the conventional CP is also due to less efficient spin-locking of the ^1H magnetization with the rf intensity of 59 kHz, which is smaller than the ^1H dipolar linewidth. Thus, the performance of polarization transfer in those previous CP techniques using the initial $\frac{\pi}{2}$ pulse at the I spin degrades when the available or tolerable rf power is limited. Moreover, the low rf intensity can cause fast spin-lattice relaxation in the rotating frame, as discussed below.

In NICP, it was found that comparable amount of enhancement factors (2.32, 2.27, 1.53) can be obtained in a single experiment using a common set of experimental parameters ($\frac{\omega_{1S}}{2\pi}$= 35 kHz, $\frac{\omega_{1I}}{2\pi}$= 48 kHz and $\frac{\Delta\omega_I}{2\pi}$= 80 kHz), as demonstrated in Fig. 5.2. The improved performance is ascribed to the following three reasons. Firstly, the magnitude of the initial effective field set along the z axis is much larger than the spectral distribution of the I spin. Thus, the I spin packets can be well locked along the effectively field, and therefore participate in the polarization transfer process even with moderate rf amplitudes. Secondly, the fact that the

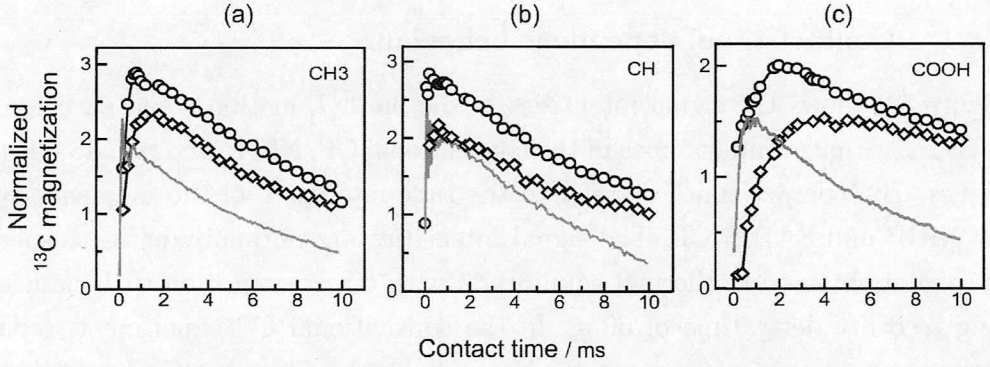

Figure 5.2: ^{13}C magnetizations for (a) CH_3, (b) CH, and (c) COOH in L-alanine for various contact times measured with conventional CP (solid lines), NICP (diamonds), and SADIS CP (circles). The vertical axis was normalized with respect to the value obtained with direct detection. For conventional CP, $\frac{\omega_{1S}}{2\pi}$ was fixed to 45 kHz and ω_{1I} was adjusted separately so that each of the isotropic chemical shifts satisfied sideband (+1) matching condition. For SADIS CP, $\frac{\omega_{1S}}{2\pi}$= 35 kHz, $\frac{\Delta\omega_S}{2\pi}$= 110 kHz and $\frac{\omega_{1I}}{2\pi}$= 48 kHz, $\frac{\Delta\omega_I}{2\pi}$= 80 kHz. For NICP, $\frac{\Delta\omega_S}{2\pi}$= 0 kHz while the rest of the parameters are the same as SADIS CP.

magnitude of the effective field changes with time permits the Hartmann-Hahn condition to be satisfied even in the presence of large spectral distribution or rf-intensity offset. Finally, the larger effective field with the off-resonance irradiation at the I channel leads to slower spin-lattice relaxation, so that larger amount of the I magnetization can be retained along the effective field before polarization transfer is completed. Since the common set of experimental parameters gave nearly the optimal enhancement factors, the sensitivity of the ^{13}C spectrum obtained with NICP (Fig. 5.3(b)) was considerably higher than that obtained with the conventional CP (Fig.5.3(a)).

In SADIS CP, the maximum enhancement factors (2.88, 2.84, 2.00) were (24%, 25%, 31%) higher than those obtained in NICP, as demonstrated in Fig. 5.2. This was achieved by employing an additional frequency sweep ($\frac{\Delta\omega_S}{2\pi}$= 110 kHz) on the S channel while other parameters were kept the same as the optimal ones for the NICP experiment. As can also be seen in Fig. 5.2, the contact times that gave the

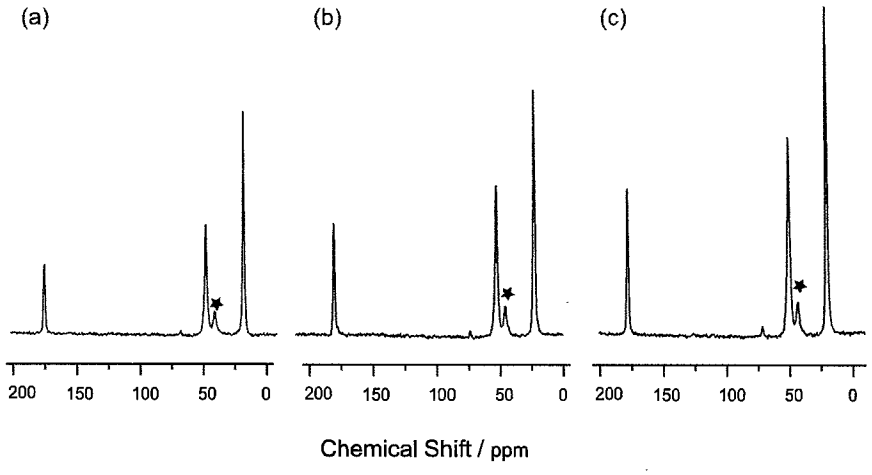

Figure 5.3: ^{13}C MAS spectra of L-alanine obtained with (a) conventional CP ($\frac{\omega_{1S}}{2\pi}$= 45 kHz, $\frac{\omega_{1I}}{2\pi}$= 58.5 kHz, contact time= 0.28 ms), (b) NICP ($\frac{\omega_{1S}}{2\pi}$= 35 kHz, $\frac{\Delta\omega_S}{2\pi}$= 0 kHz, $\frac{\omega_{1I}}{2\pi}$= 48 kHz, $\frac{\Delta\omega_I}{2\pi}$= 80 kHz, and contact time= 2 ms), and (c) SADIS CP ($\frac{\omega_{1S}}{2\pi}$= 35 kHz, $\frac{\Delta\omega_S}{2\pi}$= 110 kHz, $\frac{\omega_{1I}}{2\pi}$= 48 kHz $\frac{\Delta\omega_I}{2\pi}$= 80 kHz, and contact time= 0.8 ms), The peaks indicated by asterisks originate from impurity which was intentionally mixed for other purposes. There were no interaction between the impurity and L-alanine because it was just mechanically mixed.

maxima in SADIS CP are slightly shorter than those in NICP. This indicates that the buildup of the ^{13}C magnetizations was faster in SADIS CP, confirming the rather simplified theoretical descriptions in the chapter 3 which has neglected the homonuclear dipolar interactions among the protons. The optimized ^{13}C spectrum of SADIS CP is shown in Fig. 5.3(c).

For the purpose of clarifying the role of additional frequency sweep in the S channel, we have carried out related experiments, as described below.

5.3.2 ^{13}C magnetization buildup

In order to trace the buildup behaviour in NICP and SADIS CP, time interruption measurements were carried out, in which frequency sweep was aborted at various moments during the contact time. Fig. 5.4 shows the buildup of the methine ^{13}C

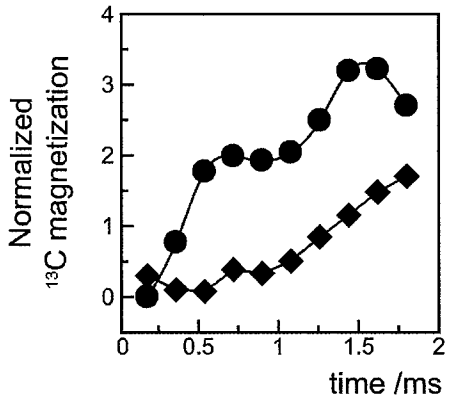

Figure 5.4: Buildup behaviour of the methine ^{13}C magnetization in L-alanine in SADIS CP (circles) and NICP (diamonds) obtained with time-interruption measurements. For SADIS CP, experimental parameters were $\frac{\Delta\omega_S}{2\pi}$ = 120 kHz, $\frac{\omega_{1S}}{2\pi}$ = 35 kHz, $\frac{\Delta\omega_I}{2\pi}$ = 100 kHz, and $\frac{\omega_{1I}}{2\pi}$ = 52 kHz. For NICP, the frequency sweep for S channel were turned off ($\frac{\Delta\omega_S}{2\pi}$= 0 kHz), while the other parameters were the same as in SADIS CP. A contact time of 1.8 ms was used. A correction factor $1/\sin(\alpha_S)$ was taken into account for SADIS CP since only the projection of the magnetization onto the xy-plane is measurable.

magnetization with T= 1.8 ms, $\frac{\omega_{1S}}{2\pi}$= 35 kHz, $\frac{\omega_{1I}}{2\pi}$= 52 kHz, $\frac{\Delta\omega_I}{2\pi}$= 100 kHz, and with $\frac{\Delta\omega_S}{2\pi}$= 0 kHz and 120 kHz for NICP and SADIS CP, respectively. Unlike the simplified calculation in Fig. 3.7, the oscillations were suppressed due to distribution of the IS dipolar frequency in the powder sample used in our study, and due to the dipolar interactions among the ^{1}H spins which were neglected in the theoretical part. For NICP, the Hartmann-Hahn crossing occured at $t \sim 1.2$ ms while for SADIS CP, the S magnetization surged up as the Hartmann-Hahn crossings occured at T= 0.5 ms and 1.3 ms, as demonstrated in Fig. 5.4. In SADIS CP, the overall attained ^{13}C magnetization was larger than that in NICP. One reason for this result is that Δ_{HH}(t) is smaller throughout the sequence in SADIS CP, which leads to the following two consequences. First, the chance of Hartmann-Hahn crossing increase when Δ_{HH}(t) is small; in this example the crossing occured twice in SADIS CP while it only occured once in NICP. Second, the smaller Δ_{HH}(t), the higher the rate of polarization transfer in each crossing. In other words, NICP requires a longer contact time to attain the same amount of polarization in SADIS CP.

In reality, however, the available time interval is limited by the effect of relaxation, which restores the spin system towards thermal equilibrium. Since the final ^{13}C magnetization is determined by the balance between the buildup and relaxation processes, both the transfer rate and the chance of the Hartmann-Hahn crossing are desirable to be maximized for a given relaxation rate. In both of these respects, SADIS CP is superior to NICP, despite that the IS dipolar interaction is weaker in SADIS CP by an additional scaling factor $\sin\alpha_S(t)$. Thus, SADIS CP opens its application to systems in which the effect of relaxation (particularly on the S spins) is so serious that the previously proposed CP techniques do not provide efficient polarization transfer. Such systems include, e.g., paramagnetics materials, samples with molecular motion whose time scale is comparable to the Larmor frequency, and samples in which the target rare spins, such as ^{13}C and ^{15}N, are isotopically enriched, because the presence of the additional homonuclear dipolar interactions among the S spins can reduce the relaxation time [49, 50]. Application of SADIS CP to such materials is shown in chapter 6.

5.3.3 Hartmann-Hahn matching profile

In order to study the efficiency of polarization transfer in terms of the Hartmann-Hahn mismatch $\Delta_{HH}(t)$ described in Eq. (3.14), we have examined the signal intensities of the methine ^{13}C as a function of the rf amplitude ω_{1I} for three frequency sweep widths $\frac{\Delta\omega_S}{2\pi}$= 0 kHz, 20 kHz, 110 kHz on the S channel (Fig. 5.5), which represents NICP, less optimal SADIS CP and the optimal SADIS CP, respectively. All other parameters were kept fixed. For $\frac{\Delta\omega_S}{2\pi}$= 110 kHz (black line), $\Delta_{HH}(t)$ is minimal throughout the sequence, providing the highest signal intensity and well-broadened matching profile over a wide range of rf amplitudes. For the case of $\frac{\Delta\omega_S}{2\pi}$= 20 kHz (gray line), the signal intensity dropped significantly as ω_{1I} was increased. In the case of NICP ($\frac{\Delta\omega_S}{2\pi}$= 0 kHz) denoted by the broken line, the signal intensity further dropped and the transfer efficiency became less robust against deviation in ω_{1I}. This is because the I effective field did not overlap with any of the Hartmann-Hahn matching conditions for $\frac{\omega_{1I}}{2\pi}$ beyond approximately 60 kHz (which corresponds to $\omega_{1S} + 2w_r$ condition).

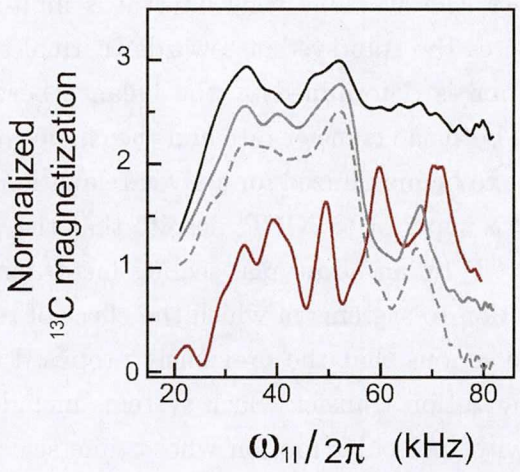

Figure 5.5: ω_{1I} dependence of the methine ^{13}C signal intensities in SADIS CP with (i) $\frac{\Delta\omega_S}{2\pi}$= 110 kHz (black line), (ii) $\frac{\Delta\omega_S}{2\pi}$= 20 kHz (gray line), and (iii) $\frac{\Delta\omega_S}{2\pi}$= 0 kHz (broken line). Note that (iii) corresponds to NICP, which is a special case of SADIS CP. Other parameters were fixed to $\frac{\Delta\omega_I}{2\pi}$ = 80 kHz, $\frac{\omega_{1S}}{2\pi}$ = 35 kHz and T = 0.8 ms. For comparison, the Hartmann-Hahn matching profile for the conventional CP with $\frac{\omega_{1S}}{2\pi}$ = 45 kHz and T = 0.80 ms is also shown in brown line.

Fig. 5.6 show the magnitudes of the effective fields during the SADIS CP and NICP sequences. As seen in Fig. 5.6(b), the Hartmann-Hahn condition is not met for the relatively stronger irradiation at the I spin in NICP. In SADIS CP, on the other hand, the Hartmann-HaHn crossings take place for a wide range of irradiation amplitudes at the I spin, as depicted in Fig. 5.6(a). Hence, the matching profile in SADIS CP is considerably wider than that in NICP, making the present scheme robust against deviation in rf intensity and spectral distribution. In this respect, SADIS CP is expected to show further advantages in experiments involving spins with large spectral distribution such as ^{19}F, ^{31}P, and paramagnetic samples.

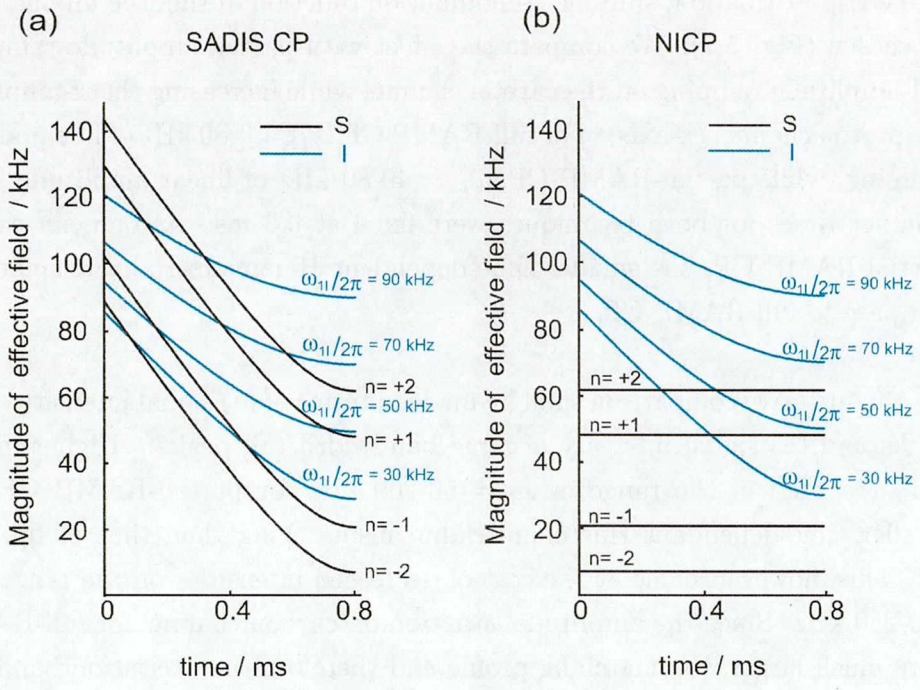

Figure 5.6: Time dependence of the magnitude of the effective field in SADIS CP for the S spin (black lines) and I spin (blue lines) with $T = 0.8$ ms, with $\Omega_S = 0$, $\frac{\omega_{1S}}{2\pi} = 35$ kHz, and $\frac{\Delta\omega_S}{2\pi} = 110$ kHz, $\Omega_I = 0$, $\frac{\Delta\omega_I}{2\pi} = 80$ kHz, and $\frac{\omega_{1I}}{2\pi} = 90$ kHz, 70 kHz, 50 kHz, and 30 kHz. In order to depict the Hartmann-Hahn crossings, the black lines are plotted with the offsets due to sample spinning frequency of $\frac{\omega_r}{2\pi} = 13.5$ kHz. (b) Time dependence of the magnitude of the effective field in NICP for the S spin (blue lines) and I spin (black lines). Parameters are the same in (a) except for $\frac{\Delta\omega_S}{2\pi} = 0$.

5.4 Effect of time-dependent Hartmann-Hahn mismatching as observed in RAMP CP

The effect of time-dependent Hartmann-Hahn mismatching was also experimentally observed in RAMP CP. Since polarization transfer is basically driven by external rf-perturbation, suitable rf-modulation function during the mixing time can be chosen (Fig. 5.7). We compare the effect with partial-amplitude ramping and full-amplitude ramping on the carbon channel while increasing the rf-amplitude on the proton channel (x-axis). For full-RAMP CP, ω_{1S}= 0-80 kHz of linear amplitude ramping, while partial-RAMP CP, ω_{1S}= 40-80 kHz of linear amplitude ramping. Contact times for both techniques were fixed at 0.5 ms. As one can easily tell, partial-RAMP CP, has smaller time-dependent Hartmann-Hahn mismatching as compare to full-RAMP CP.

Quantitative comparison shall be made in terms of (a) signal intensity of certain peaks and (b) signal intensity of large bandwidth (all peaks). Higher intensities were recorded in the range of ω_{1I}= 50-200 kHz for partial-RAMP CP, due to smaller time-dependant Hartmann-Hahn mismatching than that of full-RAMP-CP. This, however, came at the cost of decreased intensities on the range of ω_{1I}= 200-250 kHz. Since the amplitude variation on carbon channel for full-RAMP CP were much larger, the matching profile and therefore the excitation bandwidth is much larger.

Here, we can deduce that, of course, by keeping the function for proton and carbon channel exactly the same, the time-dependent Hartmann-Hahn mismatching will be zero, will therefore resulted in fastest transfer. In order to tap on a large bandwidth, effective fields should be modulated as such that it will cover large bandwidth. Therefore, keeping the first and second conditions at the same time, we shall be able to exploit fastest transfer over a large bandwidth. This is essentially the background idea of SADIS CP.

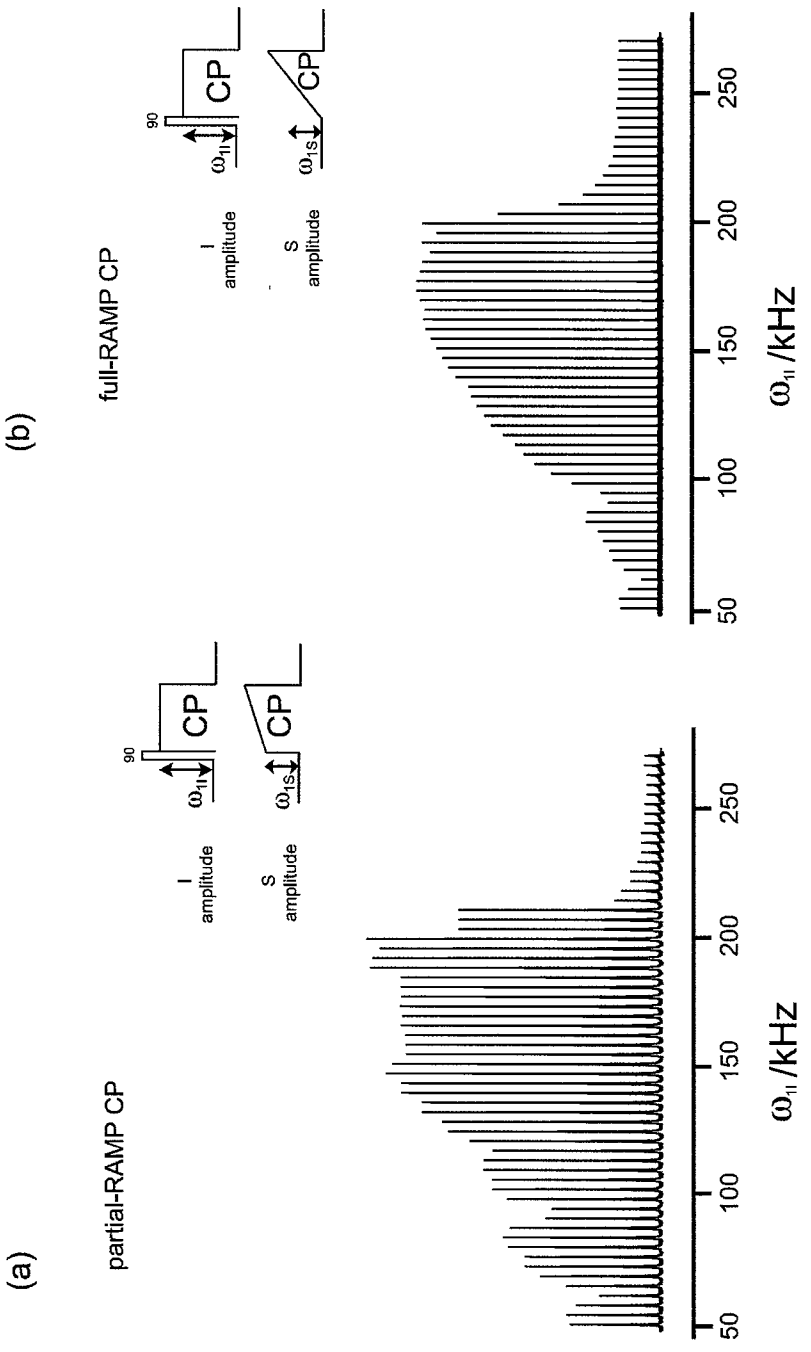

Figure 5.7: Y-axis is the arbitary carbon signal intensity of a selectively enriched ^{13}C methine in L-Alanine for (a) partial-RAMP CP, and (b) full-RAMP CP, respectively. x-axis is the incrementation of ω_{1I}. Spectra were recorded under sample spinning frequency of 50 kHz.

5.5 Issues on spin-lattice relaxation in rotating frame

Since only the magnetization along its effective field will participate in cross polarization, in practice, any decay during the spin-locking will result in reverse effect. Therefore, the upper bound of the amount of cross polarization is limited by spin-lattice relaxation in rotating frame, $T_{1\rho}$ of both the target and source spins. Spin-lattice relaxation in laboratory frame, T_1 which is usually much longer than $T_{1\rho}$ is less of a problem in CP.

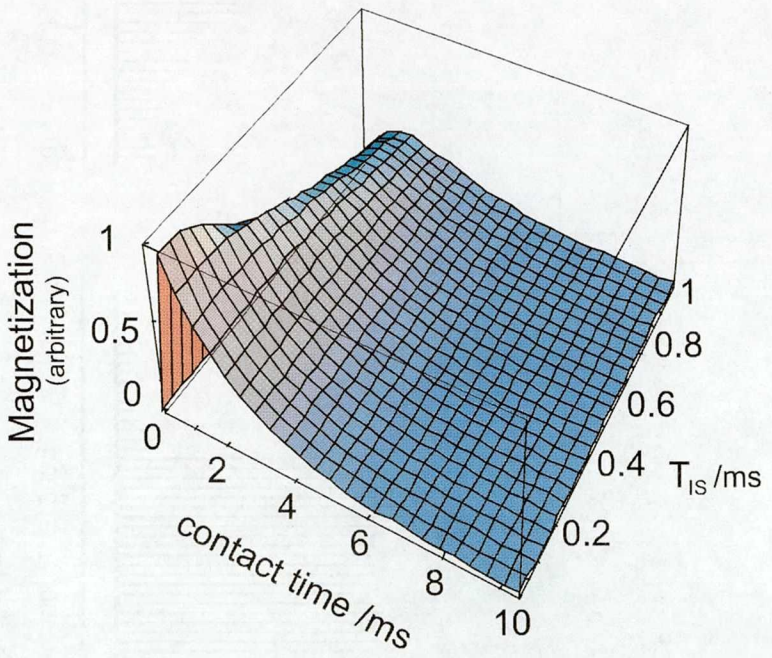

Figure 5.8: Quantification of polarization transfer calculated with double exponential model [8] as a function of contact time and cross relaxation, for a fixed $T_{1\rho}$= 2 ms.

In order to visualize the effect of relaxation on the amount of polarization transfered, phenomenological description can be employed. The speed of the polarization transfer is denoted by the cross relaxation, T_{IS} and the damping effect

is grouped into one factor known as $T_{1\rho}$. For the details, we refer readers to [8]. From Fig. 5.8, it is obvious that complete polarization will only happen provided that T_{IS} is much shorter than $T_{1\rho}$. In many systems, if the $T_{1\rho}$ is in the same order T_{IS}, full transfer is therefore impossible. If $T_{1\rho}$ is much shorter than T_{IS}, then no polarization transfer is possible.

$T_{1\rho}$ is characterized by its internal molecular properties as well as as external perturbation. Internal molecular rotation such as CH_3, couplings with other abundant spins, or enriched sample resulted in shorter $T_{1\rho}$, due to an additional path for relaxation. Other experimental aspects, e.g. temperature variation as shown in Fig. 5.9, magnetic field fluctuation, or limited rf power will contribute to the relaxation process.

SADIS CP, which make use of the offset irradiation (Fig. 5.10) on the S spins, can further suppress the effect of relaxation, because the effective field for the S spin is always larger throughout the sequence in SADIS CP as compared to NICP. Spin-lattice relaxation times in the rotating frame can be enhanced with offset irradiation, which suppresses the unwanted decay of the ^{13}C magnetization in the rotating frame. In particular, this is the case for the ^{13}C spins in L-alanine, as pointed by Akasaka et al. [51]. Thus, SADIS CP can spare longer 'contact' between both spins than NICP does.

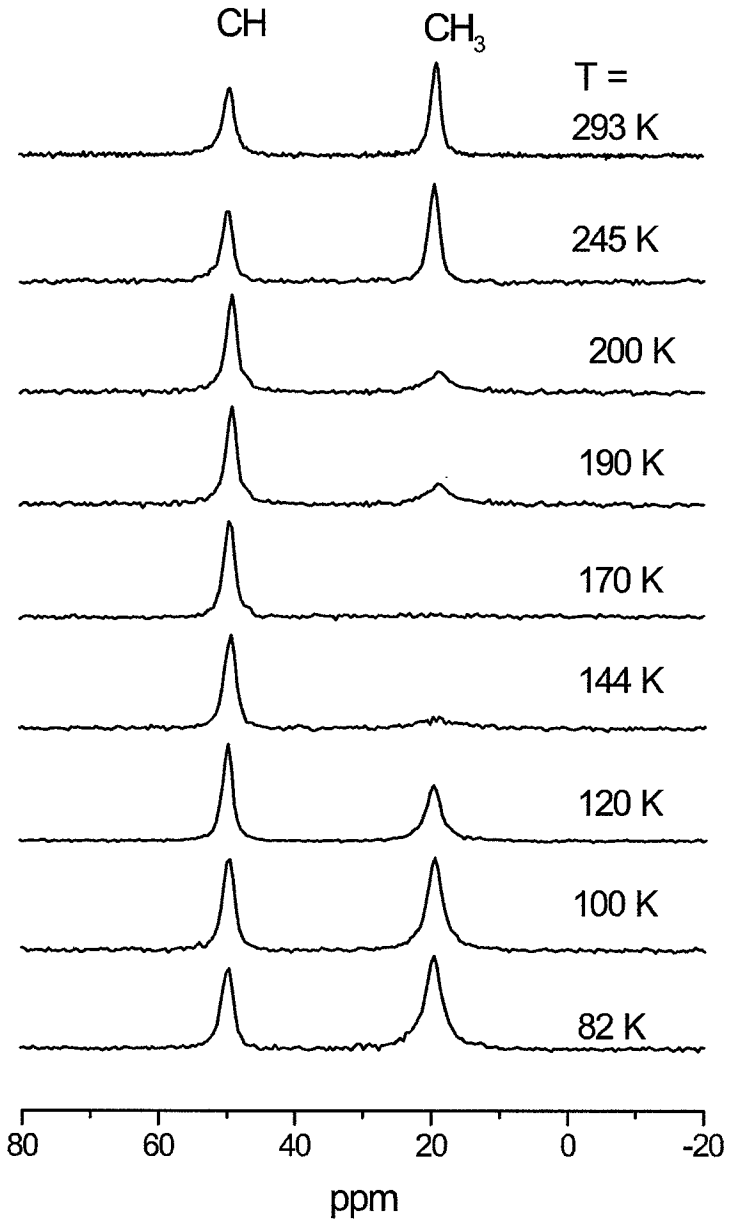

Figure 5.9: ^{13}C spectra of L-alanine observed with CPMAS as a function of temperature. The signal intensity reveals the role of spin-lattice relaxation in rotating frame in CP. These spectra were contributed by Dr. Ago Samoson (private communication).

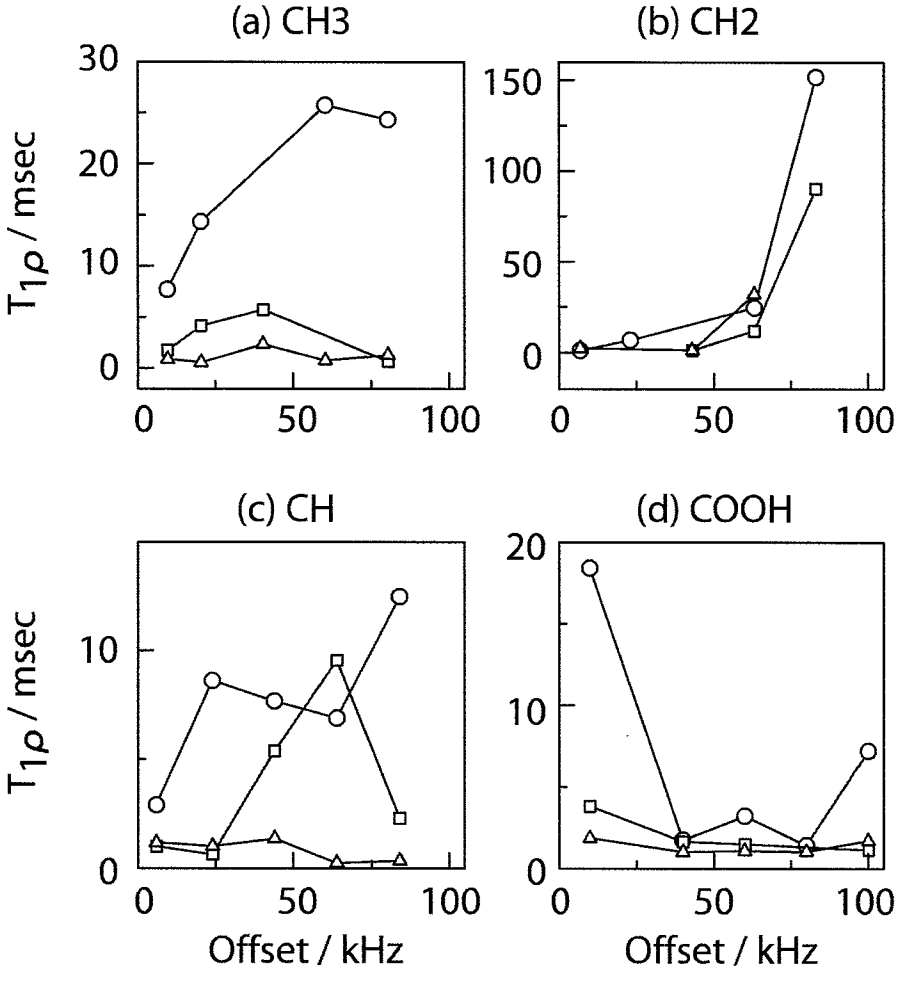

Figure 5.10: Figure shows various isotropic carbons spins and its $T_{1\rho}$ against the application of frequency offset, observed under sample spinning of 12 kHz.

6 Simultaneous Adiabatic Spin-locking Cross Polarization in Solid-State NMR of Paramagnetic Complexes under Very Fast Magic Angle Spinning

Abstract

Continuous-wave irradiations cross polarization and its variations had not been a popular choice for sensitivity enhancement in paramagnetic solids due to the large spectral broadening and the effect of fast relaxation on both the source and target spins. Furthermore, with the application of very-fast sample spinning, which is the prerequisite for high-resolution purposes, polarization transfer over a large bandwidth is further degraded. In this work, we report a wideband sensitivity enhancement in paramagnetic solids with our recently proposed cross polarization technique, Simultaneous Adiabatic Spin-locking Cross Polarization, SADIS CP. Experiments were demonstrated with Cu(II)(D,L-Alanine)$_2$.H_20 under high static field of 14.1 T and very-fast sample spinning of 31 kHz.

Solid-state NMR spectroscopy, which has been an effective tool for characterization of noncrystalline organic samples including diamagnetic organometallic complexes, has yet to be well-utilized in solid-state paramagnetic metal ions. The present of metal-ion in organic sample is notoriously known to cause huge spectral distribution or resonance line broadening, line shift and faster relaxation [7, 52] as compared to its diamagnetic state, had long impeded the quest for high resolution and high sensitivity spectroscopy. Recent report by Ishii et al. [48, 54] on very-fast

sample spinning (VFMAS) [23, 24, 25], which improved spectral resolution remarkably, has ignited new interest and hope in paramagnetic solid-state spectroscopy. Also sensitivity can be enhanced with shorter recycle delay [55] as compared to its diamagnetic counterpart. Shorter recycle delay enables the number of scans to be increased, as such the signal-to-noise ratio (SNR) can be increased.

6.1 Effect of strong paramagnetism on spectral width

Organometallic complexes are present abundantly in nature and have a wide range of applications from surface chemistry and catalysts to genome mapping. Paramagnetism is a form of induced magnetism, which only occur in the presence of external applied magnetic field. Unlike a ferromagnet, it does not retain any magnetization in the absence of external field. An element can behave like a paramagnetic if they have unpaired electron. Among them are Aluminium-13, Magnesium-12, Platinum-78 and Calcium-20. Certain salts of the d and f transitional metal group show paramagnetic behaviour, e.g. copper sulfate, ferric chloride, manganese chloride and so forth.

Molecular Complexes	Electron Spin Number	Spectral width ^{13}C [ppm]	^{1}H [ppm]	^{13}C at 14.1 T	^{1}H [kHz]
Fe(II)-DIAD	2	900	500	135	300
$Mn(acac)_3$	$\frac{5}{2}$	2600	1000	390	600
Yb(III)-dipic	$\frac{7}{2}$	-	400	-	240
Tb(III)-dipic	6	-	1200	-	720
$Cu(D,L\text{-alanine})_2.H_2O$	$\frac{1}{2}$	500	600	75	360

Table 6.1: A few selected paramagnetic sample, electron spin of the paramagnetic center and its approximate spectral width.

The anisotropic paramagnetic shifts [7] are generally proportional to

$$\frac{S(S+1)\gamma_I}{R_{IS}^3}, \tag{6.1}$$

where S is an electron spin number, γ_I is the gyromagnetic ratio of I spins and R_{IS} is the distance between I spin and the electron spin S at a paramagnetic center. Hence the higher the S spins (refer to Table 6.1), and the higher the gyromagnetic ratio of nucleus I, the anisotropic shifts tend to be larger.

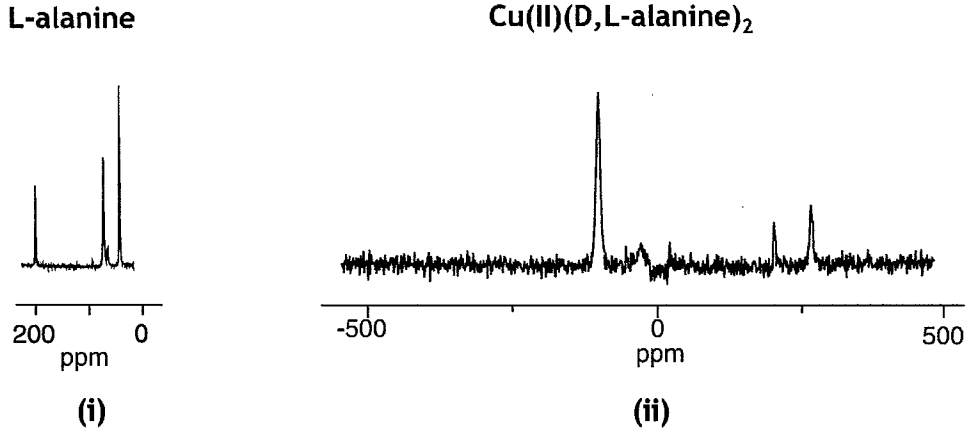

Figure 6.1: (ii) ^{13}C NMR spectra of Cu(II)(D,L-Alanine)$_2$.H_20. Huge spectral broadening, and line shift due to the effect of paramagentic center, Cu^{2+}, as compared to its diamagnetic state (i). The spectra of Cu(II)(D,L-Alanine)$_2$.H_20. was recorded with rotor-synchronous spin-echo sequence under sample spinning frequency of 35 kHz.

New terms are introduced into observed isotropic nuclear shift, δ^{obs}. In addition to orbital contribution δ^{dia} in diamagnetic molecules, which is usually observed, a few other terms

$$\delta^{obs} = \delta^{dia} + \delta^{fc} + \delta^{pc} + \delta^{BMS}, \tag{6.2}$$

appeared. δ^{fc}, δ^{pc}, δ^{BMS} are shifts due to fermi-contact, pseudo-contact (dipole interaction between electron and nuclear) and bulk magnetic susceptibility, respectively. Among others, BMS tensor due to the random orientation of each crystallite appears to be the dominating effect in spectral broadening. These effects are clearly observed as shown in Fig. 6.1 and Fig. 6.2. For further details we refer readers to excellent literature [7].

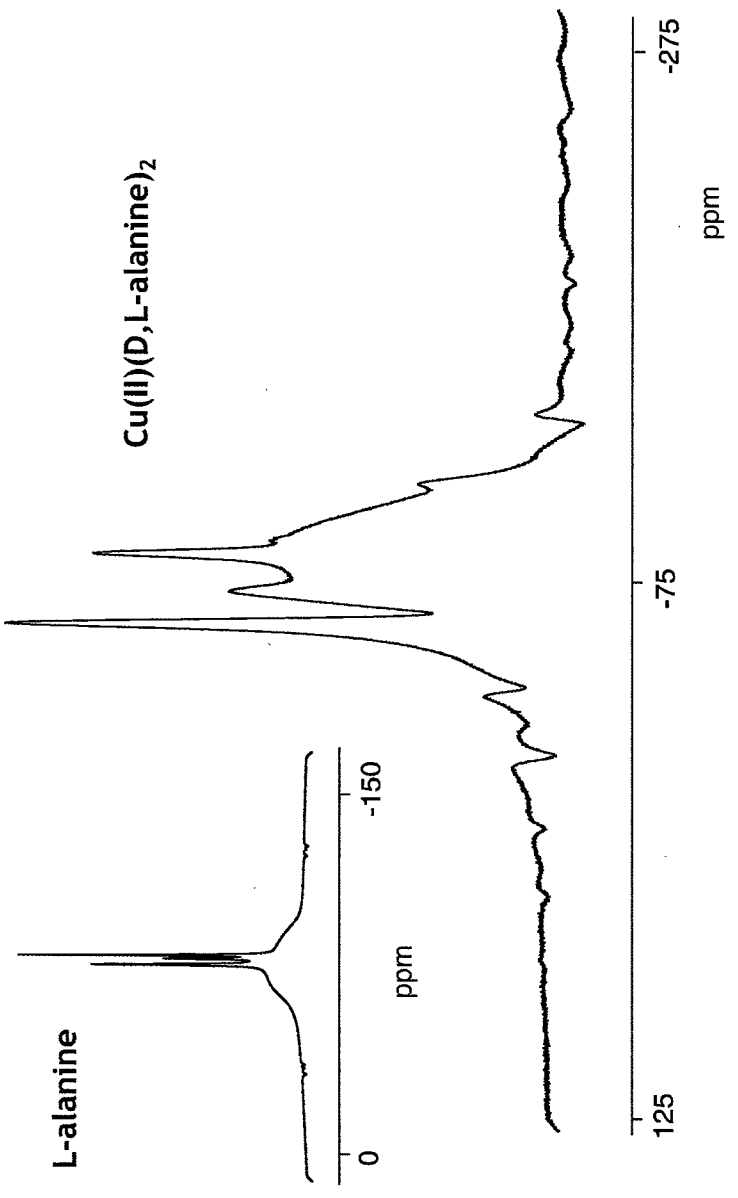

Figure 6.2: ^{1}H NMR spectra of Cu(II)(D,L-Alanine)$_2$.H_20. Huge spectral and line broadening due to the presence of paramagnetic metal-ion, Cu^{2+}, as compared to its diamagnetic state as shown in the inset. Besides, the line broadening of the isotropic chemical shift, minor anisotropic species present and spreaded over a few hundreds of ppm. The spectra of Cu(II)(D,L-Alanine)$_2$.H_20. was recorded with rotor-synchronous spin-echo sequence under sample spinning frequency of 35 kHz.

6.2 Incompability between Conventional CP and Paramagnetic Sample

Conventional cross polarization has found difficulty in its application to the paramagnetic systems [52]. Spectral broadening on both the target and source spins, spreading up to a few hundreds or even thousand of ppm, imposes strong challenges for efficient and wideband spin-locking with continuous-wave (CW) CP [10] or other single channel frequency/amplitude modulated CP, such as Amplitude-Modulated Cross Polarization [26], Adiabatic Passage through the Hartmann-Hahn condition [27, 28, 29], Amplitude-Modulated Adiabatic Passage Cross Polarization [30], Ramped-Amplitude Cross Polarization [31], Hartmann-Hahn matching via adiabatic frequency sweep [32], sinusoidally frequency-modulated Cross Polarization [33] and Ramped-Speed Cross Polarization [57]. These techniques were initially proposed during the 90's to compensate for the effect of rf-mismatching due to application of fast MAS.

Another scheme, Nuclear Integrated Cross Polarization [1], which is capable of spin-locking (even under fast MAS) large spectral broadening of the source spins was then proposed. This is achieved by applying large frequency sweep from far-off-resonance to on-resonance on the source spins while retaining the continuous wave irradiation on the target spins. As amplitude/frequency modulation on either of the channel, which was then thought to be sufficient to compensate for the rf-mismatching due to fast MAS, not much attention was paid to the influence of fast relaxation effect and huge spectral broadening which may occur in both the source and target spins such as in the case of paramagnetic solids. Note that, although very high rf-nutation is available with microcoil-probe [61], which is commonly used for mass-limited sample, we refer to 'huge' spectral broadening as to when the availability of rf-nutations/rf-powers applied are much smaller than the spectral distribution. Poor spin-locking coupled with the effect of fast relaxation, conventional CP techniques are almost helpless. Additionally, the fact that very-fast MAS is inevitably used for resolution purposes, cross polarization efficiency of large bandwidth is very much degraded.

We have shown in Chapter 5 that by applying adiabatic frequency sweep from far-off-resonance to on-resonance, on both the target and source spins simultaneously it is possible to promote faster and efficient polarization transfer over a large bandwidth. We refer to this technique as Simultaneous ADIabatic Spin-locking Cross Polarization (SADIS CP). We have successfully demonstrated this technique in diamagnetic sample of L-alanine as reported in Chapter 5. As compared to CW-irradiation, adiabatic frequency sweep from far off-resonance to on-resonance allows effective spin-locking throughout a large bandwidth, so that all the spin-packets could participate in the polarization transfer process. Since both the effective fields are now ramped through a large variable of magnitude, the chances of Hartmann-Hahn crossings over a large bandwidth are increased. Simultaneous application frequency sweeps on both the channel also reduce the degree of Hartmann-Hahn mismatching throughout the sequence and thereby polarization transfer time, bringing the desirable results particularly for spins with fast relaxation properties such as found in paramagnetic materials. Furthermore, higher effective field due to irradiation offset, in general, leads to longer $T_{1\rho}$. In this work, we experimentally demonstrated SADIS CP in paramagnetic solid with very-fast sample spinning of 31 kHz and under high-static field of 14.1 T.

6.2.1 Experimental

Experiments were performed at room temperature in a magnetic field of 14.1 T with Bruker Avance III spectrometer and home-built triple resonance probe equipped with spinning module for 1.3 mm rotor. 1.8 mg polycrystallines sample of ^{13}C-labelled Cu(II)(D,L-Alanine)$_2$.H_20 were packed into the rotor. Carrier frequencies for the ^{13}C and ^{1}H channels were 150.926 MHz and 600.175 MHz, respectively. The spectral width were 800 kHz and 200 kHz for ^{1}H and ^{13}C, respectively. The ^{13}C NMR signals were measured at sample spinning frequency, w_r of 31 kHz, and detected without the application of ^{1}H decoupling. Rotor-synchronous spin-echo sequence was applied prior to signal acquisition. Sufficiently long recycle delays of 50 ms for all CP experiments and 100 ms for ^{13}C direct observation were used to protect the probe from arching. For a common experimental time of about 42 min, the number of acquisitions were set to 50000 and 25000 for CP

experiments and direct excitation, respectively.

We compared the sensitivity enhancement (in terms of SNR) of SADIS CP with (i) RAMP CP, which represents the single channel frequency/amplitude modulated CP, and (ii) direct excitation of the rare spins. The optimal combination of rf-amplitudes and frequency widths for SADIS CP can be estimated by ensuring that the effective field for ^{13}C, ω_{eS} and that for ^{1}H, ω_{eI} were applied as such that, the initial condition (t= 0), $\omega_{eI} + w_r \leq \omega_{eS} \leq \omega_{eI} + 2w_r$, and finally at the end of the contact time, $\omega_{eS} + w_r \leq \omega_{eI} \leq \omega_{eS} + 2w_r$, or vice-versa, for sideband ± 1 matching condition to be met. For RAMP-CP, optimal rf-amplitude parameters were ^{13}C, $\frac{\omega_{1S}}{2\pi}$= 90 kHz to 125 kHz, and $\frac{\omega_{1I}}{2\pi}$= 158 kHz. An initial $\frac{\pi}{2}$ pulse of pulse width 1 μs was applied to I spin prior to spin-locking. As of standard RAMP CP, the amplitude-ramping size for ^{13}C, $\frac{\omega_{1S}}{2\pi}$ was set to approximately the frequency of sample spinning, w_r. The $\frac{\pi}{2}$ pulse width for direct observation of the rare spin is 2 μs.

6.3 Results and discussions

Among various experiments of rf-amplitudes and frequency sweep widths, the optimal results are shown in Fig. 6.3. For both CP experiments, a short contact time of 300 μs was used to minimize the effect of relaxation. The SNRs were as denoted besides each peak. One can see that through cross polarization (Fig. 6.3(a) and Fig. 6.3(b)) the SNRs were greatly enhanced (with the exception of ^{13}COOH in RAMP CP) as compare to direct excitation (Fig. 6.3(c)). For RAMP CP, SNR enhancement gains were (2.20, 0.72, 1.20) for ($^{13}CH_3$,^{13}COOH,^{13}CH), respectively, higher than that of direct excitation. Peaks assignment were based on literature [54]. However, considering that the number of scans were twice as much as that in direct excitation (due shorter recycle delay), SNR enhancement of 1.414 is to be expected. In this respect, one can deduce that the signal itself has not been improved much by the original idea of cross polarization, that is sensitivity enhancement of a ratio of the gyromagnetic ratios of both spins. Limited sensitivity enhancement in paramagnetic system with RAMP CP is not inherently the limitation of cross po-

larization, but rather caused by poor spin-locking and limited excitation bandwith due to limited rf-nutations on both the source and target spins, as described above.

With SADIS CP, we obtained a substantial signal intensity gain of as much as (1.19, 2.33, 2.17) as compared to RAMP CP, which translates to increase of the SNR to (9.25, 5.25, 6.50). These enhancements were attributed to the application of large initial frequency offset of $\frac{\Delta\omega_I}{2\pi}$= 450 kHz and $\frac{\Delta\omega_S}{2\pi}$= 500 kHz from far off-resonance to on-resonance to ^{1}H and ^{13}C, respectively. Although ^{1}H has resonance-line broadened over 600 ppm and ^{13}C has chemical isotropic shift distribution over 500 ppm, which is about 360 kHz and 75 kHz, respectively in 14.1 T field, large frequency sweep offsets in SADIS CP produce much higher effective fields that enable us to excite the whole spectra effectively and maintain a good spin-lock on both the source and target spins. As for RAMP CP, $\frac{\pi}{2}$ pulse irradiation of rf-nutation 250 kHz, and rf-amplitudes for spin-locking ($\frac{\omega_{1S}}{2\pi}$= 90-125 kHz and $\frac{\omega_{1I}}{2\pi}$= 158 kHz) were not sufficiently large as compared to its respective spectral width, therefore, resulted in poor spin-locking and decay of magnetization in the rotating frame. Moreover, since the frequency sweep offsets in SADIS CP were swept through a wide range of values, Hartmann-Hahn condition was made to satisfy over a large spectral bandwidth or chemical isotropic shift offset, as explained below.

Fig. 3.10(b) shows that in RAMP CP, if the Hartmann-Hahn condition is set to be met for S spins near to the carrier-frequency, there ought to be spins which are aligned far from the carrier frequency, due to e.g. chemical isotropic shift, where Hartmann-Hahn crossing did not occur. As such polarization transfer for RAMP CP degrades for S spins which has large chemical shift offset (Fig. 3.11(a)). As for SADIS CP as shown in Fig. 3.10, effective field for I spin can be forced to cover a large bandwidth so that Hartmann-Hahn crossings can occur to each individual S spin regardless of its chemical shifts offset (Fig. 3.11). The larger the frequency sweep width, the better the bandwidth coverage on both the source and target spins. The limit of the frequency sweeping bandwidth is only defined by the capability of the NMR spectrometer which sets the requirement for finite discrete number of steps that can be implemented for phase or frequency modulation.

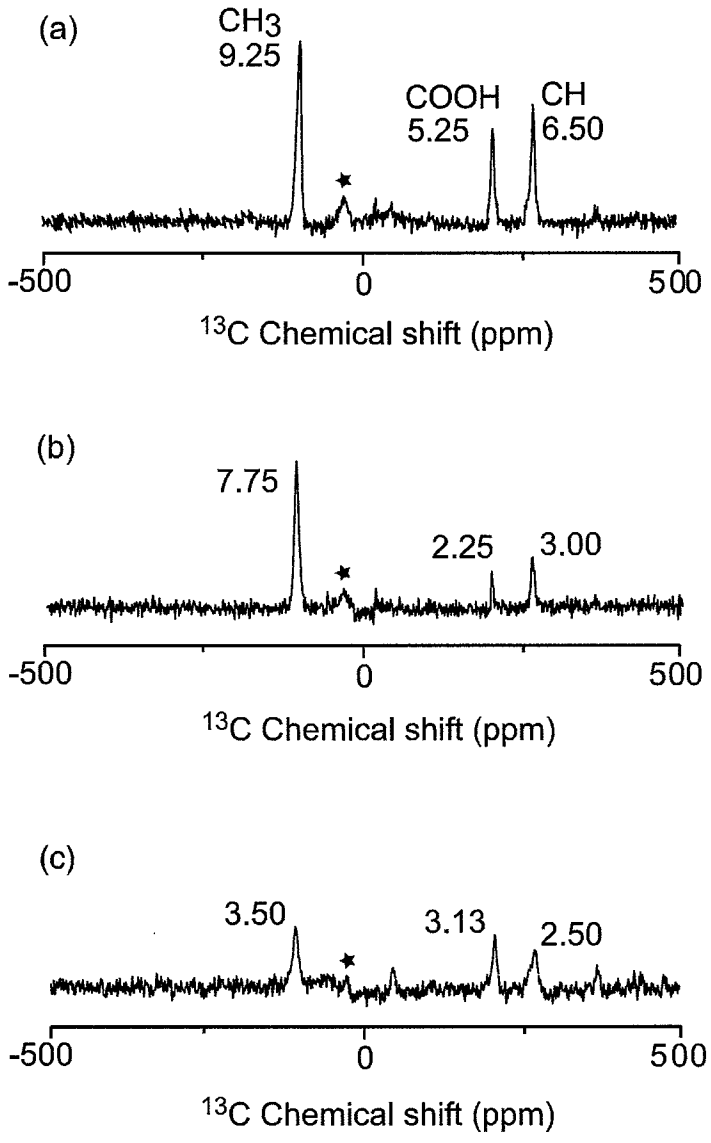

Figure 6.3: ^{13}C NMR spectrum of powder sample natural abundance Cu(II)(D,L-Alanine)$_2$.H_20, taken with (a) SADIS CP, (b) RAMP CP for a short contact time of 300 μs, and (c) single pulse direct excitation. The SNRs were noted above each respective peaks. For SADIS CP, parameters used were $\frac{\omega_{1S}}{2\pi}$= 125 kHz, $\frac{\Delta\omega_S}{2\pi}$= 500 kHz, $\frac{\omega_{1I}}{2\pi}$= 152 kHz, $\frac{\Delta\omega_I}{2\pi}$= 450 kHz. Optimal rf-amplitude parameters for RAMP CP were ^{13}C, $\frac{\omega_{1S}}{2\pi}$= 90 kHz to 125 kHz, and $\frac{\Delta\omega_I}{2\pi}$= 158 kHz. The spectra for (c) was scaled according to $N^{\frac{1}{2}}$ to display a common noise level with spectra (a) and (b). The weak peaks at 80 ppm, denoted by $\star$, are attributed to minor species.

In conclusion, we have shown a novel result of the applicability of SADIS CP in paramagnetic solid. Despite the presence of large spectral broadening and fast relaxation on both the source and target spins, substantial signal enhancement over large bandwidth can be obtained as compared to direct excitation, and RAMP CP, which represents the single-modulated CP schemes [26, 27, 28, 29, 30, 31, 32, 33]. Combined with VFMAS, high resolution and high sensitivity spectra were reported.

6.4 Future Challenges and NMR Spectrometer development

One of the future challenges for SADIS CP is certainly to be able to demonstrate a meaningful polarization transfer in other highly paramagnetic materials such as $Mn(acac)_3$ and Tb(III)-dipic, which have spectral broadening of a few thousands ppm (refer to Table 6.1). This means that application of initial frequency offset of as large as a few MHz is required in order to excite the whole spectrum. To be able to do this, new spectrometer, which has such specification, is therefore required. As far as probe is concerned, no modification is required as the FID signal is detected on-resonance. The probe channel-isolation for two concerned channels were however, need to be well-isolated as any rf-leakage will disrupt the CP performance.

From our experience, current commercial spectrometer or at least the one used in our laboratory had limitation in application of large frequency sweep. For e.g. spectrometer from Appolo Tecmag. Inc has phase modulation function in which the hardware limitation of the sampling interval is 2 μs, or maximum sampling frequency of 500 kHz. In order the reproduce a digital waveform, minimun of 4 points are required to reproduce a sinusoidal waveform. Therefore, the maximum frequency offset can be practically implemented is 125 kHz, while the one of Bruker Avancee III can practically perform up 700 kHz of phase modulation.

A home-built spectrometer (Fig. 6.4), which is capable of applying large frequency jump (in the order of more than a few MHz) is developed. The architecture of this spectrometer is based on [62] and the details can be accessed at the following link http://kuchem.kyoto-u.ac.jp/bun/indiv/takezo/opencorenmr/index.html. In this spectrometer, pulse programmer and the digital components are written with VHDL [63] code inside a FPGA system. Printed circuit boards were design and developed for each circuits (refer to Appendix C). Direct digital synthesis (DDS) is used to generate a frequency and phase-tunable signal by using digital data processing. An external DDS using AD9858 driven by external clock of 1 GHz is used to generate frequency source of up to 400 MHz. Home-made bandpass filters (refer to Appendix D) were used to cut-off spurious frequencies.

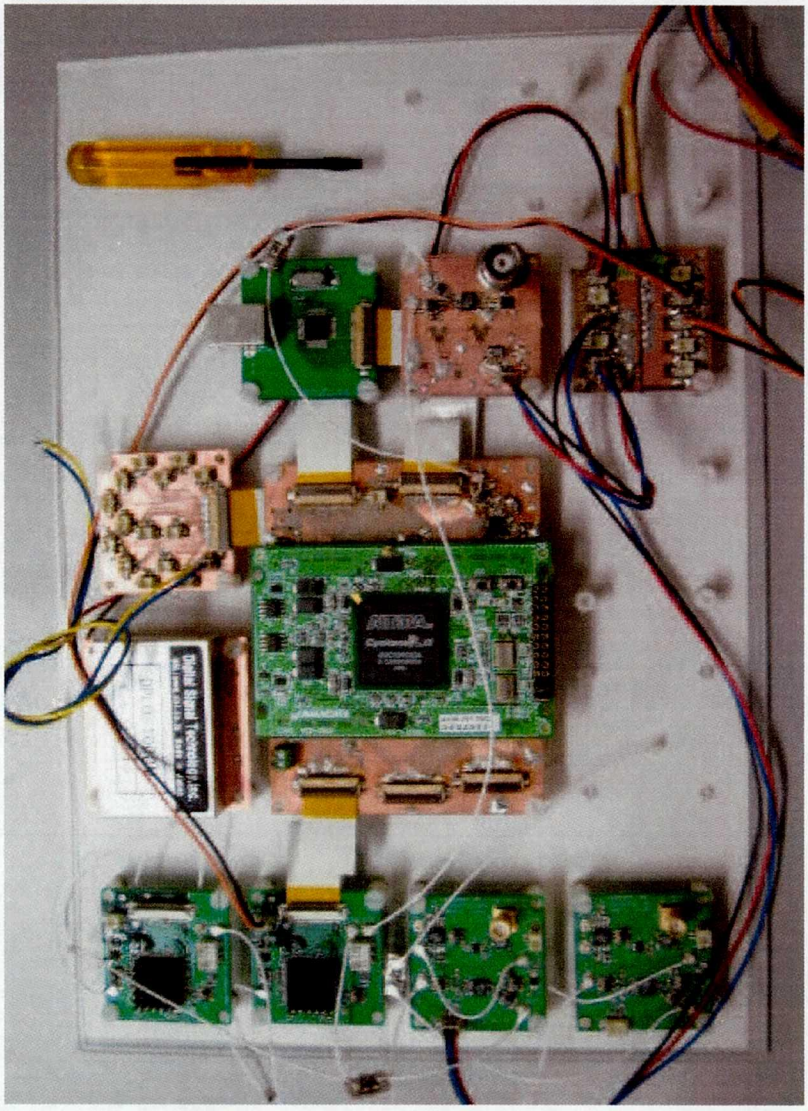

Figure 6.4: A snapshot of the 2 channels homebuilt NMR spectrometer.

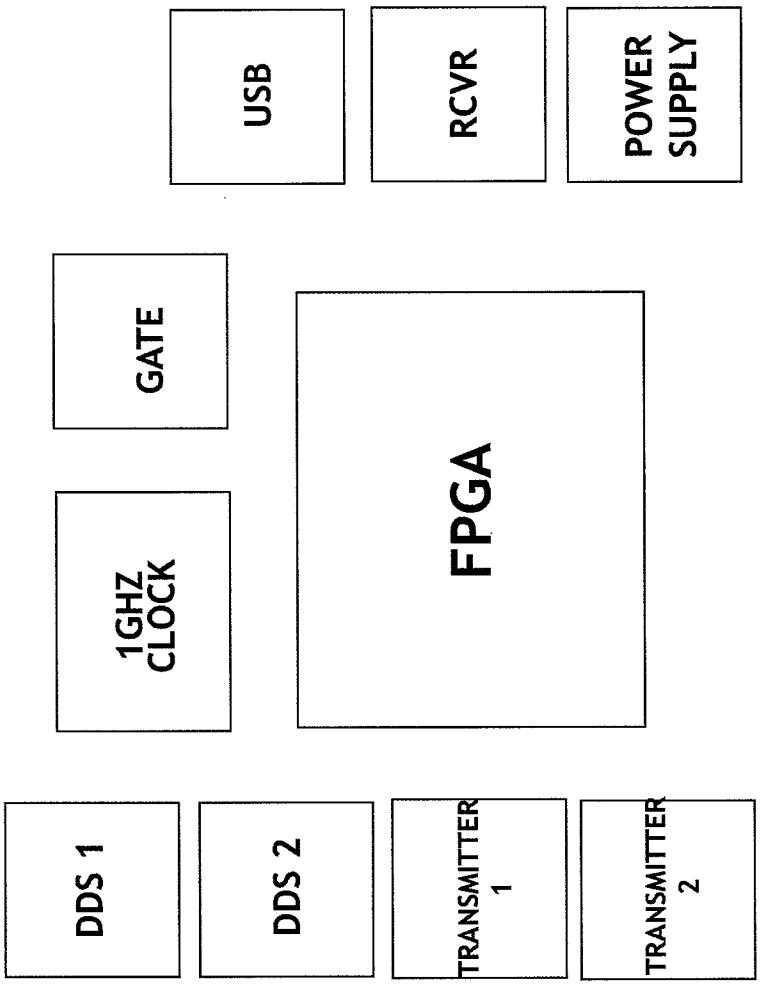

Figure 6.5: Block diagram of the spectrometer showing each of its components.

7 Concluding remarks

A study on polarization transfer by means of cross polarization in nuclear magnetic resonance was carried out. From there, two novel schemes namely, the NICP and the SADIS CP were established. Besides, our home-grown schemes, a couple of other CP schemes have also been evaluated, both theoretically and experimentally, and each of its unique features and performances were compared.

A mathematical formulation for a pair IS-spin, which serves as the fundamental understanding of spin interaction in nuclear magnetic resonance, has been developed. Our work revealed that time-dependent Hartmann-Hahn mismatching is the critical parameter that describe the ultimate magnitude of polarization transfer, while the effective coupling strength describe the speed of the exchange between the two spins or its frequency oscillation. This is true, at least, for time-scale and rf-nutations (often much larger than the coupling strengh for sufficiently strong spin-locking) in NMR. Likewise, we hope this understanding will be able to be extended to $I_{\mathrm{N}}S$ spin or even spin-diffusion of a large number of spins. With appropriate modification perhaps, the same idea may be useful for optical spectroscopy.

Qualitatively, in any of the CP schemes, as long as the Hartmann-Hahn crossing is ensured to take place, and that given sufficiently long enough of time for the magnetization buildup, full polarization transfer is possible. Quantitatively, the challenge is, of course, to increase the speed of the transfer throughout a large bandwith. This is often true in practical case, where multiple spins distributed over a large bandwidth are extremely common and also the effect of relaxation is often unnegligible. In this work, we have shown how we could drive the polarization transfer over a large bandwidth and how the speed of the polarization transfer can be accelerated at the same time. We observed this effect experimentally in L-Alanine (diamagnetic system) that an additional signal enhancement of up to 31% is possible by reducing the time-dependent Hartmann-Hahn mismatching factor. This was achieved technically by switching on an additional frequency sweep the S spins (for SADIS CP) as compared to NICP which employs only single frequency

sweep on I spins. Therefore, our scheme open for wide-range of application such as sample with fast spin relaxation, huge spectral or resonance-line broadening on both the source and target spins (such as high static field experiments or spin species which have naturally large chemical shifts dispersion such as ^{31}P and ^{19}F or paramagnetic species) as well as relatively low rf-power applications (such as heat-sensitive sample, usage of large coil to accomodate large quantity of sample, availability of power-amplifier, and so forth). On top of that since the effective-fields were ramped through a wide range of magnitude, it is compatible for fast MAS experiments. One novel application of sensitivity enhancement on paramagnetic solids under very-fast MAS was demonstrated by our group. We achieved a signal enhancement of as much as 2.33 folds higher for SADIS CP as compared to RAMP CP. Considering that both schemes are using the same idea of cross polarization where the limit of polarization transfer from ^{13}C to ^{1}H is 4 times, an additional enhancement of 2.33 times is significant !

As in any research, the end of one work usually also signifies the start of another new work. Just as this script was written, from our numerical evaluation we found that SADIS CP, may able to provide a transfer beyond the transfer bound describes by its counterpart, CW irradiation scheme. Some of the initial work is shown in Section 3.3.5. At one moment when you feel that you have known it all, at another instance you feel like a dummy. Research is an on-going effort, so as long as there is human-being there will be research to uncover the mystery of science and the challenge to build technology. We have, here, contributed a very small portion of the work, just like a drop of water dripping down a huge ocean, to the never endless work. Nevertheless, we hope that it can someday be a good jump-start for other related works. We would also like to apologize, if in any occasion, we have jumped into conclusion or making mistakes without realising them, though effort had been made to ensure that this work is as flawless as possible.

References

[1] W.K. Peng, K. Takeda, M. Kitagawa, A new technique for cross polarization in solid-state NMR compatible with high spinning frequencies and high magnetic fields, Chem. Phys. Lett. 417 (2006) 58.

[2] W.K. Peng, K. Takeda, Efficient cross polarization with simultaneous adiabatic frequency sweep on the source and target channels, J. Magn. Reson. 188 (2007) 267.

[3] W.K. Peng, A. Samoson, M. Kitagawa, Simultaneous Adiabatic Spin-locking Cross Polarization in Solid-State NMR of Paramagnetic Complexes, Chem. Phys. Lett. (under review).

[4] E.M. Purcell, H.C. Torrey, R.V. Pound, Resonance absorption nuclear magnetic moments in a solid, Phys. Rev. 69 (1946) 37.

[5] (a) F. Bloch, W.W. Hansen, M. Packard, Nuclear induction, Phys. Rev. 69 (1946) 127.
(b) F. Bloch, W.W. Hansen, M. Packard, The nuclear induction experiment, Phys. Rev. 70 (1946) 474.
(c) F. Bloch, Nuclear induction, Phys. Rev. 70 (1946) 460.

[6] H.L. Malcolm, Spin dynamics, Basics of Nuclear Magnetic Resonance, 2002.

[7] I. Bertini, C. Luchinat, G. Parigi, Magnetic susceptibilty in paramagnetic NMR, Progress in Nuc. Mag. Reson. 40 (2002) 249.

[8] M. Mehring, Principles of high resolution NMR in solids, Springer-Verlag, 1983.

[9] S.R. Hartmann, E.L. Hahn, Nuclear Double Resonance in the Rotating Frame, Phys. Rev. 128 (1962) 2042.

[10] A. Pines, M.G. Gibby, J.S. Waugh, Proton-enhanced NMR of dilute spins in solids, J. Chem. Phys. 59 (1973) 569.

[11] E.R. Andrew, A. Bradbury, R.G. Eades, Nuclear Magnetic Resonance Spectra from a Crystal rotated at High Speed, Nature 182 (1958) 1659.

[12] I.J. Lowe, Free Induction Decays of Rotating Solids, Phys. Rev. Lett. 2 (1959) 285.

[13] A.E. Bennett, C.M. Rienstra, M. Auger, K.V. Lakshmi, R.G. Griffin, Heteronuclear decoupling in rotating solids, J. Chem. Phys. 103 (1995) 6951.

[14] M. Carravetta, M. Eden, X. Zhao, A. Brinkmann, M.H. Levitt, Symmetry principles for the design of radiofrequency pulse sequences in the nuclear magnetic resonance of rotating solids, Chem. Phys. Lett. 321 (2000) 205.

[15] K. Takegoshi, J. Mizokami, T. Terao, ^{1}H decoupling with third averaging in solid NMR, Chem. Phys. Lett. 341 (2001) 540.

[16] P.K. Madhu, X. Zhao, M.H. Levitt, High-resolution ^{1}H NMR in the solid-state using symmetry-based pulse sequences, Chem. Phys. Lett. 346 (2001) 142.

[17] D. Sakellariou, A. Lesage, P. Hodgkinson, L. Emsley, Homonuclear dipolar decoupling in solid-state NMR using continuous phase modulation, Chem. Phys. Lett. 319 (2000) 253.

[18] M. Lee, W. Goldburg, Nuclear magnetic resonance line narrowing by rotating rf field, Phys. Rev. A 140 (1965) 1261.

[19] B.C. Gerstein, CRAMPS, The Encyclopedia of NMR, Wiley, London, 1997, p. 1501.

[20] J.S. Waugh, L.M. Huber, U. Haeberlen, WHH, Phys. Rev. Lett. 20 (1968) 180.

[21] W.K. Rhim, D.D. Elleman, R.W. Vaughan, Enhanced resolution for solid state NMR, J. Chem. Phys. 59 (1973) 3740.

[22] J. Schaefer, E.O. Stejskal, Carbon-13 Nuclear Magnetic Resonance of Polymers Spinning at the Magic Angle, J. Am. Chem. Soc. 98 (1976) 1031.

[23] A. Samoson, T. Tuherm, Z. Gan, Solid State Nucl. Magn. Reson. 20 (2001) 130.

[24] A. Samoson, Encyclopedia of Nuclear Magnetic Resonance 9 (2002) 59.

[25] A. Samoson, T. Tuherm, J. Past, A. Reinhold, T. Anupold, I. Heinmaa, Topics in Current Chemistry 246 (2004) 15.

[26] S. Hediger, B.H. Meier, R.R. Ernst, Cross polarization under fast magic angle sample spinning using amplitude-modulated spin-lock sequences, Chem. Phys. Lett. 213 (1993) 627.

[27] S. Hediger, B.H. Meier, N.D. Kuru, G. Bodenhausen, R.R. Ernst, NMR cross polarization by adiabatic passage through the Hartmann-Hahn condition (APHH), Chem. Phys. Lett. 223 (1994) 283.

[28] S. Hediger, B.H. Meier, R.R. Ernst, Adiabatic passage Hartmann-Hahn cross polarization in NMR under magic angle sample spinning, Chem. Phys. Lett. 240 (1995) 449.

[29] M. Baldus, D.G. Geurts, S. Hediger, B.H. Meier, Efficient ^{15}N-^{13}C Polarization Transfer by Adiabatic-Passage Hartmann-Hahn Cross Polarization, J. Magn. Reson. A118 (1996) 140.

[30] S. Hediger, P. Signer, M. Tomaselli, R.R. Ernst, B.H. Meier, A Combination of Slow and Fast RF Field Modulation for Improved Cross Polarization in Solid-State MAS NMR, J. Magn. Reson. 125 (1997) 291.

[31] G. Metz, X. Xiaoling, S. Smith, Ramped-Amplitude Cross Polarization in Magic-Angle-Spinning NMR, J. Magn. Reson. A110 (1994) 219.

[32] A.C. Kolbert, A. Bielecki, Broadband Hartmann-Hahn Matching in Magic-Angle Spinning NMR via an Adiabatic Frequency Sweep, J. Magn. Reson. A116 (1995) 29.

[33] R. Fu, P. Pelupessy, G. Bodenhausen, Frequency-modulated cross-polarization for fast magic angle spinning NMR at high fields: relaxing the Hartmann-Hahn condition, Chem. Phys. Lett. 264 (1997) 63.

[34] S.C. Shekar, D.K. Lee, A. Ramamoorthy, Chemical Shift Anisotropy and Offset Effects in Cross Polarization Solid-State NMR Spectroscopy, J. Magn. Reson. 157 (1996) 223.

[35] F. Bloch, Dynamical Theory of Nuclear Induction. II, Phys. Rev. 102 (1956) 104.

[36] R.P. Feynman, F.L. Vernon Jr., R.W. Hellwarth, J. App. Phys. 28 (1957) 49.

[37] S. Vega, Fictitious spin 1/2 operator formalism for multiple quantum nmr, J. Chem. Phys. 68 (1978) 5518.

[38] A. Abragam, Principles of Nuclear Magnetism, Clarendon Press, Oxford, 1961.

[39] B.H. Meier, Polarization Transfer and Spin-diffusion in Solid-State NMR, Adv. in Magn. and Optical, 18 (1994) 1.

[40] P. Hodgkinson, A. Pines, Cross Polarization efficiency in $I_{\mathrm{N}}S$ systems using adiabatic RF sweeps, J. Chem. Phys. 107 (1997) 8742.

[41] A. Henstra, P. Dirksen, W.Th. Wenckebach, Enhanced dynamic nuclear polarization by the integrated solid effect, Phys. Lett. A 134 (1988) 134.

[42] A. Henstra, T.-S. Lin, J. Schmidt, W.Th. Wenckebach, High dynamic nuclear polarization at room temperature, Chem. Phys. Lett. 165 (1990) 6.

[43] M. Iinuma, I. Shake, R. Takizawa, M. Daigo, H.M. Shimizu, Y. Takahashi, A. Masaike, T. Yabuzaki, High proton polarization in crystalline naphthalene by dynamic nuclear polarization with laser excitation at room temperature and liquid nitrogen temperature, Phys. Lett. A 208 (1995) 251.

[44] M. Iinuma, Y. Takahashi, I. Shaké, M. Oda, A. Masaike, T. Yabuzaki, H.M. Shimizu, High proton polarization by microwave-induced optical nuclear polarization at 77 k, Phys. Rev. Lett. 84 (2000) 171.

[45] K. Takeda, K. Takegoshi, T. Terao, Dynamic nuclear polarization by photoexcitedtriplet electron spins in polycrystalline samples, Chem. Phys. Lett. 345 (2001) 166.

[46] K. Takeda, K. Takegoshi, T. Terao, Dynamic Nuclear Polarization by Electron Spins in the Photoexcited Triplet State: I. Attainment of Proton Polarization of 0.7 at 105 K in Naphthalene, J. Phys. Soc. Japan 73 (2004) 2313.

[47] K. Takeda, K. Takegoshi, T. Terao, Dynamic Nuclear Polarization by Electron Spins in the Photoexcited Triplet State: II. High Polarization of the Residual Protons in Deuterated Naphthalene, J. Phys. Soc. Japan 73 (2004) 2319.

[48] N.P. Wickramasinghe, M. Shaibat, Y. Ishii, Enhanced Sensitivity and resolution in ^{1}H Solid-State NMR Spectroscopy of Paramagnetic Complexes under Very Fast Magic Angle Spinning, J. Am. Chem. Soc. 127 (2005) 5796.

[49] C. G. Moreland, ^{13}C-^{13}C Dipolar Interactions as Relaxation Mechanism, J. Magn. Reson. 15 (1974) 596.

[50] R.E. London, N.A. Matwiyoff, D.D. Mueller, Spin-lattice relaxation time in an AM(X_n): Application to ^{13}C relxation in enriched molecules, J. Chem. Phys. 63 (1975) 4442.

[51] K. Akasaka, S. Ganapathy, C.A. McDowell, A. Naito, Spin-spin and spin-lattice contributions to the rotating frame relaxation of ^{13}C in L-alanine, J. Chem. Phys. 78 (1983) 3567.

[52] G. Kervern, G. Pintacuda, Y. Zhang, E. Oldfield, C. Roukoss, E. Kuntz, E. Herdweck, J-M. Basset, S. Cadars, A. Lesage, C. Coperet, L. Emsley, Solid-State NMR of a Paramagnetic DIAD-Fe^{II} Catalyst: Sensitivity, Resolution Enhancement, and Structure-Based Assignments, J. Am. Chem. Soc. 128 (2006) 13545.

[53] G. Kervern, G. Pintacuda, L. Emsley, Fast Adiabatic pulses for Solid-State NMR paramagnetic systems, Chem. Phys. Lett. 475 (2007) 157.

[54] Y. Ishii, N.P. Wickramasinghe, S. Chimon, A New Approach in 1D and 2D ^{13}C High Resolution Solid-State NMR Spectroscopy of Paramagnetic Organometallic Complexes by Very Fast Magic Angle Spinning, J. Am. Chem. Soc. 125 (2003) 3438.

[55] N.P. Wickramasinghe, Y. Ishii, Sensitivity enhancement, assignment, and distance measurement in ^{13}C solid-state NMR spectroscopy for paramagnetic systems under fast magic angle spinning, J. Magn. Reson. 181 (2006) 233.

[56] N. P. Wickramasinghe, M. Kotecha, A. Samoson, J. Past, Y. Ishii, Sensitivity enhancement in ^{13}C solid-state NMR of protein microcrystals by use of paramagnetic metal ions for optimizing ^{1}H T1 relaxation, J. Magn. Reson. 184 (2007) 350.

[57] A. Samoson, T. Tuherm, J. Past, Ramped-Speed Cross Polarization MAS NMR, J. Magn. Reson. 149 (2001) 264.

[58] M. Alla, E. Lippmaa, Resolution limits in magic-angle rotation NMR spectra of polycrystalline solids, Chem. Phys. Lett. 87 (1982) 30.

[59] K. Liu, D. Ryan, K. Nakanishi, A. McDermott, Solid-Stae NMR Studies of Paramagnetic Coordination Complexes: A Comparision of Protons and Deuterons in Detection and Decoupling, J. Am. Chem. Soc. 117 (1995) 6897.

[60] A. F. McDowell, N. L. Adolphi, Operating nanoliter scale NMR microcoils in a 1 tesla field, J. Magn. Reson. 188 (2007) 74.

[61] K. Yamauchi, J. W. G. Janssen, A. P. M. Kentgens, Implementing solenoid microcoils for wide-line solid-state NMR, J. Magn. Reson. 167 (2004) 87.

[62] K. Takeda, A highly integrated FPGA-based nuclear magnetic resonance spectrometer, Rev. Scien. Ins. 78 (2007) 033103.

[63] U. Meyer-Baese, Digital Signal Processing with Field Programmable Gate Arrays, Springer-Verlag 2004.

Acknowledgement

First of all, I must express my gratitude to the following reviewers, Prof. Masahiro Kitagawa, Prof. Yoshio Kitaoka, Prof. Hideo Itozaki, and Dr. Kazuyuki Takeda for their comments and discussions. Like any part of our life, 'constructive' comments and feedbacks are essential essence for self-imporovement. For which I shall always remember that higher achievement one can get, the more likely they are to be trapped into their own self-assessment, which can be dangerous at time. A new moral-line, which were developed by them shall always be based on human-peacefulness and well being of society around them.

No word can replace my appreciation to Dr. Kazuyuki Takeda, who is my mentor and Prof. Masahiro Kitagawa, who is the group leader. Ample freedom and space as far as my research is concerned is what I appreciated much from Prof. Kitagawa. Dr. Takeda, who has been the source of my strength, patiently checked through my manuscripts, and has shown me the beauty of science and engineering. From him, I learnt to be a lot more confident and being very independent in carry out my work. By my final year, I was almost alone doing my work eversince he had moved to another university due to promotion. I would definately reckoned him as a good role-model for me, now and in future.

This work will definately not be completed without the helps of our collaborators in Kyoto University, led by Prof. Takegoshi and National Chemical Physics and Biophysics of Estonia, led by Dr. Ago Samoson. Dr. Ago Samoson, who came across my work in Experimental Nuclear Magnetic Conference 2007, promptly invited me for a short stay in his laboratory. With the state-of-the-art of his ultra fast sample spinning probe, we have then been able to demonstrate high-resolution and high sensitivity paramagnetic spectroscopy with our cp technique, which at that time many researchers have no faith on using conventional cp technique. Also thanks to all the staffs in National Chemical Physics and Biophysics, especially Dr. Heinmaa Ivo, Dr. Past Jaan and Dr. Anupold, Tiit, who made stay in Estonia wonderful.

Not forgeting about future (Dr.) Akinori Kagawa and (Dr.) Munehiro Inukai, who have been helping me in many technical aspects as well as my good buddies in Japan. Also, my others current and previous laboratory members such as Dr. Saitoh Akira and Dr. Robabeh Rahimi who have been very excellent 'sempai' to me. Our lovely secretary, Miss Hattori and Miss Hazama (of COE) who had assisted me in administration works are also greatly acknowledged.

Last but not least, thousands of thanks to everyone in my family members; my father Mr. Peng Koh Hoe, my mum Madam Oui Kim Choo and all my brothers and sisters. They have been very excellent example for me, one being a medical doctor who is currently pursuing his specialist and the other being one of the top student in the whole country. Both my younger brothers too, are currently pursuing their postgraduate study in overseas. Finally I would like to acknowledge the Japanese Government for providing me a full-scholarship throughout my master and Ph.D programme and being a fellow in 21st Century Center of Excellence, Japan for the past few years.

List of Publications

This thesis is based on the following publications, conference papers and manuscripts.

List of Peer-Reviewed Publications

[1] W.K. Peng, K. Takeda, and M. Kitagawa, A New Techniques for Cross Polarization Compatible with High Spinning Frequencies and High Magnetic Fields, Chem. Phys. Lett. 417 (2006) 58.

[2] W.K. Peng and K. Takeda, Efficient Cross Polarization with Simultaneous Adiabatic Frequency Sweep on the Source and Target Channels, J. Magn. Reson. 188 (2007) 267.

[3] W.K. Peng, A. Samoson, and M. Kitagawa, Simultaneous Adiabatic Spin-locking Cross Polarization in Solid-State NMR of Paramagnetic Complexes, Chem. Phys. Lett. (under review).

List of Peer-Reviewed Conferences

[1] W.K. Peng and K. Takeda, New Techniques for Cross Polarization with Treatment on Relaxation, 47th Experimental Nuclear Magnetic Resonance Conference, California, April 2006.

[2] W.K. Peng and K. Takeda, Efficient Cross Polarization with Simultaneous Adiabatic Sweep on the Source and Target Spins Applicable for Spins with Fast Relaxation, 48th Experimental Nuclear Magnetic Resonance Conference, Florida, April 2007.

[3] W.K. Peng, K. Takeda, and A. Samoson, Large bandwidth sensitivity enhancement in paramagnetic system with Simultaneous Adiabatic Frequency Sweep on the Source and Target Channels, SADIS CP, 49th Experimental Nuclear Magnetic

Resonance Conference, California, March 2008.

List of International and Domestic Conferences

[1] K. Takeda and W.K. Peng, A New Techniques for Cross Polarization Compatible with High Spinning Frequencies and High Magnetic Fields, PACIFICCHEM 2005, Hawaii, Dec 2005.

[2] W.K.Peng, K. Takeda, and M. Kitagawa, A New Techniques for Cross Polarization Compatible with High Spinning Frequencies and High Magnetic Fields, 1st Asia-Pacific NMR Symposium, Yokohama, Nov 2005.

[3] W.K. Peng, and K. Takeda, Cross Polarization with Simultaneous Adiabatic Sweep on I and S spins, The 45th Annual Meeting of The NMR Society of Japan, Nov 2006.

[4] W.K. Peng and K. Takeda, Cross Polarization with Simultaneous Adiabatic Sweep on I and S spins, 21st Century Center of Excellence Japan Symposium, March 2007.

[5] W.K. Peng, and M. Kitagawa, Large bandwidth sensitivity enhancement in paramagnetic system with Simultaneous Adiabatic Frequency Sweep on the Source and Target Channels, SADIS CP, 2nd International Workshop on Materials Science and Nano-Engineering, Awaji, Japan, Dec 2007.

List of International Awards

[1] *Student Travel Award*
W.K. Peng and K. Takeda, New Techniques for Cross Polarization with Treatment on Relaxation, 47th Experimental Nuclear Magnetic Resonance Conference, California, April 2006.

[2] *Student Travel Award Funded by Suraj P. Manrao Science Foundation*
W.K. Peng and K. Takeda, Efficient Cross Polarization with Simultaneous Adiabatic Sweep on the Source and Target Spins Applicable for Spins with Fast Relaxation, 48th Experimental Nuclear Magnetic Resonance Conference, Florida, April 2007.

[3] *Student Travel Award*
W.K. Peng, K. Takeda, and A. Samoson, Large bandwidth sensitivity enhancement in paramagnetic system with Simultaneous Adiabatic Frequency Sweep on the Source and Target Channels, SADIS CP, 49th Experimental Nuclear Magnetic Resonance Conference, California, March 2008.

Appendices

Appendix A

Mathematica Source Code: Spin dynamics of two interacting spins

Numerical-code for buildup curve

```
W1S;
DWS = SweepS*((-t/ct) + 1);
WeffS = ((W1S)^2 + (DWS)^2)^(1/2);
W1H;
DWH = SweepH*((-t/ct) + 1);
WeffH = ((W1H)^2 + (DWH)^2)^(1/2);
alphaS = W1S/WeffS;
alphal = W1H/WeffH;
deff = Sin[alphal]*Sin[alphaS]*d;
Δ = WeffH - WeffS;
sol =
    NDSolve[{
        mx'[t] - my[t]*Δ == 0,
        my'[t] - 2*deff*mz[t] + Δ*mx[t] == 0,
        mz'[t] + 2*deff*my[t] == 0,
        mx[0] == a, my[0] == b, mz[0] == c
        },
      {mx, my, mz},
      {t, 0, ct}
      ];
```

Numerical-code for chemical-shift dependent profile

```
Block[
{ct=0.5, do=40, ¥[CapitalOmega]I=0,   W1H=180,  SweepH=300,  SweepS=400,
      wf=100, w0=100},
  sol=
    NDSolve[{
        mx' [t]-my[t]*¥[CapitalDelta]¥[Equal]0,
        my' [t]-2*deff*mz[t]+¥[CapitalDelta]*mx[t]¥[Equal]0,
        mz' [t]+2*deff*my[t]¥[Equal]0,
        mx[0]¥[Equal]0, my[0]¥[Equal]0, mz[0]¥[Equal]1
        },
       {mx, my, mz},
       {t, 0, ct}
       ];
                ListPlot[
                   Flatten[
                         Table[
                             Table[
                               Evaluate[
            Sum[(0.01*0.5*Sin[theta] )*({0.5*(1-mz[t])}/.sol), {theta, 0, Pi, 0]
                                        ], {t, ct, ct, 0.5}
                                    ], {¥[CapitalOmega]S, 0, 100, 1}
                                ]
                          ], Filling ¥[Rule]Axis, PlotRange¥[Rule]{0, 1}
       ]
```

Appendix B
Delphi Source Code: Phase and Amplitude Modulation Table

```
unit Unit1;

interface

uses
  Windows, Messages, SysUtils, Variants, Classes, Graphics, Controls, Forms,
  Dialogs, StdCtrls, ComCtrls, math;

type
  TForm1 = class(TForm)
    Memo1: TMemo;
    GroupBox1: TGroupBox;
    GroupBox2: TGroupBox;
    Edit1: TEdit;
    Edit2: TEdit;
    Button1: TButton;
    Button2: TButton;
    StatusBar1: TStatusBar;
    Edit3: TEdit;
    Label1: TLabel;
    Label2: TLabel;
    Label3: TLabel;
    Label4: TLabel;
    Label5: TLabel;
    Edit4: TEdit;
    Edit5: TEdit;
    Edit6: TEdit;
    Edit7: TEdit;
    Edit8: TEdit;
```

```
    Label6: TLabel;
    Label7: TLabel;
    Label8: TLabel;
    Label9: TLabel;
    Label10: TLabel;
    Label11: TLabel;
    Label12: TLabel;
    procedure Button1Click(Sender: TObject);
    procedure Button2Click(Sender: TObject);
  private
    { Private 宣言 }
  public
    { Public 宣言 }
  end;

var
  Form1: TForm1;

implementation

{$R *.dfm}


procedure TForm1.Button1Click(Sender: TObject);
var
  dF,tauF:single;
  t:single;
  g:integer;
  k,n:integer;
begin
  dF:=StrToFloat(Edit1.Text);
  tauF:=StrToFloat(Edit2.Text);
  n:=StrToInt(Edit3.Text);



   Memo1.Lines.Clear;

   t:=0;
   for k:=0 to n-1 do begin

     g:= trunc(-180.0 * dF * t * (-t/tauF + 1.0)) mod 360;
     if g<0 then g:=g+360;

     Memo1.Lines.Add(IntToStr(g));

     t:=t+tauF/n;
   end;

   Memo1.SelectAll;
   Memo1.CopyToClipboard;
```

```
  Statusbar1.SimpleText:=
  '(dF, ct, n) = (' + Edit1.Text + ', '
      + Edit2.Text + ', '
      + Edit3.Text
  + '): The phase table has been copied to the Clipboard.';

end;

procedure TForm1.Button2Click(Sender: TObject);
var
  amp, tauS, s, tauF: single;
  b,t:single;
  k,n: integer;
begin

  amp:=StrToFloat(Edit4.Text);
  tauS:=StrToFloat(Edit5.Text);
  s:=StrToFloat(Edit6.Text);
  tauF:=StrToFloat(Edit7.Text);
  n:=StrToInt(Edit8.Text);


 Memo1.Lines.Clear;
   t:=0;
   for k:=0 to n-1 do begin
     if t<=tauS then
       b:=0.5* amp * (1 + Tanh(Pi * s *((2*t/tauS)-1)))
     else
       b:=amp;

     Memo1.Lines.Add(FloatToStr(b));
     t:=t+tauF/n;
   end; // for

   Memo1.SelectAll;
   Memo1.CopyToClipboard;

   Statusbar1.SimpleText:=
   '(f*amp, tauS, steep, ct, n) = (' + Edit4.Text + ', '
       + Edit5.Text + ', '
       + Edit6.Text + ', '
       + Edit7.Text + ', '
       + Edit8.Text
   + '): The amp table has been copied to the Clipboard.';

 end;

 end.
```

Appendix C
Printed Circuit Board Design

Filter Board

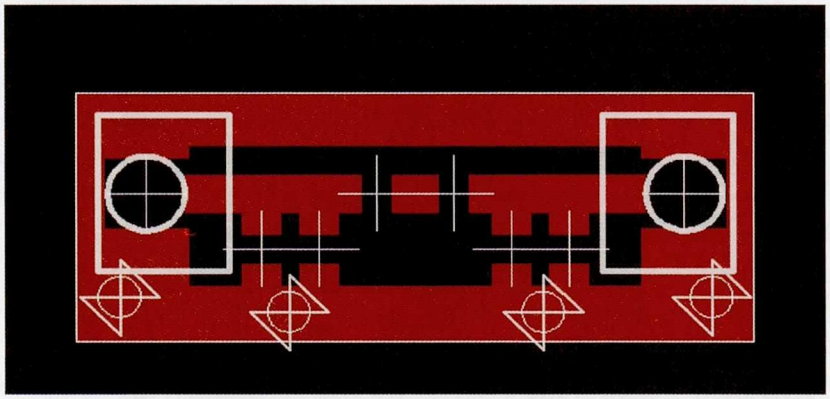

RF-feedback Switching Board

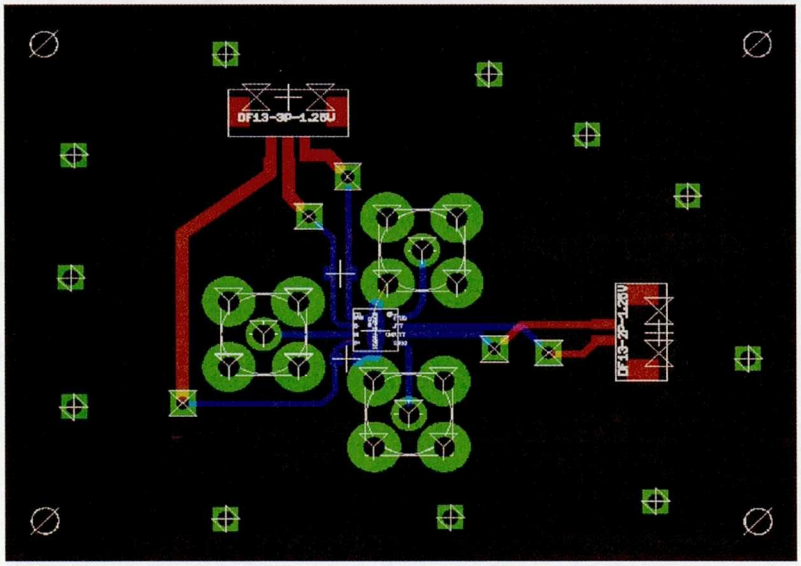

Receiver-AD9245

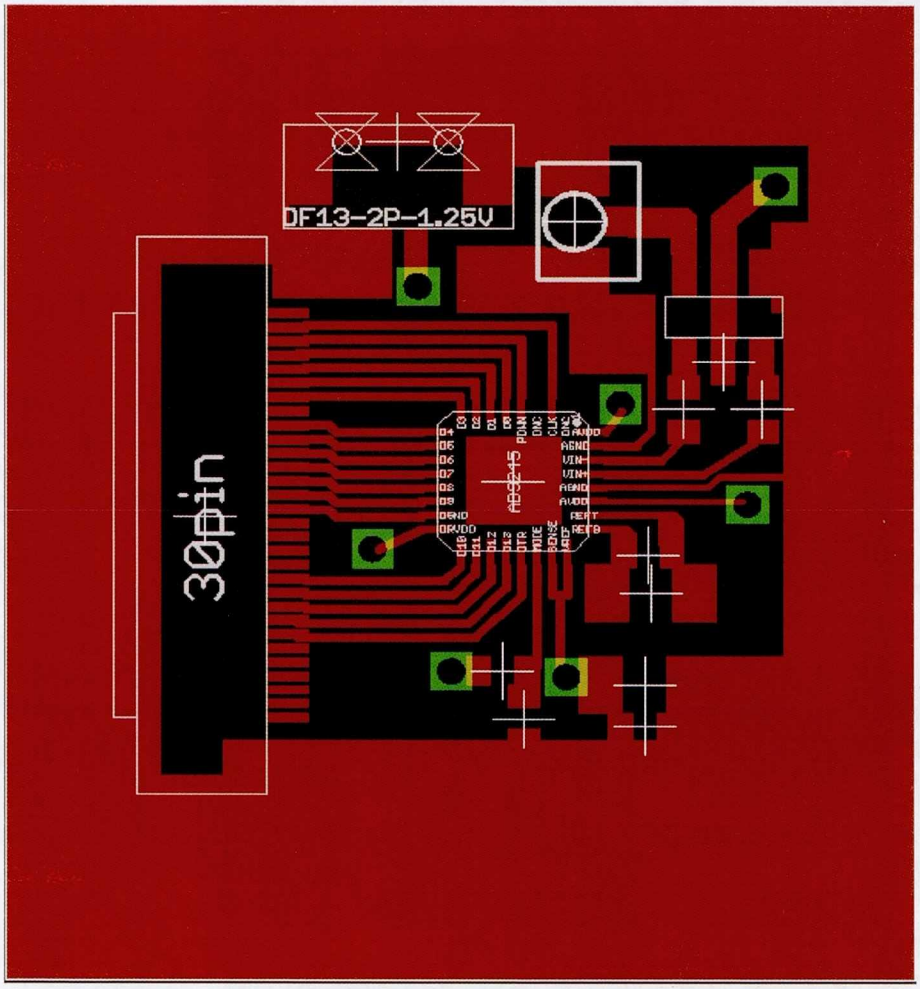

Appendix D

Circuit for home-made passive filter

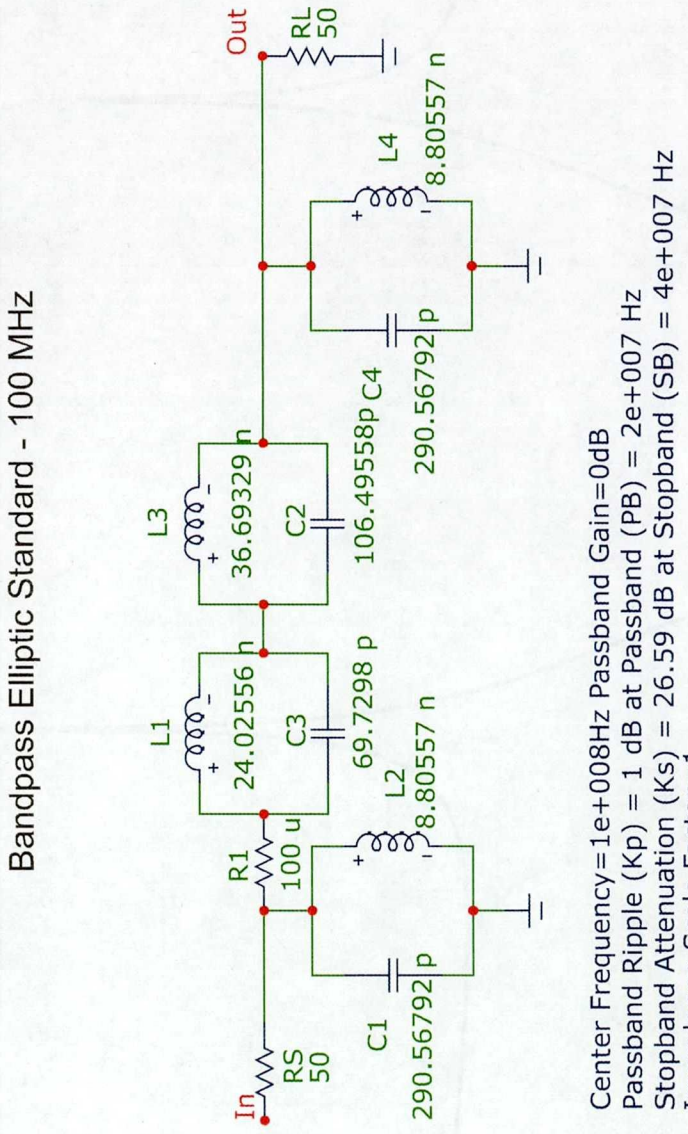

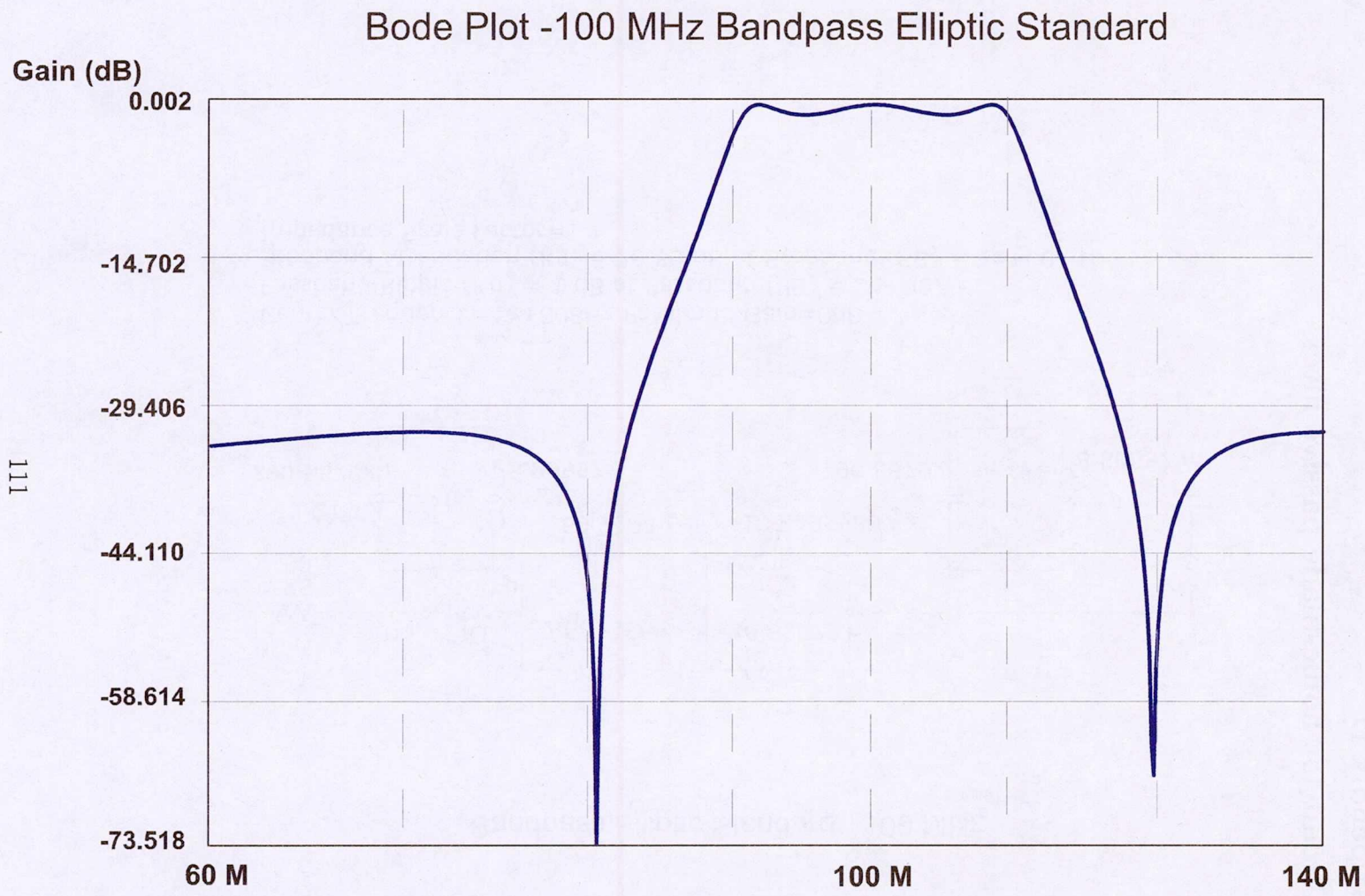
Bode Plot -100 MHz Bandpass Elliptic Standard
Gain (dB)
0.002
-14.702
-29.406
-44.110
-58.614
-73.518
60 M
100 M
140 M

Bandpass Elliptic Standard - 400 MHz

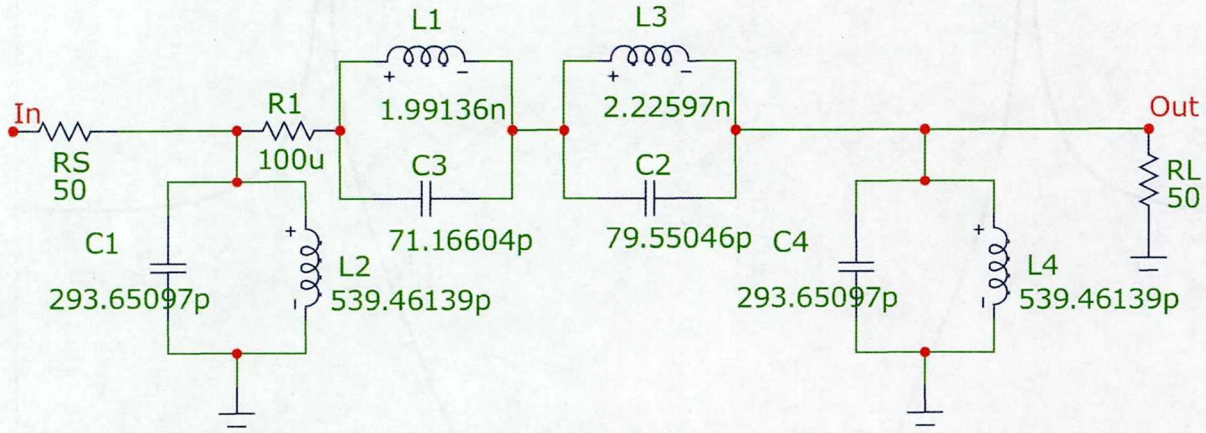

Center Frequency=4e+008Hz Passband Gain=0dB
Passband Ripple (Kp) = 1 dB at Passband (PB) = 2e+007 Hz
Stopband Attenuation (Ks) = 26.59 dB at Stopband (SB) = 4e+007 Hz
Impedance Scale Factor=1

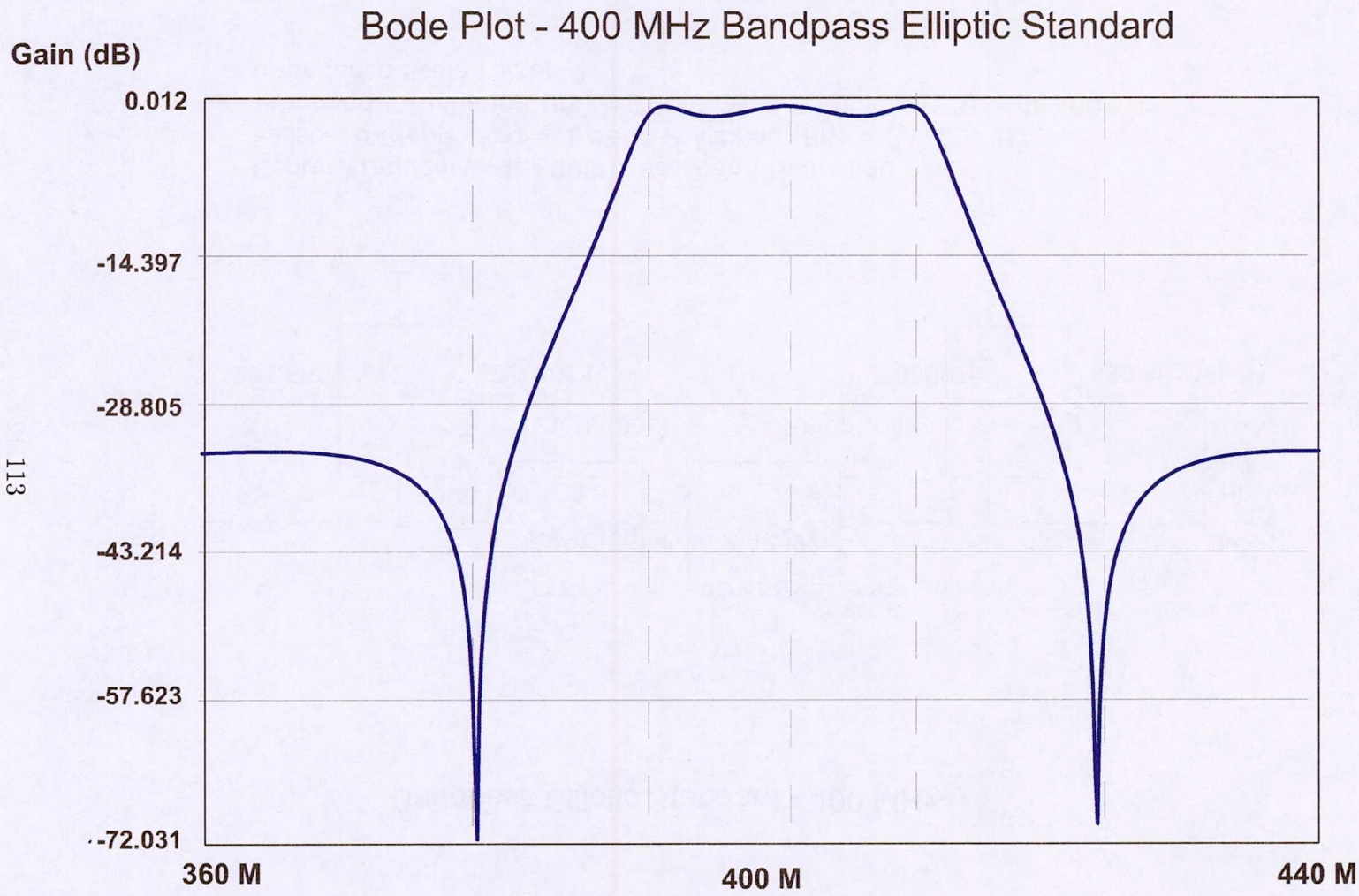
Bode Plot - 400 MHz Bandpass Elliptic Standard
Gain (dB)
0.012
-14.397
-28.805
-43.214
-57.623
-72.031
360 M
400 M
440 M

Included Papers

[1] W.K. Peng, K. Takeda, and M. Kitagawa, A New Techniques for Cross Polarization Compatible with High Spinning Frequencies and High Magnetic Fields, Chem. Phys. Lett. 417 (2006) 58.

[2] W.K. Peng and K. Takeda, Efficient Cross Polarization with Simultaneous Adiabatic Frequency Sweep on the Source and Target Channels, J. Magn. Reson. 188 (2007) 267.

[3] W.K. Peng, A. Samoson, and M. Kitagawa, Simultaneous Adiabatic Spinlocking Cross Polarization in Solid-State NMR of Paramagnetic Complexes, Chem. Phys. Lett. (under review).

Available online at www.sciencedirect.com
SCIENCE DIRECT®
Chemical Physics Letters 417 (2006) 58–62
CHEMICAL PHYSICS LETTERS
www.elsevier.com/locate/cplett

A new technique for cross polarization in solid-state NMR compatible with high spinning frequencies and high magnetic fields

Weng Kung Peng, Kazuyuki Takeda *, Masahiro Kitagawa

Division of Advanced Electronics and Optical Science, Graduate School of Engineering Science, Osaka University, D421, 1-3 Machikaneyama, Toyonaka, Osaka 560-8531, Japan

Received 23 August 2005; in final form 4 October 2005
Available online 24 October 2005

Abstract

The idea of integrated cross polarization which has been utilized for electron-to-nucleus polarization transfer is applied to nucleus-to-nucleus polarization transfer. Instead of using a $\frac{\pi}{2}$ pulse followed by a $\frac{\pi}{2}$ phase-shifted locking pulse like in the conventional cross polarization, irradiation with a single phase is applied together with adiabatic frequency sweep from far off-resonance toward on-resonance. This is capable of locking individual spin packets even in the presence of considerable spectral distribution and/or line broadening. Thus, this technique can provide efficient polarization transfer for spin species having large chemical shifts and experiments in high static fields.

1. Introduction

Cross polarization (CP) [1,2] is widely used in solid-state NMR spectroscopy to enhance sensitivity of nuclear spin species having relatively small gyromagnetic ratios such as ^{13}C and ^{15}N. In particular, CP combined with magic angle spinning (MAS) [3,4], namely CP-MAS [5], is one of the most successful methodologies in solid-state NMR, and is utilized to investigate static structure and dynamics of solid materials. Recent technological development has brought very fast MAS into practice, which can considerably improve spectral resolution [6–8]. On the other hand, the Hartmann–Hahn matching profile splits into narrow sidebands under fast MAS, making polarization-transfer experiments sensitive to rf-intensity mismatch. In order to improve such mismatch-tolerance, a number of techniques have been proposed which employ modulation of rf amplitude or frequency [9–16].

In parallel, the available static magnetic fields have been increased remarkably, which is preferred to further enhance sensitivity and spectral resolution. However, like fast MAS led to the problem of the sensitive Hartmann–Hahn condition, rise in static field has also brought a challenge into CP due to the increased spectral distribution or resonance-line broadening by isotropic and anisotropic chemical shifts. Large spectral distribution inevitably leads to off-resonance irradiation, which results in incomplete spin lock. Since only those components of the spin magnetization which is locked along the effective field contribute to polarization transfer, high fields comes into conflict with CP.

What will be required henceforth is a new CP technique which is compatible with both fast MAS and high fields, that is, a CP technique that is robust against rf-mismatch and is capable of wideband spin lock. The purpose of this work is to present one such. Instead of applying a $\frac{\pi}{2}$ pulse followed by the locking pulse whose phase is shifted by $\frac{\pi}{2}$ with respect to the first pulse, this technique uses irradiation with a single phase together with an adiabatic frequency sweep from far off-resonance toward on-resonance. In this technique, the effective field has the maximum amplitude at the beginning and is decreased gradually as the frequency gets close to on-resonance. Thus, the Hartmann–Hahn condition is fulfilled during the sweep for a wide range of rf amplitudes. In previous works on

* Corresponding author. Fax: +81 6 6850 6321.
E-mail address: takeda@qc.ee.es.osaka-u.ac.jp (K. Takeda).

0009-2614/$ - see front matter © 2005 Elsevier B.V. All rights reserved.
doi:10.1016/j.cplett.2005.10.012

frequency sweep CP (FSCP) [13], a $\frac{\pi}{2}$ pulse is initially applied and then frequency is swept from on-resonance to far off-resonance. Although the Hartmann–Hahn condition is relaxed, the problem of incomplete spin lock remain unsolved. On the other hand, the present technique is free from the initial $\frac{\pi}{2}$ pulse and employs the converse frequency sweep, making it possible to lock the individual spin packets with relatively low rf powers. Improvement in spin locking efficiency is also expected in homogeneously-broadened spin systems such as protons in rigid solids. The present approach would also be advantageous when strong rf irradiation should be avoided for investigations of heat-sensitive biological materials.

The technique in which adiabatic passage serves for both efficient spin lock and error-tolerant Hartmann–Hahn matching has originally been demonstrated in electron-to-proton polarization transfer [17–23], and originally called integrated solid effect, and then integrated cross polarization (ICP). Accordingly, we call the present nuclear-spin-version technique nuclear integrated cross polarization (NICP). We demonstrate NICP in powder mixture of L-alanine and glycine, and show that the Hartmann–Hahn matching profile is as insensitive as FSCP, and the ^{1}H-^{13}C polarization transfer is more efficient than that by the FSCP scheme, as a consequence of effective locking of the homogeneously broadened ^{1}H spins even with relatively low rf amplitudes.

2. Theory

We consider here an isolated pair of heteronuclear spins $I = \frac{1}{2}$ and $S = \frac{1}{2}$, and suppose that linear frequency sweep is applied at I from far off-resonance toward on-resonance, while on-resonance cw irradiation is applied at S, as schematically described in Fig. 1c. The rotating-frame Hamiltonian during NICP is represented as

$$H = \omega_{1S}S_x + \Delta\omega_I(t)I_z + \omega_{1I}I_x + D(t)I_zS_z. \tag{1}$$

Here, ω_{1I} and ω_{1S} are the amplitudes of rf irradiation at I and S, respectively. $D(t)$ is the magnitude of the dipolar coupling between them, which is modulated by MAS and is given by [24,25]

$$D(t) = d_{IS}[G_1\cos(\omega_r t) + G_2\cos(2\omega_r t)], \tag{2}$$

$$d_{IS} = \frac{\mu_0\gamma_I\gamma_S\hbar}{4\pi r_{IS}^3}, \tag{3}$$

where ω_r is a spinning frequency, and G_1 and G_2 describe the orientation of the internuclear vector in the rotor-fixed coordinate, and r_{IS} is the internuclear distance between I and S. Under the linear frequency sweep, $\Delta\omega_I(t)$ is represented as

$$\Delta\omega_I(t) = \Delta F\left(1 - \frac{t}{\tau}\right), \tag{4}$$

where ΔF and τ is the range and the duration of the frequency sweep. When the sweep rate is slow enough to satisfy the adiabatic condition [26]

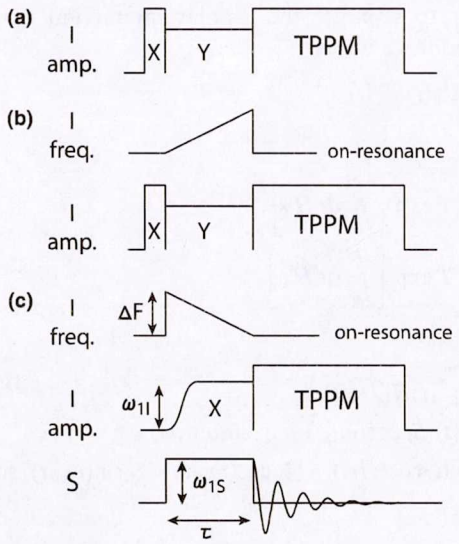

Fig. 1. Pulse sequences for (a) conventional CP, (b) frequency-sweep CP (FSCP), and (c) NICP. Instead of irradiating at the I spin with a $\pi/2$ pulse followed by the spin lock pulse whose phase is shifted by $\pi/2$ with respect to the initial pulse, a single phase irradiation is applied together with frequency sweep from far off-resonance toward on-resonance. For better spin locking efficiency, the rf irradiation may be switched on tangentially, as shown in (c).

$$\left|\frac{d\Delta\omega_I(t)}{dt}\right| \ll \frac{\omega_{\text{eff}}^2}{\sin\alpha} \quad \text{or} \quad \frac{\Delta F}{\tau} \ll \frac{\omega_{\text{eff}}^2}{\sin\alpha} \tag{5}$$

the magnetization of the I spin follows the direction of the effective field, which is initially points in the z axis and is gradually tilted toward the x axis. Here, ω_{eff} is the amplitude of the effective field and α is the tilt angle of the effective field from the z axis:

$$[\omega_{\text{eff}}(t)]^2 = [\Delta\omega_I(t)]^2 + \omega_{1I}^2, \tag{6}$$

$$\alpha(t) = \tan^{-1}\left[\frac{\omega_{1I}}{\Delta\omega_I(t)}\right]. \tag{7}$$

When the initial frequency offset ΔF is much larger than the spectral distribution or resonance-line broadening of the I spin species, all spin packets can be locked along the effective field. For better spin lock performance, the irradiation amplitude may be switched on gradually, as described in Fig. 1c.

Now we transform H into the tilted rotating frame in which the effective fields for both spins point in the z axis. This is accomplished by the interaction representation with respect to αI_y and $\frac{\pi}{2}S_y$, leading to

$$H^{\text{TR}} = H_Z + H_D, \tag{8}$$

$$H_Z = \omega_{1S}S_z + \omega_{\text{eff}}(t)I_z, \tag{9}$$

$$H_D = D(t)S_x(I_z\cos\alpha + I_x\sin\alpha). \tag{10}$$

The evolution of the system during NICP is described by the propagator $U(t)$ written as

$$U(t) = T\exp\left[\int_0^t dt' H^{\text{TR}}\right]. \tag{11}$$

In order to separate the dipolar interaction from the rf interaction, we write

$$U(t) = U_0(t)U_1(t), \tag{12}$$

where

$$U_0(t) = T\exp\left[\int_0^t \mathrm{d}t' H_Z\right], \tag{13}$$

$$U_1(t) = T\exp\left[\int_0^t \mathrm{d}t' \widetilde{H}_D\right] \tag{14}$$

with

$$\widetilde{H}_D = U_0^{-1}(t)H_D U_0(t) \tag{15}$$

$$= D(t)(S_x\cos(\omega_{1S}t) - S_y\sin(\omega_{1S}t)) \times [I_z\cos(\alpha(t)) + (I_x\cos(\omega_{\mathrm{eff}}t) - I_y\sin(\omega_{\mathrm{eff}}t))\sin(\alpha(t))] \tag{16}$$

$$= \frac{1}{4}D(t)\{\sin(\alpha(t)) \times [\cos(\Delta(t)t)(I_+S_- + I_-S_+) + \mathrm{i}\sin(\Delta(t)t)(I_+S_- - I_-S_+) + \cos(\Sigma(t)t)(I_+S_+ + I_-S_-) + \mathrm{i}\sin(\Sigma(t)t)(I_+S_+ - I_-S_-)] + 2\cos\alpha(t)[\exp(\mathrm{i}\omega_{1S}t)S_+ + \exp(-\mathrm{i}\omega_{1S}t)S_-]I_z\}, \tag{17}$$

and with

$$\Delta(t) = \omega_{\mathrm{eff}}(t) - \omega_{1S}, \tag{18}$$

$$\Sigma(t) = \omega_{\mathrm{eff}}(t) + \omega_{1S}. \tag{19}$$

When the Hartmann–Hahn condition $\Delta(t) = n\omega_r$ ($n = -2,-1,1,2$) is satisfied, interference between the spatial part and the spin part in $\widetilde{H}_D$ leads to the non-vanishing zeroth-order average Hamiltonian

$$\overline{\widetilde{H}}_D = \frac{1}{8}d_{IS}G_n\sin\alpha(I_+S_- + I_-S_+). \tag{20}$$

Thus, transition between the states $|+\,-\rangle$ and $|-\,+\rangle$, and thereby transfer of polarization from I to S, is induced by the flip-flop term of the dipolar interaction given in Eq. (20), provided that the density operator has populations on the diagonal states $|+\,-\rangle\langle+\,-|$ and $|-\,+\rangle\langle-\,+|$ in the tilted rotating frame. This is ensured in NICP when the adiabatic condition given in Eq. (5) is fulfilled, so that the I spin magnetization is locked along the effective field, or equivalently, the quantization axis in the tilted rotating frame. It is worth noting here that the Hartmann–Hahn condition $\Delta(t) = n\omega_r$ is realized for considerable ranges of ω_{1S} and ω_{1I}, because the amplitude of the effective field starts with the maximum ($\sim\Delta F$) and ends with the minimum (ω_{1I}) values, and thereby takes a wide range during NICP.

In order to provide a crude but visual account for the polarization transfer process, we introduce the zero-quantum (ZQ) subspace spanned by the states $|+\,-\rangle$ and $|-\,+\rangle$, in which time evolution is independent of that in the double-quantum (DQ) subspace spanned by the states $|+\,+\rangle$ and $|-\,-\rangle$ [10]. Dropping the nonsecular terms, we express the zero-quantum Hamiltonian H^{ZQ} as

$$H^{\mathrm{ZQ}} = \begin{pmatrix} \Delta(t) - n\omega_r & \frac{1}{8}d_{IS}G_n\sin\alpha \\ \frac{1}{8}d_{IS}G_n\sin\alpha & -\Delta(t) + n\omega_r \end{pmatrix} \tag{21}$$

$$= 2(\Delta(t) - n\omega_r)I_z^{\mathrm{ZQ}} + \frac{1}{4}d_{IS}G_n\sin\alpha I_x^{\mathrm{ZQ}}, \tag{22}$$

where I_z^{ZQ} and I_x^{ZQ} are fictitious spin-$\frac{1}{2}$ operators given by [27,25]

$$I_z^{\mathrm{ZQ}} = \frac{1}{2}[|+\,-\rangle\langle+\,-| - |-\,+\rangle\langle-\,+|], \tag{23}$$

$$I_x^{\mathrm{ZQ}} = \frac{1}{2}[|+\,-\rangle\langle-\,+| + |-\,+\rangle\langle+\,-|]. \tag{24}$$

According to the vector representation scheme for a general two-level system [28], H^{ZQ} gives the 'effective field' $\omega_{\mathrm{eff}}^{\mathrm{ZQ}} = (\frac{1}{4}d_{IS}G_n\sin\alpha, 0, 2(\Delta(t) - n\omega_r))$ in the ZQ subspace. Fig. 2a and b describes how $(\omega_{\mathrm{eff}}^{\mathrm{ZQ}})_z$ and $(\omega_{\mathrm{eff}}^{\mathrm{ZQ}})_x$ change in time during NICP for $\omega_{1I}/2\pi = 35$ kHz, $\omega_{1S}/2\pi = 45$ kHz, $\Delta F/2\pi = 100$ kHz, and $\tau = 7.2$ ms. For simplicity, we assumed here that $\omega_r = 0$ and chose a IS dipolar interaction (40 kHz) arbitrarily. As is found in Fig. 2 c or d, the trajectory of the effective field in the ZQ subspace during NICP is reminiscent to that in the conventional rotating frame under a passage from far above-resonance to below-resonance. By an analogy with the conventional adiabatic

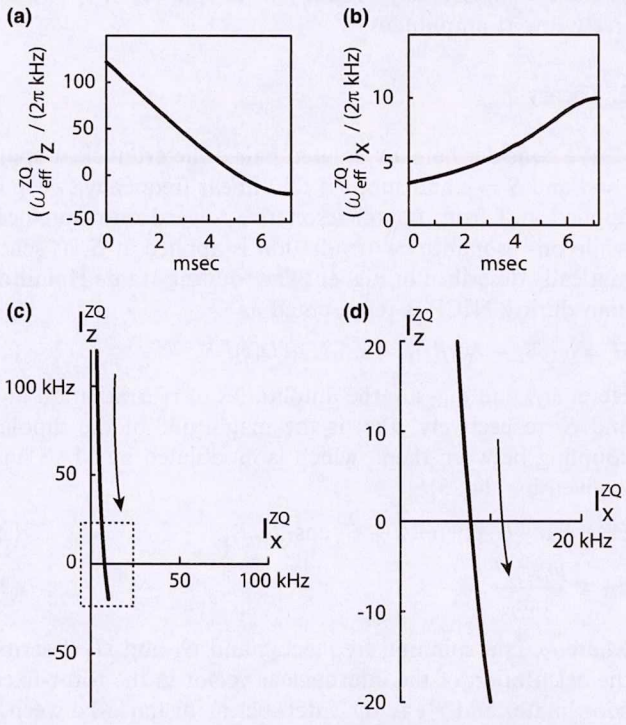

Fig. 2. (a) and (b) Calculated z and x components of the ZQ effective field $\omega_{\mathrm{eff}}^{\mathrm{ZQ}}$ for $\omega_{1I}/2\pi = 35$ kHz, $\omega_{1S}/2\pi = 45$ kHz, $\Delta F/2\pi = 100$ kHz, and $\tau = 7.2$ ms. For simplicity, $\omega_r = 0$ was assumed and an arbitrary IS dipolar interaction (40 kHz) was chosen. The trajectory of the effective field in the ZQ subspace, shown in (c), gives a crude but visual account for exchange of the spin states and thereby transfer of polarization, in analogy with the inversion of magnetization in the rotating frame by a passage from above to below resonance. (d) An expanded view of the region indicated by a dotted square in (c).

inversion, one can also expect that the 'inversion' takes place in the ZQ subspace, if the change of the ZQ effective field in time is sufficiently slow. The condition for the slow passage, which may be referred to as the adiabatic condition in the ZQ subspace, can be derived in the same manner as in the case of the conventional adiabatic condition [26], as follows. Using a general formula for vector kinetics, change of $\omega_{\text{eff}}^{\text{ZQ}}$ in time is described by

$$\frac{\mathrm{d}}{\mathrm{d}t}\omega_{\text{eff}}^{\text{ZQ}} = \mathbf{\Omega} \times \omega_{\text{eff}}^{\text{ZQ}} + \Omega_1 \omega_{\text{eff}}^{\text{ZQ}}, \tag{25}$$

where the vector $\mathbf{\Omega}$ and the scalar Ω_1 have dimension of frequency. Since $(\omega_{\text{eff}}^{\text{ZQ}})_y = 0$ in the present case, the only non-vanishing component of $\mathbf{\Omega}$ is Ω_y, whose expression is obtained from Eq. (25) as

$$\Omega_y = \frac{d_{IS}G_n}{2(\omega_{\text{eff}}^{\text{ZQ}})^2}[\Delta(t)\dot{\alpha}\cos\alpha - \dot{\Delta}(t)\sin\alpha]. \tag{26}$$

The adiabatic condition is satisfied when Ω_y has a negligible Fourier component at the frequency $\omega_{\text{eff}}^{\text{ZQ}}$, or $\Omega_y \ll \omega_{\text{eff}}^{\text{ZQ}}$. That is, if

$$\frac{d_{IS}G_n}{2}[\Delta(t)\dot{\alpha}(t)\cos\alpha - \dot{\Delta}(t)\sin\alpha] \ll (\omega_{\text{eff}}^{\text{ZQ}})^3 \tag{27}$$

is satisfied, NICP causes inversion in the ZQ subspace. Since inversion in the ZQ subspace is equivalent to swap of populations between the states $|+\,-\rangle\langle+\,-|$ and $|-\,+\rangle\langle-\,+|$, polarization transfer is shown to take place by NICP.

If the two-spin system is well isolated, the adiabatic inversion in the ZQ subspace causes complete exchange of spin polarizations between I and S, when only a single sideband of the Hartmann–Hahn matching profile is swept through. However, if a sweep is performed through multiple sidebands, polarization would be transferred back [12]. The way to avoid such multiple contacts in NICP is to choose ω_{1I} such that $\omega_{1S} + \omega_r < \omega_{1I} < \omega_{1S} + 2\omega_r$.

3. Experimental

Powder mixture of non-labeled L-alanine and glycine was packed in a Doty 5 mm rotor, and experiments were carried out in a magnetic field of 12.7 T at room temperature with a spinning speed of 10 kHz. The carrier frequencies for the ^{1}H and ^{13}C resonances were 499.789 and 125.686 MHz, respectively. After performing the NICP sequence, the ^{13}C magnetizations of the methyl (CH_3), the methylene (CH_2), the methine (CH), and the carboxyl (COOH) groups were measured under TPPM ^{1}H decoupling [29]. NICP experiments were performed for various ^{1}H irradiation amplitudes (ω_{1I}), while that (ω_{1S}) at the ^{13}C spins was fixed to 45 kHz. For better spin lock performance, the ^{1}H irradiation amplitude was tangentially turned on at the beginning of the frequency sweep.

For comparison, we have also performed the conventional CP and the FSCP experiments, whose pulse sequences are shown in Fig. 1a and b. In conventional CP and FSCP, a $\frac{\pi}{2}$ pulse was firstly applied, and then was the locking pulse whose phase was shifted by $\frac{\pi}{2}$ with respect to the first pulse. No rf modulation was used in conventional CP, while frequency sweep from on-resonance to far off-resonance was employed in FSCP.

4. Results and discussion

Among a number of experiments for various contact times and frequency sweep widths, the optimal results are shown in Fig. 3 for conventional CP (squares), FSCP (triangles), and NICP (circles). In the conventional CP experiment, the Hartmann–Hahn matching profiles show sidebands splitted by the spinning frequency (10 kHz) for the methyl and the carboxyl group, which is ascribed to relatively weak dipolar couplings between the ^{13}C and the ^{1}H spins. Such a sideband splitting was considerably suppressed in FSCP, because the amplitude of the ^{1}H effective field is ramped by the frequency sweep, so that the Hartmann–Hahn condition can be fulfilled for wide range of irradiation amplitudes. As demonstrated in Fig. 3, the flat matching profiles were also realized in NICP. This is

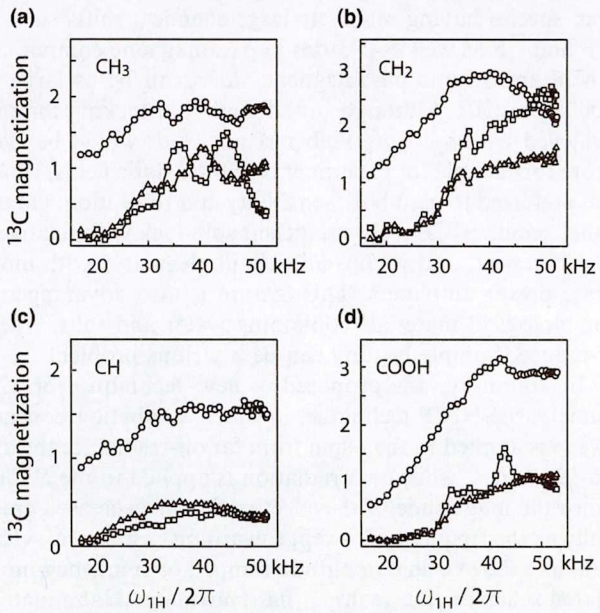

Fig. 3. ^{13}C magnetizations of (a) the methyl (CH_3), (b) the methylene (CH_2), (c) the methine (CH), and (d) the carboxyl (COOH) groups in powder mixture of L-alanine and glycine obtained with conventional CP (squares), FSCP (triangles), and NICP (circles) for various ^{1}H irradiation amplitudes. The spinning frequency was 10 kHz, and the carrier frequencies for the ^{1}H and ^{13}C channels were 499.789 and 125.686 MHz, respectively. Among a number of experimental results for various contact times and frequency-sweep widths, the optimal results were shown here for each carbon group. In conventional CP, the optimal contact times were 0.2, 5.5, 0.2 and 5.5 ms for the methyl, the methylene, the methine, and the carboxyl groups, respectively. In FSCP, the optimal sets of contact time and sweep width were (0.2 ms, 50 kHz), (5.5 ms, 80 kHz), (0.2 ms, 34 kHz), and (5.5 ms, 50 kHz), and in NICP were (7.2 ms, 100 kHz), (7.2 ms, 200 kHz), (7.2 ms, 100 kHz), and (7.2 ms, 100 kHz). The ^{13}C magnetizations were normalized with respect to those in thermal equilibrium.

because the trajectory of the effective field during NICP is nearly the same as that during FSCP except for its direction. Moreover, the ^{13}C magnetizations obtained in NICP were considerably larger than those in conventional CP and FSCP. This is ascribed to that the rf amplitude $\omega_{1I}/2\pi = 56$ kHz used for the initial $\frac{\pi}{2}$ pulse in conventional CP and FSCP was not sufficiently large as compared to the ^{1}H resonance-line broadening of the order of several tens of kilohertz, so that some amount of the spin packets could not be locked and were lost. On the other hand, the amplitude of the initial effective field (~100 kHz) in NICP was large enough to effectively lock the ^{1}H spin and let all the spin packets to participate in the polarization transfer process, even when the rf intensity was relatively small.

We have also found that the optimal sets of contact time and frequency-sweep width are nearly the same for the four carbon groups in NICP. The theoretical account for this favorable feature will require evaluation of the ZQ adiabatic condition in (27) by taking account of powder averaging and sample spinning, and will be published elsewhere.

The characteristic of NICP that the effective field has the maximum amplitude at the beginning of the sequence would also be advantageous for polarization transfer from spin species having relatively large chemical shifts such as ^{19}F and ^{31}P as well as protons in paramagnetic compounds where anisotropic paramagnetic shifts can be as large as 1000 ppm [30]. Although broadband spin locking may be achieved by employing higher rf power, it would be even more formidable for experiments in high static fields, which are preferred to gain both sensitivity and resolution. On the other hand, NICP realizes efficient spin lock with relatively low rf power, and is conveniently implemented with moderate power amplifiers. This feature is also advantageous for biological materials containing water and salts, where rf-induced sample heating can be a serious problem.

In summary, we proposed a new technique for CP, namely, the NICP technique, in which adiabatic frequency sweep is applied to the I spin from far off-resonance toward on-resonance, while cw irradiation is applied to the S spin. Since the magnitude of the effective field is decreased gradually as the frequency is swept toward on-resonance, NICP can, like the existing amplitude-ramped or frequency-modulated schemes can, realize a flat Hartmann–Hahn matching profile even for high spinning speeds. Adiabatic passage from far off- to on-resonance is capable of lock the individual spin packets even in the presence of considerable spectral distribution and/or line-broadening. Thus, NICP is useful when available rf power is limited, or for polarization transfer from spin species having large chemical shifts, or for experiments in high static fields.

Acknowledgement

This work was supported by the CREST program of the Japan Science and Technology Corporation.

References

[1] S.R. Hartmann, E.L. Hahn, Phys. Rev. 128 (1962) 2042.
[2] A. Pines, M.G. Gibby, J.S. Waugh, J. Chem. Phys. 59 (1973) 569.
[3] E.R. Andrew, A. Bradbury, R.G. Eades, Nature 182 (1958) 1659.
[4] I.J. Lowe, Phys. Rev. Lett. 2 (1959) 285.
[5] J. Schaefer, E.O. Stejskal, J. Am. Chem. Soc. 98 (1976) 1031.
[6] A. Samoson, T. Tuherm, Z. Gan, Solid State Nucl. Magn. Reson. 20 (2001) 130.
[7] A. Samoson, Encyclopedia of Nuclear Magnetic Resonance 9 (2002) 59.
[8] A. Samoson, T. Tuherm, J. Past, A. Reinhold, T. Anupold, I. Heinmaa, Topics in Current Chemistry 246 (2004) 15.
[9] S. Hediger, B.H. Meier, R.R. Ernst, Chem. Phys. Lett. 213 (1993) 627.
[10] S. Hediger, B.H. Meier, N.D. Kurur, G. Bodenhausen, R.R. Ernst, Chem. Phys. Lett. 223 (1994) 283.
[11] G. Metz, X. Xiaoling, S. Smith, J. Magn. Reson. A110 (1994) 219.
[12] S. Hediger, B.H. Meier, R.R. Ernst, Chem. Phys. Lett. 240 (1995) 449.
[13] A.C. Kolbert, A. Bielecki, J. Magn. Reson. A116 (1995) 29.
[14] M. Baldus, D.G. Geurts, S. Hediger, B.H. Meier, J. Magn. Reson. A118 (1996) 140.
[15] R. Fu, P. Pelupessy, G. Bodenhausen, Chem. Phys. Lett. 264 (1997) 63.
[16] S. Hediger, P. Signer, M. Tomaselli, R.R. Ernst, B.H. Meier, J. Magn. Reson. 125 (1997) 291.
[17] A. Henstra, P. Dirksen, W.Th. Wenckebach, Phys. Lett. A 134 (1988) 134.
[18] A. Henstra, T.-S. Lin, J. Schmidt, W.Th. Wenckebach, Chem. Phys. Lett. 165 (1990) 6.
[19] M. Iinuma, I. Shake, R. Takizawa, M. Daigo, H.M. Shimizu, Y. Takahashi, A. Masaike, T. Yabuzaki, Phys. Lett. A 208 (1995) 251.
[20] M. Iinuma, Y. Takahashi, I. Shaké, M. Oda, A. Masaike, T. Yabuzaki, H.M. Shimizu, Phys. Rev. Lett. 84 (2000) 171.
[21] K. Takeda, K. Takegoshi, T. Terao, Chem. Phys. Lett. 345 (2001) 166.
[22] K. Takeda, K. Takegoshi, T. Terao, J. Phys. Soc. Japan 73 (2004) 2313.
[23] K. Takeda, K. Takegoshi, T. Terao, J. Phys. Soc. Japan 73 (2004) 2319.
[24] M.M. Maricq, J.S. Waugh, J. Chem. Phys. 70 (1979) 3300.
[25] M. Mehring, Principles of High Resolution NMR in Solids, Springer-Verlag, 1983.
[26] A. Abragam, Principles of Nuclear Magnetism, Clarendon Press, Oxford, 1961.
[27] S. Vega, J. Chem. Phys. 68 (1978) 5518.
[28] R.P. Feynman, F.L. Vernon Jr., R.W. Hellwarth, J. Appl. Phys. 28 (1957) 49.
[29] A.E. Bennett, C.M. Rienstra, M. Auger, K.V. Lakshmi, R.G. Griffin, J. Chem. Phys. 103 (1995) 6951.
[30] N.P. Wickramasinghe, M. Shaibat, Y. Ishii, J. Am. Chem. Soc. 127 (2005) 5796.

Available online at www.sciencedirect.com
ScienceDirect
Journal of Magnetic Resonance 188 (2007) 267–274
JMR Journal of Magnetic Resonance
www.elsevier.com/locate/jmr

Efficient cross polarization with simultaneous adiabatic frequency sweep on the source and target channels

Weng Kung Peng *, Kazuyuki Takeda

Division of Advanced Electronics and Optical Science, Graduate School of Engineering Science, Osaka University, Toyonaka, Osaka 560-8531, Japan

Received 13 April 2007; revised 21 June 2007
Available online 3 August 2007

Abstract

In this work, we propose a new and efficient heteronuclear cross polarization scheme, in which adiabatic frequency sweeps from far off-resonance toward on-resonance are applied simultaneously on both the source and target spins. This technique, which we call as Simultaneous ADIabatic Spin-locking Cross Polarization (SADIS CP), is capable of efficiently locking both the source and target spins with moderate power even in the presence of large spectral distribution and fast relaxation. It is shown that by keeping the time-dependent Hartmann–Hahn mismatch minimal throughout the mixing period, polarization transfer can be accelerated. Experiments are demonstrated in a powder sample of L-alanine.

Keywords: Cross polarization; Simultaneous adiabatic frequency sweep; Spin–lattice relaxation time in the rotating frame; Time-dependent Hartmann–Hahn mismatch

1. Introduction

Cross polarization (CP) [1,2] is routinely used in solid-state nuclear magnetic resonance spectroscopy to enhance the sensitivity of nuclear spins (S spins) with relatively low gyromagnetic ratio, by transferring the larger polarization of nuclear spins (I spins) such as ^{1}H.

The original CP technique [2] employs a $\frac{\pi}{2}$ pulse at I followed by simultaneous irradiations at I and S so that the Hartmann–Hahn condition is satisfied. Since 1990s, a lot of modifications to the pulse sequence have been proposed to improve the efficiency of polarization transfer. For example, under high-speed MAS [3–7], the Hartmann–Hahn matching profile splits into sidebands. As a result, efficiency of the polarization transfer becomes sensitive to the mismatch of the rf amplitudes. In order to make transfer robust against the mismatch, a number of techniques [8–15] have been proposed which employ modulation of rf amplitude or frequency during the contact time. They include Amplitude-Modulated Cross Polarization (AMCP) [8], Adiabatic Passage through the Hartmann–Hahn condition (APHH) [9–11], Amplitude-Modulated Adiabatic Passage Cross Polarization (AMAP-CP) [12], Ramped-Amplitude Cross Polarization (RAMP-CP) [13], Hartmann–Hahn matching via adiabatic frequency sweep [14], sinusoidally frequency-modulated cross polarization [15], and so forth. Since the magnitude of the effective field in the rotating frame changes in time, the Hartmann–Hahn condition can be made to be fulfilled on the way during the contact time.

Another viewpoint for improving the CP performance has recently been put forth, in which the efficiency of spin-locking is enhanced while the favorable properties of the modulation schemes are still retained. In the proposed technique, referred to as Nuclear Integrated Cross Polarization (NICP) [16], the initial $\frac{\pi}{2}$ pulse on the I spin is removed, and the frequency of the I channel is adiabatically swept from far-off resonance toward on-resonance. The far-off to on-resonance frequency sweep serves the following two purposes: (i) even in the presence of considerable spectral distribution due to chemical shift or dipolar line broadening, the I spin packets follow, i.e., locked along

* Corresponding author. Fax: +81 668506321.
E-mail address: peng@qc.ee.es.osaka-u.ac.jp (W.K. Peng).

1090-7807/$ - see front matter © 2007 Elsevier Inc. All rights reserved.
doi:10.1016/j.jmr.2007.06.015

the effective field, which is initially pointing in the z direction and gradually tilted toward the xy plane. Since it is the locked components of the I spin packets that participate in polarization transfer, this approach leads to increase in the enhancement factor when available/tolerable rf power is not large enough to flip the entire spin packets with the $\frac{\pi}{2}$ pulse in the previous CP techniques. (ii) The magnitude of the effective field takes the maximum value at the beginning of the sweep and decreases gradually. Thus, transfer is expected to be insensitive to rf-mismatch.

In order to further increase the attainable magnetization, we present in this work an improved scheme for NICP, in which adiabatic frequency sweeps from far-off resonance toward on-resonance are applied simultaneously on both the source and target spins. This technique, which we call as Simultaneous ADIabatic Spin-locking Cross Polarization (SADIS CP), has the following advantages: (i) simultaneous sweep reduces the amount of Hartmann–Hahn offset throughout the whole sequence as compared to that in NICP, therefore allowing faster polarization transfer. (ii) Offset irradiation leads to higher effective field. The higher effective field, in general, results in a longer spin–lattice relaxation time in the rotating frame. The property that the effective field is initially the largest is particularly attractive, because both the I and S magnetization can be well kept during the sequence. Offset assisted power reduction is also attractive for application to power lossy biological samples [17]. (iii) The favorable properties of NICP mentioned above are retained in this new approach. We present here, the principle behind SADIS CP and demonstrate its performance in ^{1}H–^{13}C double resonance experiments using a powder sample of L-alanine. As shown later, the above merits are more than enough to compensate the cost of the decreased I–S dipolar interaction with offset irradiation.

2. Principle

Let us consider an isolated heteronuclear spin pair $I = \frac{1}{2}$ and $S = \frac{1}{2}$ and suppose that simultaneous linear frequency sweeps are applied at both the I and S spins under rf irradiations with intensities ω_{1I} and ω_{1S}, respectively. For simplicity, homonuclear dipolar interactions among the abundant protons are neglected. We write the rotating-frame Hamiltonian as

$$H = -(\Delta\Omega_I(t) + \Omega_I)I_z - \omega_{1I}I_x - (\Delta\Omega_S(t) + \Omega_S)S_z - \omega_{1S}S_x + D(t)I_zS_z. \quad (1)$$

Here, Ω_I and Ω_S are the isotropic chemical shifts for I and S. $D(t)$ is the magnitude of the dipolar interaction between them, which is modulated by MAS and is given by

$$D(t) = d_{IS}[G_1\cos(w_r t) + G_2\cos(2w_r t)] \quad (2)$$

where w_r is the spinning frequency and G_k $(k = 1, 2)$ depends on the orientation of the internuclear vector in a reference frame fixed to the rotor. d_{IS} is the dipolar coupling constant. In the pulse sequence of SADIS CP as depicted in Fig. 1(c), the frequency-offset terms $\Delta\Omega_I$ and $\Delta\Omega_S$ change in time according to

$$\Delta\Omega_\epsilon(t) = -\Delta\omega_\epsilon\left(1 - \frac{t}{T}\right), \quad (3)$$

where $\epsilon = I$ or S, T is the period of frequency sweep, and $\Delta\omega_\epsilon$ is the frequency sweep width. Note that the special case of SADIS CP in which $\Delta\omega_S = 0$ (no frequency sweep on the S channel) corresponds to the NICP sequence described in Fig. 1(b).

We assume that the rate of frequency sweep is slow enough for both I and S and consider the doubly tilted rotating frame in which the effective fields for both spins point in the z axis. When the adiabatic conditions are met, transformation from the rotating frame into the doubly tilted rotating frame does not have significant effects on the density matrix, whereas the Hamiltonian H^{TR} in this new frame is given by

$$H^{TR} = H_Z + H_D, \quad (4)$$

where

$$H_Z = \omega_{eI}(t)I_z + \omega_{eS}(t)S_z \quad (5)$$

$$H_D = D(t)[I_z\cos(\alpha_I(t)) + I_x\sin(\alpha_I(t))][S_z\cos(\alpha_S(t)) + S_x\sin(\alpha_S(t))], \quad (6)$$

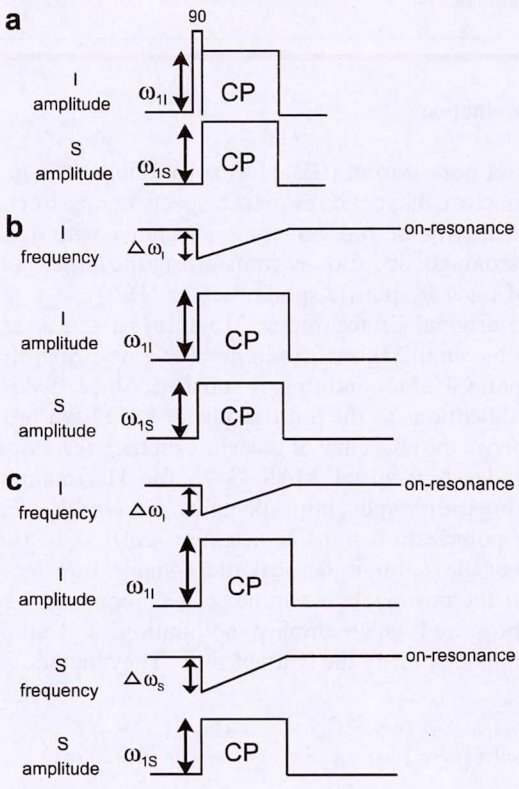

Fig. 1. Pulse sequences for (a) the conventional CP, (b) NICP, and (c) SADIS CP.

with

$$\omega_{e\epsilon}^2(t) = \omega_{1\epsilon}^2 + (\Delta\Omega_\epsilon(t) + \Omega_\epsilon)^2, \tag{7}$$

and

$$\alpha_\epsilon(t) = \tan^{-1}\frac{\omega_{1\epsilon}(t)}{\Delta\Omega_\epsilon(t) + \Omega_\epsilon}. \tag{8}$$

The evolution of the system is governed by the propagator $U(t)$ given by

$$U(t) = T\exp\left[\int_0^t \mathrm{d}t' H^{\mathrm{TR}}\right] = U_0(t)U_1(t), \tag{9}$$

where

$$U_0(t) = T\exp\left[\int_0^t \mathrm{d}t' H_Z\right], \tag{10}$$

$$U_1(t) = T\exp\left[\int_0^t \mathrm{d}t' \widetilde{H}_D\right], \tag{11}$$

with

$$\widetilde{H}_D = U_0^{-1}(t)H_D U_0(t) \tag{12}$$

$$\begin{aligned} &= D(t)[S_z\cos(\alpha_S(t)) + (S_x\cos(\omega_{eS}t) \\ &\quad - S_y\sin(\omega_{eS}t))\sin(\alpha_S(t))][I_z\cos(\alpha_I(t)) \\ &\quad + (I_x\cos(w_{eI}t) - I_y\sin(w_{eI}t))\sin(\alpha_I(t))]. \end{aligned} \tag{13}$$

When the time-dependent Hartmann–Hahn condition

$$\Delta_{\mathrm{HH}}(t) \equiv \omega_{eI}(t) - \omega_{eS}(t) - nw_r = 0, (n = -2, -1, 1, 2) \tag{14}$$

is satisfied, interference between the spatial and spin parts in $\widetilde{H}_D$ leads to the non-vanishing average Hamiltonian

$$\overline{\widetilde{H}}_D = \frac{1}{8}d_{IS}G_n\sin\alpha_I(t)\sin\alpha_S(t)(I_+S_- + I_-S_+). \tag{15}$$

In order to discuss the exchange of the spin states between I and S, we focus on the zero-quantum (ZQ) subspace spanned by states $|+-\rangle$ and $|-+\rangle$, in which the secular Hamiltonian H^{ZQ} is represented by

$$H^{\mathrm{ZQ}} = 2\Delta_{\mathrm{HH}}(t)I_z^{\mathrm{ZQ}} + \frac{1}{4}D_{\mathrm{eff}}(t)I_x^{\mathrm{ZQ}}, \tag{16}$$

where $D_{\mathrm{eff}}(t)$, which we call the effective dipolar frequency, is given by

$$D_{\mathrm{eff}}(t) = d_{IS}G_n\sin\alpha_I(t)\sin\alpha_S(t), \tag{17}$$

and I_z^{ZQ} and I_x^{ZQ} are the ZQ fictitious spin $-\frac{1}{2}$ operators given by

$$I_z^{\mathrm{ZQ}} = \frac{1}{2}[|+-\rangle\langle+-| - |-+\rangle\langle-+|], \tag{18}$$

$$I_x^{\mathrm{ZQ}} = \frac{1}{2}[|+-\rangle\langle-+| + |-+\rangle\langle+-|]. \tag{19}$$

We assume that initially the state $|+-\rangle$ is idempotently populated, so that the ZQ density matrix $\rho^{\mathrm{ZQ}}(t=0)$ is

$$\rho^{\mathrm{ZQ}}(t=0) = \begin{pmatrix} 1 & 0 \\ 0 & 0 \end{pmatrix} = \frac{1}{2}\mathbf{1} + I_Z^{\mathrm{ZQ}}. \tag{20}$$

When the I and S spins have exchanged their spin states, the density matrix would be

$$\rho^{\mathrm{ZQ}}(t=ct) = \begin{pmatrix} 0 & 0 \\ 0 & 1 \end{pmatrix} = \frac{1}{2}\mathbf{1} - I_Z^{\mathrm{ZQ}}. \tag{21}$$

Hence, the transverse magnetization $\langle S_x\rangle$ of the S spin is correlated with $\langle I_Z^{\mathrm{ZQ}}\rangle$ through

$$\langle S_x\rangle(t) = \frac{1}{2} - \langle I_Z^{\mathrm{ZQ}}\rangle \tag{22}$$

$$= \frac{1}{2} - \mathrm{Tr}[I_Z^{\mathrm{ZQ}}\rho^{\mathrm{ZQ}}(t)]. \tag{23}$$

Since the problem has now been reduced to the two-level system, geometric state representation is possible, i.e., a general state ρ^{ZQ} in the ZQ-subspace is given by employing a vector $\mathbf{M}$ as

$$\rho^{\mathrm{ZQ}}(t) = M_x(t)I_x^{\mathrm{ZQ}} + M_y(t)I_y^{\mathrm{ZQ}} + M_z(t)I_z^{\mathrm{ZQ}}, \tag{24}$$

and the dynamics of $\mathbf{M}$ is governed by the Bloch equation [18]

$$\frac{\mathrm{d}}{\mathrm{d}t}\mathbf{M} = \mathbf{M}\times\omega_{\mathrm{eff}}^{\mathrm{ZQ}}, \tag{25}$$

where $\omega_{\mathrm{eff}}^{\mathrm{ZQ}}$ is the vector of effective field in the ZQ-subspace which is represented by

$$\omega_{\mathrm{eff}}^{\mathrm{ZQ}} = \begin{pmatrix} (\omega_{\mathrm{eff}}^{\mathrm{ZQ}})_x \\ (\omega_{\mathrm{eff}}^{\mathrm{ZQ}})_y \\ (\omega_{\mathrm{eff}}^{\mathrm{ZQ}})_z \end{pmatrix} = \begin{pmatrix} \frac{1}{4}D_{\mathrm{eff}}(t) \\ 0 \\ 2\Delta_{\mathrm{HH}}(t) \end{pmatrix}. \tag{26}$$

Substituting Eq. (26) into Eq. (25), we arrive at

$$\frac{\mathrm{d}}{\mathrm{d}t}\begin{pmatrix} M_x \\ M_y \\ M_z \end{pmatrix} = \begin{pmatrix} 2\Delta_{\mathrm{HH}}(t)M_y \\ \frac{1}{4}D_{\mathrm{eff}}(t)M_z - 2\Delta_{\mathrm{HH}}(t)M_x \\ -\frac{1}{4}D_{\mathrm{eff}}(t)M_y \end{pmatrix}\begin{pmatrix} M_x \\ M_y \\ M_z \end{pmatrix}. \tag{27}$$

In order to make a simple comparison on transfer efficiencies between SADIS CP and NICP, we consider one specific crystallite orientation in a static sample. We also neglect the effect of relaxation here, which will be discussed later. Assuming the initial magnetization $(0, 0, 1)$, we evaluated numerically (Fig. 2) the dynamics of the S magnetization for an arbitrarily given set of parameters ($\frac{\omega_{IS}}{2\pi} = 35$ kHz, $\frac{\omega_{1I}}{2\pi} = 40$ kHz, $\frac{\Delta\omega_I}{2\pi} = 80$ kHz, $T = 2$ ms, and $\frac{d_{IS}}{2\pi} = 45$ kHz). The difference between SADIS CP (blue line) and NICP (green line) is the application of the frequency sweep on the S channel, in which $\frac{\Delta\omega_S}{2\pi} = 90$ kHz for SADIS CP while $\frac{\Delta\omega_S}{2\pi} = 0$ kHz for NICP.

As shown in Fig. 2, the calculated buildup of the S magnetization is faster in SADIS CP than in NICP. Thus, the same amount of S polarization can be achieved with SADIS CP in a relatively shorter period of time as compared to NICP. This feature is particularly attractive for spins with short relaxation times, where polarization transfer should be as fast as possible before overwhelmed by the effect of relaxation. The oscillation at the I–S dipolar frequency is also visible in the build up curve. It is worth

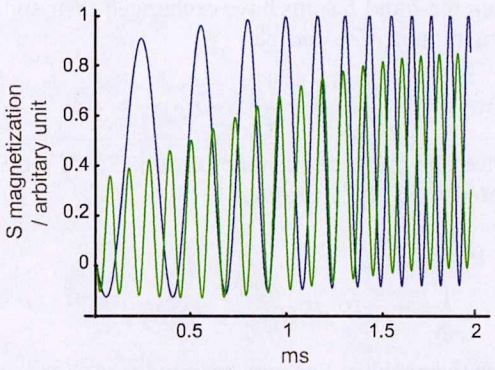

Fig. 2. Numerically calculated buildup curves for SADIS CP (blue line) and NICP (green line). $\frac{\Delta\omega_S}{2\pi} = 90$ kHz and $\frac{\Delta\omega_S}{2\pi} = 0$ were used for SADIS CP and NICP, respectively. Other parameters were $\frac{\omega_{1S}}{2\pi} = 35$ kHz, $\frac{\omega_{1I}}{2\pi} = 40$ kHz $\frac{\Delta\omega_I}{2\pi} = 80$ kHz, and $T = 2$ ms. (For interpretation of the references to color in this figure legend, the reader is referred to the web version of this paper.)

noting here that the effective dipolar frequency $D_{\text{eff}}(t)$ given in Eq. (17) is lower in SADIS CP than in NICP by the scaling factor $\sin\alpha_S(t)$. For this reason, NICP shows faster oscillation than SADIS CP, as revealed in Fig. 2. In NICP, however, the buildup of the amplitude profile of the oscillation is rather slower because of the larger Hartmann–Hahn offset. In actual situations, this oscillation is expected to be suppressed due to distribution of the *I–S* dipolar frequency in powder samples, and due to the effect of homonuclear dipolar interactions among the *I* spins.

The efficient polarization transfer in SADIS CP is ascribed to the smaller time-dependent Hartmann–Hahn offset $\Delta_{\text{HH}}(t)$ than that in NICP throughout the sequence. In the ZQ subspace, $\Delta_{\text{HH}}(t)$ appears in the I_Z^{ZQ} term which corresponds to the resonance offset in the conventional nutation. For relatively smaller $\Delta_{\text{HH}}(t)$ as in the case of SADIS CP, the ZQ effective field is tilted more toward the *xy* plane. Since the inversion of the magnetization requires on-resonance nutation, polarization transfer is expected to be faster in SADIS CP. Furthermore, the aforementioned attractive features of NICP can be retained when the adjustable parameters (ω_{1S}, ω_{1I}, $\Delta\omega_I$, $\Delta\omega_S$) are appropriately chosen.

The time-dependent Hartmann–Hahn offset should be kept small as long as the Hartmann–Hahn condition is satisfied for the individual target spins. Generally speaking, experiments should be arranged in such a way that the magnitude of the effective fields are initially different, and so they are the other way around at the end of the sequence. For example, for the case of simple isolated two-spin system under sample spinning,

(1) at $t = 0$

$$\omega_{eI} + w_r \leqslant \omega_{eS} \leqslant \omega_{eI} + 2w_r, \tag{28}$$

and

(2) at $t = T$

$$\omega_{eS} + w_r \leqslant \omega_{eI} \leqslant \omega_{eS} + 2w_r, \tag{29}$$

or vice versa so that the crossing will be limited to $|n| = 1$ matching condition, where the magnitude of the dipolar coefficient is the largest. The reversal of the magnitude relation between the effective fields guarantees that the Hartmann–Hahn condition is satisfied during the simultaneous sweep.

3. Experimental

Experiments were performed at room temperature in a magnetic field of 11.7 T using a home-built triple resonance probe equipped with a Varian 4 mm spinning module. Carrier frequencies for the ^{13}C and ^{1}H channels were 125.675 and 499.789 MHz, respectively. The ^{13}C NMR signals in a polycrystallines sample of ^{13}C-labelled L-alanine were measured at a spinning frequency of 13.5 kHz under ^{1}H TPPM decoupling [19]. Recycle delays were 60 s for ^{13}C direct observation and 2 s for all other CP experiments.

4. Results and discussion

4.1. 'Contact-time'-dependent behavior

Fig. 3 shows the signal intensities of the methyl, methine, and carboxyl ^{13}C spins for various contact times

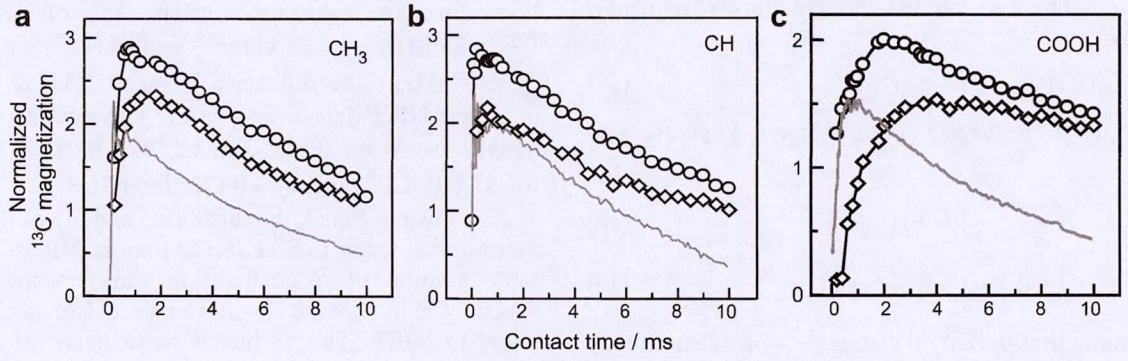

Fig. 3. ^{13}C magnetizations for (a) CH_3, (b) CH, and (c) COOH in L-alanine for various contact times measured with conventional CP (—), NICP (◇), and SADIS CP (○). The vertical axis was normalized with respect to the value obtained with direct detection. For conventional CP, $\frac{\omega_{1S}}{2\pi}$ was fixed to 45 kHz and ω_{1I} was adjusted separately so that each of the isotropic chemical shifts satisfied sideband (+1) matching condition. For SADIS CP, $\frac{\omega_{1S}}{2\pi} = 35$ kHz, $\frac{\Delta\omega_S}{2\pi} = 110$ kHz and $\frac{\omega_{1I}}{2\pi} = 48$ kHz, $\frac{\Delta\omega_I}{2\pi} = 80$ kHz. For NICP, $\frac{\Delta\omega_S}{2\pi} = 0$ kHz while the rest of the parameters are the same as SADIS CP.

in the conventional CP, NICP, and SADIS CP techniques. By 'contact time' we refer to the time interval T of the frequency-sweep for NICP and SADIS CP. The signal intensities are normalized with respect to the signal obtained in thermal equilibrium with direct excitation with sufficiently long recovery delay time of 60 s. In the conventional CP experiment, separate measurements were carried out for the individual carbon groups by setting the carrier frequency at on-resonance and adjusting the $n = +1$ Hartmann–Hahn condition, and the maximum enhancement factors recorded were 2.26, 2.32, 1.52 for the methyl, methine, and carboxyl ^{13}C spins with contact times of 0.16, 0.10, and 0.68 ms, respectively. This result indicates that it is impossible to choose a common set of optimal contact time and rf power. This problem would be more serious for samples with large chemical shift distribution or experiments under high static field where the Hartmann–Hahn matching profile is shifted according to the individual chemical shifts. The relatively smaller signal enhancement for the conventional CP is also due to less efficient spin-locking of the ^{1}H magnetization with the rf intensity of 59 kHz, which is smaller than the ^{1}H dipolar linewidth. Thus, the performance of polarization transfer in those previous CP techniques using the initial $\frac{\pi}{2}$ pulse at the I spin degrades when the available or tolerable rf power is limited. Moreover, the low rf intensity can cause fast spin–lattice relaxation in the rotating frame, as discussed below.

In NICP, it was found that comparable amount of enhancement factors (2.32, 2.27, 1.53) can be obtained in a single experiment using a common set of experimental parameters $\left(\frac{\omega_{1S}}{2\pi} = 35 \text{ kHz}, \frac{\omega_{1I}}{2\pi} = 48 \text{ kHz} \text{ and } \frac{\Delta\omega_I}{2\pi} = 80 \text{ kHz}\right)$, as demonstrated in Fig. 3. The improved performance is ascribed to the following three reasons. First, the magnitude of the initial effective field set along the z axis is much larger than the spectral distribution of the I spin. Thus, the I spin packets can be well locked along the effectively field, and therefore participate in the polarization transfer process even with moderate rf amplitudes. Second, the fact that the magnitude of the effective field changes with time permits the Hartmann–Hahn condition to be satisfied even in the presence of large spectral distribution or rf-intensity offset. Finally, the larger effective field with the off-resonance irradiation at the I channel leads to slower spin–lattice relaxation, so that larger amount of the I magnetization can be retained along the effective field before polarization transfer is completed. Since the common set of experimental parameters gave nearly the optimal enhancement factors, the sensitivity of the ^{13}C spectrum obtained with NICP (Fig. 4(b)) was considerably higher than that obtained with the conventional CP (Fig. 4(a)).

In SADIS CP, the maximum enhancement factors (2.88, 2.84, 2.00) were (24%, 25%, 31%) higher than those obtained in NICP, as demonstrated in Fig. 3. This was achieved by employing an additional frequency sweep $\left(\frac{\Delta\omega_S}{2\pi} = 110 \text{ kHz}\right)$ on the S channel while other parameters were kept the same as the optimal ones for the NICP experiment. As can also be seen in Fig. 3, the contact times that gave the maxima in SADIS CP are slightly shorter than those in NICP. This indicates that the buildup of the ^{13}C magnetizations was faster in SADIS CP, confirming the rather simplified theoretical descriptions in the previous section which neglected the homonuclear dipolar interactions among the protons. The optimized ^{13}C spectrum of SADIS CP is shown in Fig. 4(c).

For the purpose of clarifying the role of additional frequency sweep in the S channel, we have carried out related experiments, as described below.

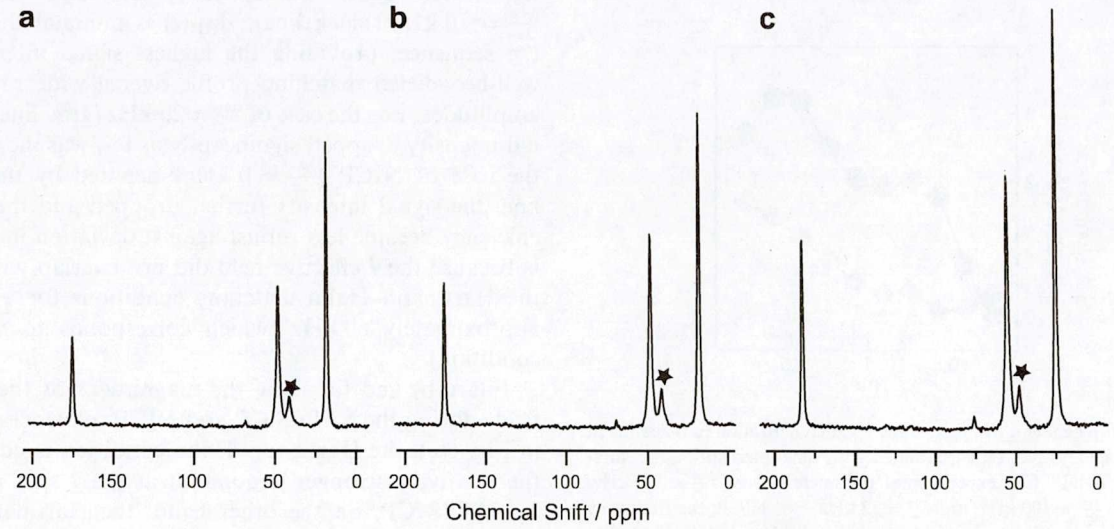

Fig. 4. ^{13}C MAS spectra of L-alanine obtained with (a) conventional CP ($\frac{\omega_{1S}}{2\pi}$ =45 kHz, $\frac{\omega_{1I}}{2\pi}$ =58.5 kHz, contact time = 0.28 ms), (b) NICP ($\frac{\omega_{1S}}{2\pi}$ =35 kHz, $\frac{\Delta\omega_S}{2\pi}$ =0 kHz, $\frac{\omega_{1I}}{2\pi}$ =48 kHz, $\frac{\Delta\omega_I}{2\pi}$ =80 kHz, and contact time = 2 ms), and (c) SADIS CP ($\frac{\omega_{1S}}{2\pi}$ =35 kHz, $\frac{\Delta\omega_S}{2\pi}$ =110 kHz, $\frac{\omega_{1I}}{2\pi}$ =48 kHz, $\frac{\Delta\omega_I}{2\pi}$ =80 kHz, and contact time = 0.8 ms). The peaks indicated by asterisks originate from impurity which was intentionally mixed for other purposes. There were no interaction between the impurity and L-alanine because it was just mechanically mixed.

4.2. ^{13}C magnetization buildup

In order to trace the buildup behavior in NICP and SADIS CP, time interruption measurements were carried out, in which frequency sweep was aborted at various moments during the contact time. Fig. 5 shows the buildup of the methine ^{13}C magnetization with $T = 1.8$ ms, $\frac{\omega_{1S}}{2\pi} = 35$ kHz, $\frac{\omega_{1I}}{2\pi} = 52$ kHz, $\frac{\Delta\omega_I}{2\pi} = 100$ kHz, and with $\frac{\Delta\omega_S}{2\pi} = 0$ and 120 kHz for NICP and SADIS CP, respectively. Unlike the simplified calculation in Fig. 2, the oscillations were suppressed due to distribution of the *IS* dipolar frequency in the powder sample used in our study, and due to the dipolar interactions among the ^{1}H spins which were neglected in the theoretical part. For NICP, the Hartmann–Hahn crossing occurred at $t \sim 1.2$ ms while for SADIS CP, the *S* magnetization surged up as the Hartmann–Hahn crossings occured at $T = 0.5$ and 1.3 ms, as demonstrated in Fig. 5. In SADIS CP, the overall attained ^{13}C magnetization was much larger than that in NICP. One reason for this result is that $\Delta_{HH}(t)$ is smaller throughout the sequence in SADIS CP, which leads to the following two consequences. First, the chance of Hartmann–Hahn crossing increase when $\Delta_{HH}(t)$ is small; in this example the crossing occured twice in SADIS CP while it only occured once in NICP. Second, the smaller $\Delta_{HH}(t)$, the higher the rate of polarization transfer in each crossing. In other words, NICP requires a longer contact time to attain the same amount of polarization in SADIS CP.

In reality, however, the available time interval is limited by the effect of relaxation, which restores the spin system toward thermal equilibrium. Since the final ^{13}C magnetization is determined by the balance between the buildup and relaxation processes, both the transfer rate and the chance of the Hartmann–Hahn crossing are desirable to be maximized for a given relaxation rate. In both of these respects, SADIS CP is superior to NICP, despite that the *IS* dipolar interaction is weaker in SADIS CP by an additional scaling factor $\sin\alpha_S(t)$. Thus, SADIS CP opens its application to systems in which the effect of relaxation (particularly on the *S* spins) is so serious that the previously proposed CP techniques do not provide efficient polarization transfer. Such systems include, e.g., paramagnetic materials, samples with molecular motion whose time scale is comparable to the Larmor frequency, and samples in which the target rare spins, such as ^{13}C and ^{15}N, are isotopically enriched, because the presence of the additional homonuclear dipolar interactions among the *S* spins can reduce the relaxation time [20,21]. Application of SADIS CP to such materials is under progress.

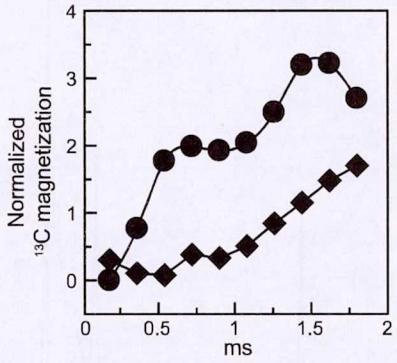

Fig. 5. Buildup behavior of the methine ^{13}C magnetization in L-alanine in SADIS CP (●) and NICP (◆) obtained with time-interruption measurements. For SADIS CP, experimental parameters were $\frac{\Delta\omega_S}{2\pi} = 120$ kHz, $\frac{\omega_{1S}}{2\pi} = 35$ kHz, $\frac{\Delta\omega_I}{2\pi} = 100$ kHz, and $\frac{\omega_{1I}}{2\pi} = 52$ kHz. For NICP, the frequency sweep for *S* channel were turned off $\left(\frac{\Delta\omega_S}{2\pi} = 0 \text{ kHz}\right)$, while the other parameters were the same as in SADIS CP. A contact time of 1.8 ms was used. A correction factor $1/\sin(\alpha_S)$ was taken into account for SADIS CP since only the projection of the magnetization onto the *xy* plane is measurable.

Moreover, SADIS CP, which make use of the offset irradiation on the *S* spins, can further suppress the effect of relaxation, because the effective field for the *S* spin is always larger throughout the sequence in SADIS CP as compared to NICP. Spin–lattice relaxation times in the rotating frame can be enhanced with offset irradiation, which suppresses the unwanted decay of the ^{13}C magnetization in the rotating frame. In particular, this is the case for the ^{13}C spins in L-alanine, as pointed by Akasaka et al. [22]. Thus, SADIS CP can spare longer 'contact' between both spins than NICP does.

4.3. Hartmann–Hahn matching profile

In order to study the efficiency of polarization transfer in terms of the Hartmann–Hahn mismatch $\Delta_{HH}(t)$ described in Eq. (14), we have examined the signal intensities of the methine ^{13}C as a function of the rf amplitude ω_{1I} for three frequency sweep widths $\frac{\Delta\omega_S}{2\pi} = 0$, 20, and 110 kHz on the *S* channel (Fig. 6(a)), which represents NICP, less optimal SADIS CP and the optimal SADIS CP, respectively. All other parameters were kept fixed. For $\frac{\Delta\omega_S}{2\pi} = 110$ kHz (black line), $\Delta_{HH}(t)$ is minimal throughout the sequence, providing the highest signal intensity and well-broadened matching profile over a wide range of rf amplitudes. For the case of $\frac{\Delta\omega_S}{2\pi} = 20$ kHz (gray line), the signal intensity dropped significantly as ω_{1I} was increased. In the case of NICP $\left(\frac{\Delta\omega_S}{2\pi} = 0 \text{ kHz}\right)$ denoted by the broken line, the signal intensity further dropped and the transfer efficiency became less robust against deviation in ω_{1I}. This is because the *I* effective field did not overlap with any of the Hartmann–Hahn matching conditions for $\frac{\omega_{1I}}{2\pi}$ beyond approximately 60 kHz (which corresponds to $\omega_{1S} + 2w_r$ condition).

Fig. 6(b) and (c) show the magnitudes of the effective fields during the SADIS CP and NICP sequences. As seen in Fig. 6(c), the Hartmann–Hahn condition is not met for the relatively stronger irradiation at the *I* spin in NICP. In SADIS CP, on the other hand, the Hartmann–Hahn crossings take place for a wide range of irradiation amplitudes at the *I* spin, as depicted in Fig. 6(b). Hence, the matching profile in SADIS CP is considerably wider than that in NICP, making the present scheme robust against

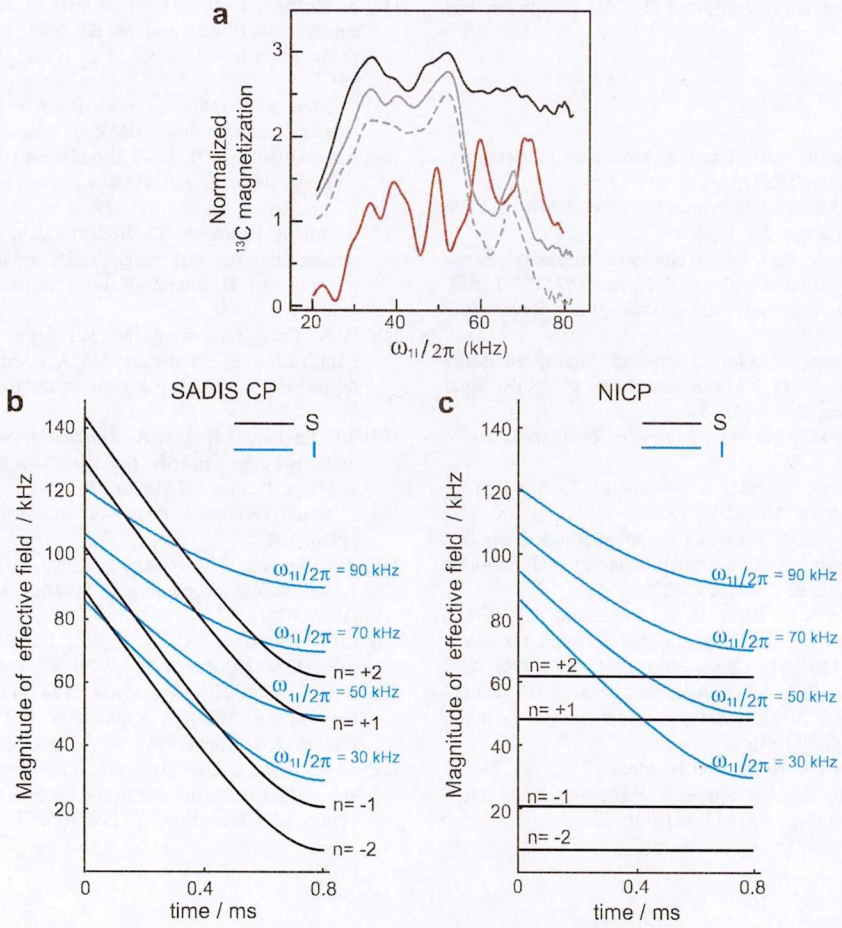

Fig. 6. (a) ω_{1I} dependence of the methine ^{13}C signal intensities in SADIS CP with (i) $\frac{\Delta\omega_S}{2\pi}$ =110 kHz (black line), (ii) $\frac{\Delta\omega_S}{2\pi}$ =20 kHz (gray line), and (iii) $\frac{\Delta\omega_S}{2\pi}$ =0 kHz (broken line). Note that (iii) corresponds to NICP, which is a special case of SADIS CP. Other parameters were fixed to $\frac{\Delta\omega_I}{2\pi}$ = 80 kHz, $\frac{\omega_{1S}}{2\pi}$ = 35 kHz and T = 0.8 ms. For comparison, the Hartmann–Hahn matching profile for the conventional CP with $\frac{\omega_{1S}}{2\pi}$ = 45 kHz and T = 0.80 ms is also shown in brown line. (b) Time dependence of the magnitude of the effective field in SADIS CP for the S spin (black lines) and I spin (blue lines) with T = 0.8 ms, with Ω_S = 0, $\frac{\omega_{1S}}{2\pi}$ = 35 kHz, and $\frac{\Delta\omega_S}{2\pi}$ = 110 kHz, Ω_I = 0, $\frac{\Delta\omega_I}{2\pi}$ = 80 kHz, and $\frac{\omega_{1I}}{2\pi}$ = 90 kHz, 70 kHz, 50 kHz, and 30 kHz. In order to depict the Hartmann–Hahn crossings, the black lines are plotted with the offsets due to sample spinning frequency of $\frac{\omega_r}{2\pi}$ = 13.5 kHz. (c) Time dependence of the magnitude of the effective field in NICP for the S spin (blue lines) and I spin (black lines). Parameters are the same in (b) except for $\frac{\Delta\omega_S}{2\pi}$ = 0. (For interpretation of the references to color in this figure legend, the reader is referred to the web version of this paper.)

deviation in rf intensity and spectral distribution. In this respect, SADIS CP is expected to show further advantages in experiments involving spins with large spectral distribution such as ^{19}F, ^{31}P, and paramagnetic samples.

5. Conclusions

In summary, an improved scheme for heteronuclear cross polarization, which we call as SADIS CP, has been proposed, demonstrated and analyzed. In this technique, adiabatic frequency sweep from far-off to on-resonance is employed on both the source and target spins simultaneously. As compared to the previously proposed NICP technique, which has been shown to be a special case of SADIS CP with zero frequency-sweep width on the target channel, SADIS CP keeps the Hartmann–Hahn mismatch $\Delta_{HH}(t)$ smaller throughout the sequence, allowing the faster magnetization buildup of the target spin and more robust transfer against deviation in the rf amplitudes. And yet, SADIS CP retains the favorable properties of NICP, and is thus compatible with fast sample spinning and large spectral distribution of the source spins, as discussed in our previous work [16]. Since the off-resonance irradiation on the S channel increases the magnitude of the effective field on the target spins, which can suppress the loss of magnetization due to the effect of relaxation, SADIS CP is also expected to be well applicable to experiments where either or both of the source and target spins are subjected to fast relaxation.

Acknowledgments

This work was supported by the CREST program of the Japan Science and Technology Agency and W.K.P thanks

the 21st Century Center of Excellence (COE) program for financial support.

References

[1] S.R. Hartmann, E.L. Hahn, Nuclear double resonance in the rotating frame, Phys. Rev. 128 (1962) 2042.
[2] A. Pines, M.G. Gibby, J.S. Waugh, Proton-enhanced NMR of dilute spins in solids, J. Chem. Phys. 59 (1973) 569.
[3] E.R. Andrew, A. Bradbury, R.G. Eades, Nuclear magnetic resonance spectra from a crystal rotated at high speed, Nature 182 (1958) 1659.
[4] I.J. Lowe, Free induction decays of rotating solids, Phys. Rev. Lett. 2 (1959) 285.
[5] A. Samoson, T. Tuherm, Z. Gan, High-field high-speed MAS resolution enhancement in ^{1}H NMR spectroscopy of solids, Solid State Nucl. Magn. Reson. 20 (2001) 130.
[6] A. Samoson, Encyclopedia of Nuclear Magnetic Resonance, vol. 9, Wiley, Chichester, 2002, p. 59.
[7] A. Samoson, T. Tuherm, J. Past, A. Reinhold, T. Anupold, I. Heinmaa, Top. Curr. Chem. 246 (2004) 15.
[8] S. Hediger, B.H. Meier, R.R. Ernst, Cross polarization under fast magic angle sample spinning using amplitude-modulated spin-lock sequences, Chem. Phys. Lett. 213 (1993) 627.
[9] S. Hediger, B.H. Meier, N.D. Kuru, G. Bodenhausen, R.R. Ernst, NMR cross polarization by adiabatic passage through the Hartmann–Hahn condition (APHH), Chem. Phys. Lett. 223 (1994) 283.
[10] S. Hediger, B.H. Meier, R.R. Ernst, Adiabatic passage Hartmann–Hahn cross polarization in NMR under magic angle sample spinning, Chem. Phys. Lett. 240 (1995) 449.
[11] M. Baldus, D.G. Geurts, S. Hediger, B.H. Meier, Efficient ^{15}N–^{13}C polarization transfer by adiabatic-passage Hartmann–Hahn cross polarization, J. Magn. Reson. A118 (1996) 140.
[12] S. Hediger, P. Signer, M. Tomaselli, R.R. Ernst, B.H. Meier, A combination of slow and fast RF field modulation for improved cross polarization in solid-state MAS NMR, J. Magn. Reson. 125 (1997) 291.
[13] G. Metz, X. Xiaoling, S. Smith, Ramped-amplitude cross polarization in magic-angle-spinning NMR, J. Magn. Reson. A110 (1994) 219.
[14] A.C. Kolbert, A. Bielecki, Broadband Hartmann–Hahn matching in magic-angle spinning NMR via an adiabatic frequency sweep, J. Magn. Reson. A116 (1995) 29.
[15] R. Fu, P. Pelupessy, G. Bodenhausen, Frequency-modulated cross polarization for fast magic angle spinning NMR at high fields: relaxing the Hartmann–Hahn condition, Chem. Phys. Lett. 264 (1997) 63.
[16] W.K. Peng, K. Takeda, M. Kitagawa, A new technique for cross polarization in solid-state NMR compatible with high spinning frequencies and high magnetic fields, Chem. Phys. Lett. 417 (2006) 58.
[17] S.C. Shekar, D.K. Lee, A. Ramamoorthy, Chemical shift anisotropy and offset effects in cross polarization solid-state NMR spectroscopy, J. Magn. Reson. 157 (1996) 223.
[18] F. Bloch, Dynamical theory of nuclear induction. II, Phys. Rev. 102 (1956) 104.
[19] A.E. Bennett, C.M. Rienstra, M. Auger, K.V. Lakshmi, R.G. Griffin, Heteronuclear decoupling in rotating solids, J. Chem. Phys. 103 (1995) 6951.
[20] C.G. Moreland, ^{13}C–^{13}C dipolar interactions as relaxation mechanism, J. Magn. Reson. 15 (1974) 596.
[21] R.E. London, N.A. Matwiyoff, D.D. Mueller, Spin–lattice relaxation time in an $AM(X_n)$: application to ^{13}C relaxation in enriched molecules, J. Chem. Phys. 63 (1975) 4442.
[22] K. Akasaka, S. Ganapathy, C.A. McDowell, A. Naito, Spin–spin and spin–lattice contributions to the rotating frame relaxation of ^{13}C in L-alanine, J. Chem. Phys. 78 (1983) 3567.

Simultaneous Adiabatic Spin-locking Cross Polarization in Solid-State NMR of Paramagnetic Complexes

Weng Kung Peng[1] *, Ago Samoson[2], Masahiro Kitagawa[1]

[1] *Division of Advanced Electronics and Optical Science, Graduate School of Engineering Science, Osaka University, Toyonaka, Osaka 560-8531, Japan*

[2] *National Institute of Chemical Physics and Biophysics, Tallinn, Estonia*

Abstract

Continuous-wave irradiations cross polarization and its variations had not been a popular choice for sensitivity enhancement in paramagnetic solids due to the large spectral broadening and the effect of fast relaxation on both the source and target spins. Furthermore, with the application of very-fast sample spinning, which is the prerequisite for high-resolution purposes, polarization transfer over a large bandwidth is further degraded. In this work, we report a wideband sensitivity enhancement in paramagnetic solid with our recently developed technique, Simultaneous Adiabatic Spin-locking Cross Polarization, SADIS CP. Experiments were demonstrated with Cu(II)(D,L-Alanine)$_2$.H_20 under high static field of 14.1 T and very-fast sample spinning of 31 kHz.

Key words: paramagnetic solids, wideband cross polarization, simultaneous adiabatic frequency sweep, fast relaxation spins

* corresponding author

Email address: peng@qc.ee.es.osaka-u.ac.jp (Weng Kung Peng[1]).

1 Introduction

Organometallic complexes are present abundantly in nature and have a wide range of applications from surface chemistry and catalysts to genome mapping. Solid-state NMR spectroscopy, which has been an effective tool for characterization of noncrystalline organic samples including diamagnetic organometallic complexes, has yet to be well-utilized in condensed phase with paramagnetic metal ions. The presence of metal-ion in organic sample is known to cause huge lineshifts and broadenings, and accelerate relaxation [1,2] as compared to its diamagnetic counterparts. These features had long impeded the quest for adequate high resolution and high sensitivity spectroscopy. Recent report by [3,4] on very-fast magic-angle sample spinning (VFMAS) [5–7] demonstrated a remarkably improved spectral resolution and has ignited a new interest and perspective in spectroscopy of compounds with paramagnetic doping. Very important methodological benefit is sensitivity enhancement due to a shorter recycle delay [8] permitting more scans in a unit time.

Cross polarization (CP) [9,10] is routinely used in diamagnetic solid-state NMR spectroscopy to enhance sensitivity of nuclear spin species having relatively small gyromagnetic ratios (S spins) such as ^{13}C and ^{15}N, by transferring the larger polarization of nuclear spins (I spins) such as ^{1}H or ^{19}F. Sensitivity enhancement of a factor $\frac{\gamma_I}{\gamma_S}$ is then possible, provided that (i) the number of abundant spins is very much larger than the rare spins, and (ii) relaxation time of both the source spins and target spins are long enough. Furthermore, shorter relaxation rate of abundant spins often allows shorter recycle delay, which will again increase the signal-to-noise ratio (SNR) as compared to direct

excitation of the rare spins.

However, conventional cross polarization has found difficulty in its application to the paramagnetic systems [2]. Spectral broadening on both the target and source spins, spreading up to a few hundreds or even thousand of ppm, imposes strong challenges for efficient and wideband spin-locking with continuous-wave (CW) CP [10] or other single channel frequency/amplitude modulated CP, such as Amplitude-Modulated Cross Polarization (AMCP) [11], Adiabatic Passage through the Hartmann-Hahn condition (APHH) [12–14], Amplitude-Modulated Adiabatic Passage Cross Polarization (AMAP-CP) [15], Ramped-Amplitude Cross Polarization (RAMP-CP) [16], Hartmann-Hahn matching via adiabatic frequency sweep [17], sinusoidally frequency-modulated Cross Polarization [18] and Ramped-Speed Cross Polarization [19]. These techniques were initially proposed during the 90's to compensate for the effect of rf-mismatching due to application of fast MAS. Another scheme, Nuclear Integrated Cross Polarization [20], which is capable of spin-locking (even under fast MAS) large spectral broadening of the source spins was then proposed. This is achieved by applying large frequency sweep from far-off-resonance to on-resonance on the source spins while retaining the continuous wave irradiation on the target spins. As amplitude/frequency modulation on either of the channel, which was then thought to be sufficient to compensate for the rf-mismatching due to fast MAS, not much attention was paid to the influence of fast relaxation effect and huge spectral broadening which may occur in both the source and target spins such as in the case of paramagnetic solids. Note that, although very high rf-nutation is available with microcoil-probe [21], which is commonly used for mass-limited sample, we refer to 'huge' spectral

broadening as to when the availability of rf-nutations/rf-powers applied are much smaller than the spectral distribution. Poor spin-locking coupled with the effect of fast relaxation, conventional CP techniques are almost helpless. Additionally, the fact that very-fast MAS is inevitably used for resolution purposes, cross polarization efficiency of large bandwidth is very much degraded.

We have recently shown in [22] that by applying adiabatic frequency sweep from far-off-resonance to on-resonance, on both the target and source spins simultaneously it is possible to promote faster and efficient polarization transfer over a large bandwidth. We refer to this technique as Simultaneous ADIabatic Spin-locking Cross Polarization (SADIS CP). We have successfully demonstrated this technique in diamagnetic sample of L-alanine as reported in [22]. As compared to CW-irradiation, adiabatic frequency sweep from far off-resonance to on-resonance allows effective spin-locking throughout a large bandwidth, so that all the spin-packets could participate in the polarization transfer process. Since both the effective fields are now ramped through a large variable of magnitude, the chances of Hartmann-Hahn crossings over a large bandwidth are increased. Simultaneous application frequency sweeps on both the channel also reduce the degree of Hartmann-Hahn mismatching throughout the sequence and thereby polarization transfer time, bringing the desirable results particularly for spins with fast relaxation properties such as found in paramagnetic materials. Furthermore, higher effective field due to irradiation offset, in general, leads to longer spin-lattice relaxation time in rotating frame, $T_{1\rho}$.

In this work, we experimentally demonstrated SADIS CP in paramagnetic

solid with very-fast sample spinning of 31 kHz and under high-static field of 14.1 T. The results were then compared to the one obtained from direct excitation and RAMP CP. The effect of large dispersion of chemical shift offset on its transfer efficiencies were analyzed and discussed.

2 Theoretical

Under the application of very-fast MAS, the chemical shift anisotropy as well as the heteronuclear and homonuclear dipolar couplings in the system are essentially removed [3,4]. Here, a simplified theoretical description, which is sufficiently for us to show the effect of chemical shift offset on its transfer efficiency, is presented. We focus on short contact time transfer, so that polarization transfer from remote protons which require long contact time can be safely neglected. This is true especially in the case of fast relaxation spins in paramagnetic sample, where long contact time is not favorable. We therefore, reduce the description to an isolated heteronuclear spin pair $I = \frac{1}{2}$ and $S = \frac{1}{2}$ transfer. Suppose that simultaneous linear frequency sweeps are applied at both the I and S spins under rf irradiations with intensities ω_{1I} and ω_{1S}, respectively, the rotating-frame Hamiltonian is written as

$$H = -(\Delta\Omega_I(t) + \Omega_I)I_z - \omega_{1I}(t)I_x - (\Delta\Omega_S(t) + \Omega_S)S_z - \omega_{1S}(t)S_x + D(t)I_zS_z. \quad (1)$$

$D(t)$ is the magnitude of the dipolar interaction between them, which is modulated by MAS and is given by

$$D(t) = d_{\mathrm{IS}}[G_1 \cos(w_r t) + G_2 \cos(2w_r t)] \quad (2)$$

where w_r is the spinning frequency and G_k ($k = 1,2$) depends on the orientation of the internuclear vector in a reference frame fixed to the rotor. d_{IS} is the dipolar coupling constant.

Here, Ω_I and Ω_S are the isotropic chemical shifts for I and S. For brevity, anisotropic chemical shift has been neglected. In the pulse sequence of SADIS CP (Fig. 1a), the frequency-offset terms $\Delta\Omega_I$ and $\Delta\Omega_S$ change in time according to

$$\Delta\Omega_\epsilon(t) = -\Delta\omega_\epsilon(1 - \frac{t}{T}) \tag{3}$$

where $\epsilon = I$ or S, T is the period of frequency sweep, and $\Delta\omega$ is the frequency sweep width. Note that for RAMP CP (Fig. 1b), the term $\Delta\Omega_S$(t) and $\Delta\Omega_I$(t) do not exist, while the rf-irradiation on S channel is linearly ramped through with an initial offset, as described by

$$\omega_{1S}(t) = \frac{(\omega_{\mathrm{f}} - \omega_{\mathrm{i}})}{T}t + \omega_{\mathrm{i}} \tag{4}$$

where ω_{i} and ω_{f} are the initial and final rf-intensity, respectively.

In order to track the evolution of the system, we adopt the non-interacting virtual spin-$\frac{1}{2}$ description known as double quantum (DQ) and zero-quantum (ZQ) subspace [12,20]. Since strong rf-amplitudes are usually applied, the entire system evolves in the ZQ subspace. We have shown in [22] that the secular ZQ Hamiltonian is represented by

$$H^{\mathrm{ZQ}} = 2\Delta_{\mathrm{HH}}(t)I_z^{\mathrm{ZQ}} + \frac{1}{4}D_{\mathrm{eff}}(t)I_x^{\mathrm{ZQ}}, \tag{5}$$

where the effective dipolar frequency, $D_{\text{eff}}(t)$ is given by

$$D_{\text{eff}}(t) = d_{\text{IS}} G_n \sin\alpha_I(t) \sin\alpha_S(t), \tag{6}$$

and the time-dependent Hartmann-Hahn condition

$$\Delta_{\text{HH}}(t) \equiv \omega_{eI}(t) - \omega_{eS}(t) - n w_r = 0, (n = -2, -1, 1, 2). \tag{7}$$

I_z^{ZQ} and I_x^{ZQ} are the ZQ fictitious spin-$\frac{1}{2}$ operators [23]. Here, $\omega_{eI}(t)$ and $\omega_{eS}(t)$ are its respective effective fields,

$$\omega_{e\epsilon}^2(t) = \omega_{1\epsilon}^2 + (\Delta\Omega_\epsilon(t) + \Omega_\epsilon)^2, \tag{8}$$

which are tilted to an angle,

$$\alpha_\epsilon(t) = \tan^{-1} \frac{\omega_{1\epsilon}(t)}{\Delta\Omega_\epsilon(t) + \Omega_\epsilon} \tag{9}$$

with respective to the z-axis.

In order to visualize the transfer efficiencies due to the effect of chemical shift offsets, and since only the magnetizations locked along its effective fields do participate in the polarization transfer (Eq. (7)), we show the trajectory of the effective fields as evaluated with Eq. (8) in Fig. 2. Arbitrary set of parameters were chosen for fair comparison between SADIS CP and RAMP CP schemes. At this point, for the purpose of clarity, w_r= 0 is assumed so that all other sideband-matching conditions can be dropped. In RAMP CP (Fig. 2a), if the matching parameters were adjusted as such that Hartmann-Hahn conditions are met for S spins near to the S carrier-frequency (e.g. Ω_S= 0, in this case), there ought to be many other S spins, due to e.g. isotropic chemical shift (e.g. Ω_S= 0.3 MHz, in this case) where its trajectories are aligned far

from the trajectory of the I spin. As such Hartmann-Hahn crossing cannot be satisfied simultaneously over a large bandwidth. Therefore, the efficiency of the polarization transfer degrades for S spins which have large chemical shift offset (Fig. 3). Likewise, as for the case of fast sample spinning, additional effective field trajectories for I spin separated by the spinning frequency, w_r due to sideband conditions appear. As such, only S spins of approximately $\Omega_S \leq 2w_r$ fall in the region where Hartmann-Hahn crossings are viable but not for S spins of $\Omega_S \geq 2w_r$. In paramagnetic solids, isotropic chemical shifts are typical in the order of a few hundred of kHz, while w_r of 30-60 kHz are commonly used.

As for SADIS CP as shown in Fig. 2b, effective field for I spin can be forced to cover a large bandwidth so that Hartmann-Hahn crossings can occur to each individual S spin regardless of its chemical shifts offset (Fig. 3). In RAMP CP, since CW irradiation is applied on the I spin, its effective field trajectory does not ramp through a large variable of values as in the case of effective field trajectory of the I spin in SADIS CP. This is a unique feature of applying simultaneous adiabatic frequency in SADIS CP as compared to other single channel frequency/amplitude modulated schemes [11–18]. The limit of the frequency sweeping width is only defined by the capability of the NMR spectrometer which sets the requirement for finite discrete number of steps that can be implemented for phase or frequency modulation. It is worth noting that in SADIS CP, the transfered S magnetization are much higher than the one of RAMP CP as depicted in Fig. 3. Furthermore complete inversion is possible with longer contact time (results not shown) similar to other adiabatic inversion schemes [12–14]. As for RAMP CP, the final S transfered magnetization saturated at those points as shown in Fig. 3 and do not increase further even

with longer contact time. Complete inversion in adiabatic schemes is however oftenly not practical due to the decay in spin-lattice relaxation in rotating frame. In this respect, SADIS CP as compared to other adiabatic inversion schemes [12–14], may hold slight advantage due to its larger effective fields (due to off-resonance irradiations) which can in general enhance the $T_{1\rho}$ [24] of the spins.

3 Experimental

Experiments were performed at room temperature in a magnetic field of 14.1 T with Bruker Avance III spectrometer and home-built triple resonance probe equipped with spinning module for 1.3 mm rotor. 1.8 mg polycrystallines sample of natural abundance Cu(II)(D,L-Alanine)$_2$.H_20 were packed into the rotor. Carrier frequencies for the ^{13}C and ^{1}H channels were 150.926 MHz and 600.175 MHz, respectively. The spectral width were 800 kHz and 200 kHz for ^{1}H and ^{13}C, respectively. The ^{13}C NMR signals were measured at sample spinning frequency, w_r of 31 kHz, and detected without the application of ^{1}H decoupling. Rotor-synchronous spin-echo sequence was applied prior to signal acquisition. Sufficiently long recycle delays of 50 ms for all CP experiments and 100 ms for ^{13}C direct observation were used to protect the probe from arching. For a common experimental time of about 42 min, the number of acquisitions (N) were set to 50000 and 25000 for CP experiments and direct excitation, respectively.

We compared the sensitivity enhancement (in terms of SNR) of SADIS CP with (i) RAMP CP, which represents the single channel frequency/amplitude modulated CP, and (ii) direct excitation of the rare spins. The optimal combi-

nation of rf-amplitudes and frequency widths for SADIS CP can be estimated by ensuring that the effective field for ^{13}C, ω_{eS} and that for ^{1}H, ω_{eI} were applied as such that, the initial condition (t= 0), $\omega_{eI} + w_r \leq \omega_{eS} \leq \omega_{eI} + 2w_r$, and finally at the end of the contact time ($t = T$), $\omega_{eS} + w_r \leq \omega_{eI} \leq \omega_{eS} + 2w_r$, or vice-versa, for one of the sideband ± 1 matching condition to be met. For RAMP-CP, optimal rf-amplitude parameters were ^{13}C, $\frac{\omega_{1S}}{2\pi}$= 90 kHz to 125 kHz, and $\frac{\omega_{1I}}{2\pi}$= 158 kHz. An initial $\frac{\pi}{2}$ pulse of pulse width 1 μs was applied to I spin prior to spin-locking. As of standard RAMP CP, the amplitude-ramping width for ^{13}C, $\frac{\omega_{1S}}{2\pi}$ was set to approximately the frequency of sample spinning, w_r. The $\frac{\pi}{2}$ pulse width for ^{13}C direct excitation was 2 μs.

4 Results and discussions

Among various experiments of rf-amplitudes and frequency sweep widths, the optimal results are shown in Fig. 4. For both CP experiments, a short contact time of 300 μs was used to minimize the effect of relaxation. The SNRs were as denoted besides each peak. One can see that through cross polarization (Fig. 4a and Fig. 4b) the SNRs were greatly enhanced (with the exception of ^{13}COOH in RAMP CP) as compare to direct excitation (Fig. 2c). For RAMP CP, SNR enhancement gains were (2.20, 0.72, 1.20) for ($^{13}CH_3$,^{13}COOH,^{13}CH), respectively, higher than that of direct excitation. Peaks assignment were based on literature [3]. However, considering that the number of scans were twice as much as that in direct excitation (due shorter recycle delay), SNR enhancement of 1.414 is to be expected. In this respect, one can deduce that the signal itself has not been improved much by the original idea of cross po-

larization, that is sensitivity enhancement of a ratio of the gyromagnetic ratios of both spins. Limited sensitivity enhancement in paramagnetic system with RAMP CP is not inherently the limitation of cross polarization, but rather caused by poor spin-locking and limited excitation bandwith due to limited rf-nutations on both the source and target spins, as described above.

With SADIS CP, we obtained a substantial signal intensity gain of as much as (1.19, 2.33, 2.17) as compared to RAMP CP, which translates to increase of the SNR to (9.25, 5.25, 6.50). These enhancements were attributed to the application of large initial frequency offset of $\frac{\Delta\omega_I}{2\pi}$= 450 kHz and $\frac{\Delta\omega_S}{2\pi}$= 500 kHz from far off-resonance to on-resonance to ^{1}H and ^{13}C, respectively. Although ^{1}H has resonance-line broadened over 600 ppm and ^{13}C has isotropic chemical shift distribution over 500 ppm, which is about 360 kHz and 75 kHz, respectively in 14.1 T field, large frequency sweep offsets in SADIS CP produce much higher effective fields that enable us to excite the whole spectra effectively and maintain a good spin-lock on both the source and target spins. As for RAMP CP, $\frac{\pi}{2}$ pulse irradiation of rf-nutation 250 kHz, and rf-amplitudes for spin-locking ($\frac{\omega_{1S}}{2\pi}$= 90-125 kHz and $\frac{\omega_{1I}}{2\pi}$= 158 kHz) were not sufficiently large as compared to its respective spectral width, therefore, resulted in poor spin-locking and decay of magnetization in the rotating frame. Moreover, since the frequency sweep offsets in SADIS CP were swept through a wide range of values, Hartmann-Hahn condition was made to satisfy over a large spectral bandwidth or isotropic chemical shift offset, as explained in the theoretical section.

In conclusion, we have shown that simultaneous adiabatic spin-locking cross polarization is applicable to spins with large chemical shift dispersion or when the practical achievable rf-amplitude is not sufficiently large to cover the whole

spectral distribution as is often true as in the case of paramagnetic solid. Despite the presence of large spectral broadening and fast relaxation on both the source and target spins, substantial signal enhancements over large bandwidth has been obtained with SADIS CP as compared to RAMP CP, and direct excitation. Combined with VFMAS, high resolution and high sensitivity spectra were reported. Work on other highly paramagnetic species is currently under progress at our laboratory and will be reported elsewhere.

Acknowledgement

This work was supported by the CREST program of the Japan Science and Technology Agency, FP6 UPMAN project and Estonian Science Foundation. W.K. Peng would like to thank the 21st Century Center of Excellence (COE) program for financial support.

References

[1] I. Bertini, C. Luchinat, G. Parigi, Prog. in Nuc. Mag. Reson. 40 (2002) 249.

[2] G. Kervern, G. Pintacuda, Y. Zhang, E. Oldfield, C. Roukoss, E. Kuntz, E. Herdweck, J-M. Basset, S. Cadars, A. Lesage, C. Coperet, L. Emsley, J. Am. Chem. Soc. 128 (2006) 13545.

[3] Y. Ishii, N.P. Wickramasinghe, S. Chimon, J. Am. Chem. Soc. 125 (2003) 3438.

[4] N.P. Wickramasinghe, M. Shaibat, Y. Ishii, J. Am. Chem. Soc. 127 (2005) 5796.

[5] A. Samoson, T. Tuherm, Z. Gan, Solid State Nucl. Magn. Reson. 20 (2001) 130.

[6] A. Samoson, Encyclopedia of Nuclear Magnetic Resonance, vol. 9, Wiley, Chichester, 2002, p.59.

[7] A. Samoson, T. Tuherm, J. Past, A. Reinhold, T. Anupold, I. Heinmaa, Topics in Current Chemistry 246 (2004) 15.

[8] N.P. Wickramasinghe, Y. Ishii, J. Magn. Reson. 181 (2006) 233.

[9] S.R. Hartmann, E.L. Hahn, Phys. Rev. 128 (1962) 2042.

[10] A. Pines, M.G. Gibby, J.S. Waugh, J. Chem. Phys. 59 (1973) 569.

[11] S. Hediger, B.H. Meier, R.R. Ernst, Chem. Phys. Lett. 213 (1993) 627.

[12] S. Hediger, B.H. Meier, N.D. Kuru, G. Bodenhausen, R.R. Ernst, Chem. Phys. Lett. 223 (1994) 283.

[13] S. Hediger, B.H. Meier, R.R. Ernst, Chem. Phys. Lett. 240 (1995) 449.

[14] M. Baldus, D.G. Geurts, S. Hediger, B.H. Meier, J. Magn. Reson. A118 (1996) 140.

[15] S. Hediger, P. Signer, M. Tomaselli, R.R. Ernst, B.H. Meier, J. Magn. Reson. 125 (1997) 291.

[16] G. Metz, X. Xiaoling, S. Smith, J. Magn. Reson. A110 (1994) 219.

[17] A.C. Kolbert, A. Bielecki, J. Magn. Reson. A116 (1995) 29.

[18] R. Fu, P. Pelupessy, G. Bodenhausen, Chem. Phys. Lett. 264 (1997) 63.

[19] A. Samoson, T. Tuherm, J. Past, J. Magn. Reson. 149, (2001) 264.

[20] W.K. Peng, K. Takeda, M. Kitagawa, Chem. Phys. Lett. 417 (2006) 58.

[21] K. Yamauchi, J.W.G. Janssen, A.P.M. Kentgens, J. Magn. Reson. 167 (2004) 87.

[22] W.K. Peng, K. Takeda, J. Magn. Reson. 188 (2007) 267.

[23] S. Vega, J. Chem. Phys. 68 (1978) 5518.

[24] S.C. Shekar, D.K. Lee, A. Ramamoorthy, J. Magn. Reson. 157 (1996) 223.

Figure Captions

Figure 1

(a) A pulse sequence for SADIS CP. Single phase continuous wave irradiation is applied together with frequency sweep from far off-resonance towards on-resonance simultaneously on both the source and target channels. For better spin-locking performance, the rf-amplitudes may be switched on gradually as shown above.

(b) A pulse sequence for RAMP CP. For both schemes, rotor-synchronous spin-echo sequence was applied prior to signal acquisition. τ_R denoted the period of one-rotor cycle.

Figure 2

(a) Instantaneous magnitude of the effective fields in RAMP CP for the I spin (dash line) and S spins (solid lines) of two different isotropic chemical shifts, $\Omega_S = 0$ and 300 kHz. The arbitrary chosen set of parameters were $\frac{\omega_{1S}}{2\pi} = 530 - 580$ kHz, $\frac{\omega_{1I}}{2\pi} = 550$ kHz, and T= 400 μs. For simplicity, $\Omega_I = 0$ is assumed.

(b) Instantaneous magnitude of the effective fields in SADIS CP for the I spin (dash line) and S spins (solid lines) of two different isotropic chemical shifts, $\Omega_S = 0$ and 300 kHz. The arbitrary chosen set of parameters were $\frac{\omega_{1S}}{2\pi} = 350$ kHz, $\frac{\Delta\omega_S}{2\pi} = 1200$ kHz, $\frac{\omega_{1I}}{2\pi} = 580$ kHz, $\frac{\Delta\omega_I}{2\pi} = 1000$ kHz, and T= 400 μs. For simplicity, $\Omega_I = 0$ is assumed.

Figure 3

Numerically calculated powder-averaged signal intensity of S spins for various isotropic chemical shift offsets, Ω_S ranging from 0-300 kHz with respect to a fixed S carrier-frequency. Carrier-frequency for I channel is assumed to be applied at on-resonance for all other spin-pairs. Polarization transfer for SADIS CP (dark line) is almost insensitive over large isotropic chemical shift distribution. For RAMP CP (gray line), the signal intensity drops as the isotropic chemical shift offset increases. Heteronuclear dipolar coupling constant for all the IS-spin pairs with different isotropic chemical shift were arbitrarily chosen as d_{IS}= 20 kHz. All other rf-amplitude and/or frequency sweep width paramaters for both the pulse sequences were as shown in caption of Fig. 2. The signal intensity is the weighted-sum of each crystallite signal for 314 different angles.

Figure 4

^{13}C NMR spectrum of powder sample of Cu(II)(D,L-Alanine)$_2$.H_20, taken with (a) SADIS CP, (b) RAMP CP for a short contact time of 300 μs, and (c) single pulse direct excitation. The SNRs were noted above each respective peaks. For SADIS CP, parameters were $\frac{\omega_{1S}}{2\pi}$= 125 kHz, $\frac{\Delta\omega_S}{2\pi}$= 500 kHz, $\frac{\omega_{1I}}{2\pi}$= 152 kHz, $\frac{\Delta\omega_I}{2\pi}$= 450 kHz. Optimal rf-amplitude parameters for RAMP CP were $\frac{\omega_{1S}}{2\pi}$= 90 kHz to 125 kHz, and $\frac{\omega_{1I}}{2\pi}$= 158 kHz. The spectra for (c) was scaled according to $N^{\frac{1}{2}}$ to display a common noise level with spectra (a) and (b). The weak peaks at 80 ppm, denoted by $\star$, are attributed to minor species.

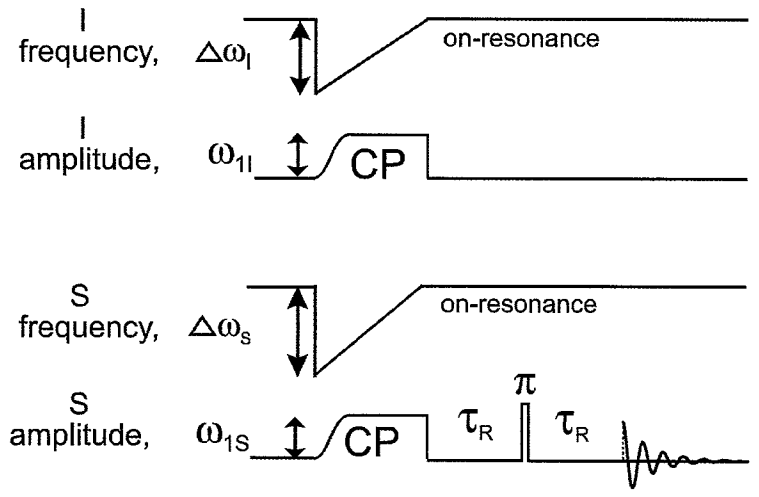

(a)

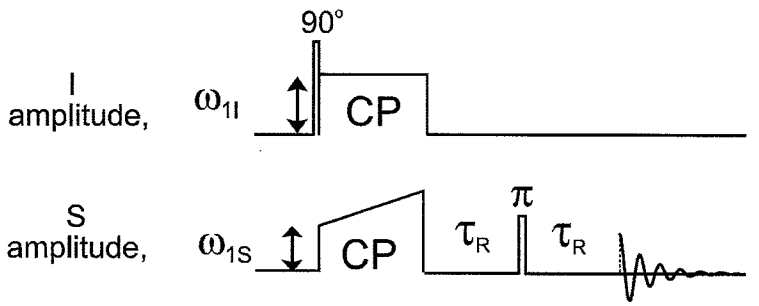

(b)

Fig. 1

Simultaneous Adiabatic Spin-locking ...

Peng et al.

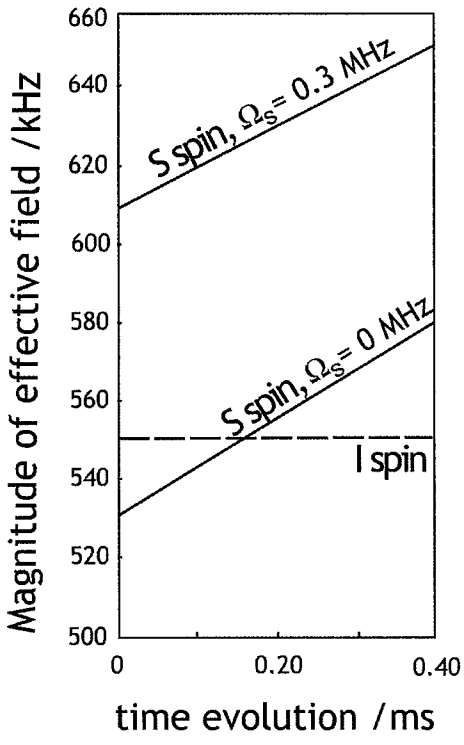

(a)

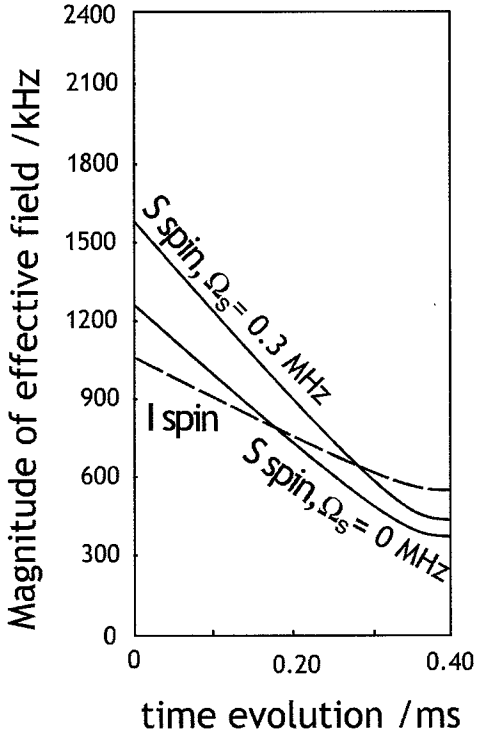

(b)

Fig. 2

Simultaneous Adiabatic Spin-locking ...

Peng et al.

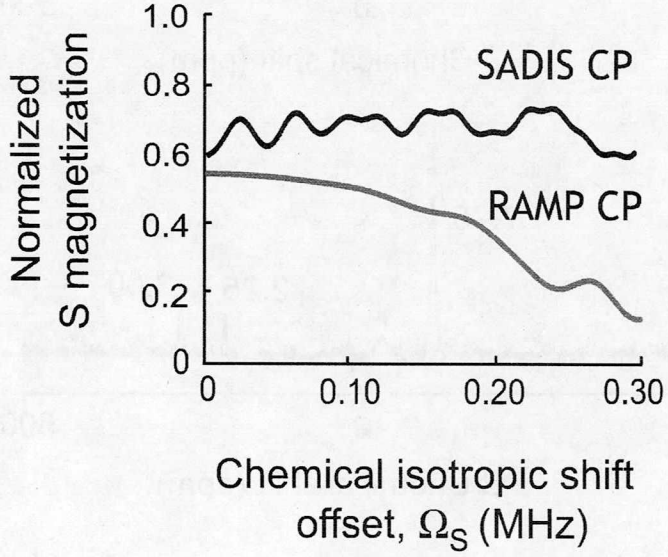

Fig. 3

Simultaneous Adiabatic Spin-locking ...

Peng et al.

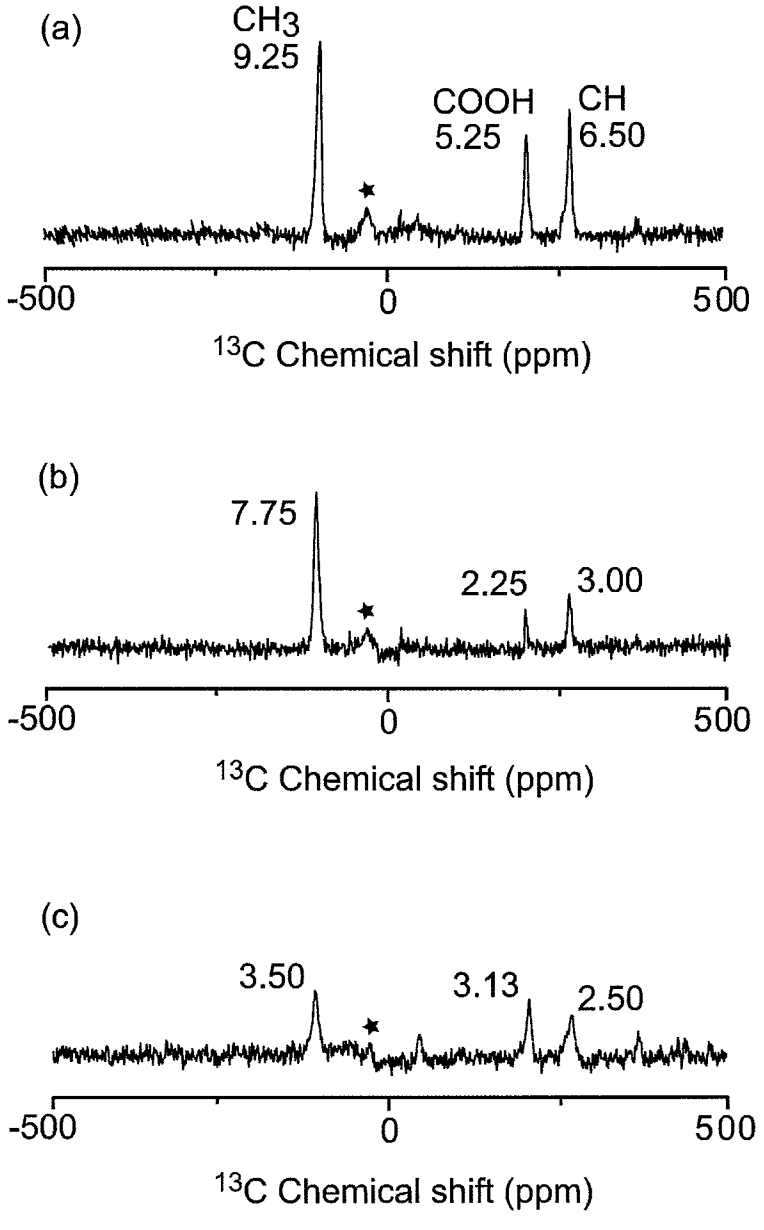

Fig. 4

Simultaneous Adiabatic Spin-locking ...

Peng et al.